Water and Heavy Metal Fluxes in Paved Urban Soils

vorgelegt von:
Dipl. Geoökologe Thomas Nehls
aus Berlin

von der Fakultät VI der Technischen Universität Berlin
zur Erlangung des akademischen Grades
Doktor der Naturwissenschaften
Dr.rer.nat.

genehmigte Dissertation

Promotionsausschuss:
Vorsitzender: Prof. Dr. Martin Kaupenjohann
Berichter: Prof. Dr. Gerd Wessolek
Berichter: Prof. Dr. Wolfgang Burghardt

Tag der wissenschaftlichen Aussprache: 27.01.2007

Berlin 2007

D83

"Man darf nie an die ganze Straße auf einmal denken, verstehst du? Man muss nur an den nächsten Schritt denken, an den nächsten Atemzug, an den nächsten Besenstrich. Und immer wieder nur an den nächsten... Dann macht es Freude; das ist wichtig, dann macht man seine Sache gut... Auf einmal merkt man, dass man Schritt für Schritt die ganze Straße gemacht hat. Man hat gar nicht gemerkt wie, und man ist nicht außer Puste."

Beppo Strassenkehrer in Michael Endes "Momo"

Danksagung

Ich danke

für das in mich gesetzte Vertrauen, die mir gewährte Freiheit, für Unterstützung und Förderung sowie die fruchtbaren und anregenden Diskussionen ganz herzlich Prof. Gerd Wessolek,

für wertvolle Impulse, aussergewöhnliche Sichtweisen und die Bereitschaft, diese Arbeit zu begutachten, Prof. Wolfgang Burghardt aus Essen,

für Nachsicht gegenüber "blauen Wundern", Hilfsbereitschaft und viele nützliche Tipps und Diskussionen, auch im Namen meiner Diplomanden, allen Mitarbeitern der Fachgebiete Standortkunde & Bodenschutz sowie Bodenkunde, ganz besonders Dr. Heiner Stoffregen, Michael Facklam und Claudia Kuntz,

meinen polnischen Kollegen Zosia, Mietek und Gzregorz für die Zusammenarbeit und die warme Herzlichkeit, welche die Aufenthalte im kalten Lublin prägten - Dziekuje!

Prof. Dieter Scherer für den "Werkzeugkasten", den er mir mit dem Einstieg in die Programmiersprache IDL zur Verfügung stellte und für seine spontane Bereitschaft, mir über diverse Hürden der Bildverarbeitung zu helfen,

Dr. Sonja Brodowski, für die Einblicke in die Kunst der Analyse schwarzen Kohlenstoffs,

Susanne Bley, Aude Delboe (merci!) und Kristofer Proll für ihre Hilfe beim Erforschen der Fließwege, für viel Wirbel und die interessanten Diplomarbeiten,

Cora für Berlin und viel Unterstüzung,

und schliesslich meinen Eltern dafür, dass sie mir mein Studium ermöglichten, mich dabei unterstützten und ganz besonders dafür, dass sie nie fragten, was man als Geoökologe denn später mal machen würde.

Preface

I studied the seam material as a member of the DFG–Graduate school GK 780/1 “Perspectives on Urban Ecology - The Metropolis Berlin”. This PhD thesis is part of the interdisciplinary scientific programme of this graduate school, in which we investigated different aspects of urban ecology. Partners of the Graduate school are the Humboldt–University of Berlin, the Technical University of Berlin, the Freie University Berlin, the Institute of Regional Science and Structural Studies from the Leibniz Research Association, and the Leibniz-Institute of Freshwater Ecology and Inland Fisheries.

The stipendiaries investigated interactions between abiotic (soil, water, air), biotic (vegetation, insects, birds) and human (human behaviour, psychology) components of the urban ecosystem. Thereby, the biodiversity was of special interest. A comprehensive introduction on the graduate school can be found under: www.stadtoekologie-berlin.de

In the project A1 “Water and Heavy Metal Fluxes in Urban Soils” I investigated partially sealed urban soils as strongly anthropogenically influenced soils. In other words, I was interested in pavements and all signs of living soils and vivid soils functions in them. It was the special goal of this work also to derive suggestions for town planners, how “soil nature” can be supported, designed and redesigned inside the city for the well-being of the city dwellers.

Special scientific topics of this study had been conducted together with national and international partners because of the interdisciplinarity of the scientific question. A part of the work is already published (Nehls et al., 2006), other parts are prepared for publication. Therefore, the dissertation was written in english rather a collection of chapters then a monography. I hope to broaden the auditory rather than to exclude people from reading about the most stressed and most stepped soil in the city dwellers life.

Now, I hope the well-disposed reader will have the same fun reading this work, which I had doing the research!

Zusammenfassung

Weltweit werden in Städten die Strassen und Gehwege gepflastert. Diese Befestigungen erlauben eine gewisse Infiltration von Regenwasser und vermindern so den Oberflächenabfluss. Pflastersysteme bestehen aus Pflastersteinen, technogenem Sand und dem sogenannten Fugenmaterial. Es wurde angenommen, dass alle drei Komponenten den Transport von Wasser und gelösten Substanzen beeinflussen.

Das Fugenmaterial ist die oberste Schicht des Bodens zwischen den Pflastersteinen. Es ist unklar, woraus es sich zusammensetzt. Es wurde vermutet, dass es durch Einwaschung von Stäuben gebildet wird und das ein großer Teil seiner organischen Substanz aus Black Carbon besteht. Dies würde dessen dunkle Färbung erklären. Aufgrund der Einträge müsste das Fugenmaterial eine spezielle Poren- und Oberflächenstruktur und damit spezielle physikalische und chemische Filtereigenschaften aufweisen.

Fugenmaterialien wurden in Berlin, Warschau und Paris beprobt und erstmals auf ihre Materialeigenschaften hin untersucht. Dabei wurden neben allgemeinen bodenchemischen Parametern die Korngrößenverteilungen, die Porengrößen und -strukturen, die Oberflächengrößen und -formen, die Adsorptionsenergieverteilungen und die Schwermetalladsorptionsisothermen untersucht. Es wurde festgestellt, dass Black Carbon bis zu 30 % der organischen Fraktion des Fugenmaterials ausmachen kann. Die organische Substanz hat verglichen mit der naturnaher Böden eine kleine spezifische Oberfläche und weist eine geringe Ladungsdichte auf, was auf ihren unpolaren Charakter schliessen lässt. Adsorptionsenergieverteilungen bestätigen dies. Zusammengenommen erklärt sich dadurch die sehr geringe Kationenaustauschkapazität des Fugenmaterials verglichen mit naturnahen sandigen Böden. Vergleicht man das Fugenmaterial jedoch mit dem ursprünglichen Bausand, so weist es allgemein günstigere ökologische Eigenschaften auf: es hat eine höhere nutzbare Feldkapazität, eine höhere Kationenaustauschkapazität und hält Schwermetalle effektiver zurück, wie die Schwermetalladsorptionsisothermen beweisen.

Nach allem, was bislang über präferenzielle Fließwege in Böden bekannt

war, müsste die Anordnung der Pflastersteine in teilversiegelten Böden ebenfalls zur Ausbildung bevorzugter Fliessbahnen führen. Untersucht wurde diese These an fünf Standorten in Berlin durch Versickerung mit Brilliant Blue gefärbten Wassers. Für die qualitative und quantitative Auswertung dieser Versuche wurde die digitale Bildverarbeitung eingesetzt. Aufgrund der heterogenen Färbung der urbanen Böden musste dazu eigens eine neue Methode entwickelt werden. Abhängig von der Größe der Pflastermaterialien und dem Aufbau der darunterliegenden Schichten kommt es zur Ausprägung präferentieller Fließwege in teilversiegelten Böden. Dabei nehmen die Fließwege teilweise die Form der Fugengeometrie an. Der effektive Fließquerschnitt verringert sich so teilweise auf 60 %.

Welchen Einfluß Fugenmaterial und präferentielle Fließwege auf die Verlagerung von Blei und Cadmium haben, wurde in numerischen Simulationen mit den Programmen HYDRUS 1D und HYDRUS 2D untersucht. Dazu wurden sämtliche gemessenen Eigenschaften des Pflastersystems verwendet. Eine akute Gefährdung der Verlagerung von Blei besteht nicht. Anders sieht es es bei Cadmium aus: es ist zu erwarten, dass die Speicherkapazität des Pflastersystems bereits nach wenigen Dekaden ausgeschöpft ist und dann ein Austrag aus dem Pflastersystem einsetzt. Partikulärer Transport und schnelles Fließen durch Makroporen wurden im Modell dabei noch nicht berücksichtigt.

Aufgrund der positiven Wirkung auf den urbanen Wasserkreislauf sind Teilversiegelungen der Verwendung total versiegelnder Materialien wie Beton oder Teer vorzuziehen. Die Speicherung von Black Carbon und Schwermetallen zeigt außerdem, dass offene Bodenoberflächen in urbanen Gebieten wichtige Senkenfunktionen wahrnehmen.

Summary

Worldwide, the streets and sidewalks in urban areas are often perviously paved. This kind of sealing allows at least a little infiltration of rainwater and thereby decreases the run-off. Pavements consist of the pavers, a construction material and the so called seam material. It was hypothesized, that these three components influence the transport of water and solved substances.

The seam material is the first layer of soil material which is situated in the gaps between single pavestones. It was hypothesized, that it develops by incorporation of different deposits of urban dust and that it contains great portions of Black Carbon. This would explain its dark colour. Because of this inputs, the seam material was expected to have a special surface and pore structure. Therefore, special chemical and physical filter properties were expected. Seam materials have been sampled in Berlin, Warsaw and Paris and their properties have been investigated for the first time. Beside the general soil chemical properties, the following parameters have been measured: grain size distribution, pore size distribution and pore structure, specific surface area and surface form, adsorption energy distribution function, and the heavy metal adsorption isotherm. Up to 30 % of the organic matter consists of Black Carbon. The organic substance of seam materials has small specific surface area and a low surface charge density. This indicates a non-polar character. The seam material shows a high fractions of low adsorption energy, which proves this statement. However, the seam material shows positive ecological properties compared to the original construction sand: it has a higher available water capacity, a higher cation exchange capacity and shows a higher heavy metal retardation, as seen from the heavy metal adsorption isotherms.

From what we know about preferential flow paths, the arrangement of pavers and seams would have to introduce preferential flow patterns. This hypothesis was tested on five sites in Berlin, were brilliant blue coloured water was infiltrated. Digital image analysis has been used for the qualitative and quantitative investigation of the dye tracer experiments. Because of the heterogeneous background colouration of urban soils, a special method was developed. Preferential flow paths were frequently found. Their develop-

ment depends on the size of the pavestones and the structure of the soils underneath the pavement. Sometimes, the preferential flow patterns show the same geometry like the pavement seams. The effective cross sectional flow area decreased to 60 %.

The influence of the seam material and the preferential flow patterns has been evaluated by a simulation of Pb and Cd displacement using HYDRUS 1D and HYDRUS 2D. Thereby, all investigated features of the pavement system have been included in the analysis. There is no acute danger of a displacement of Pb. Cd behaves different, here the retardation capacity is exhausted after some decades. Thereby, particulate transport and fast flow in macro pores has not been considered.

Because of its positive influence on the water cycle inside urban areas, pervious pavements are favorable to complete sealing by tar or concrete. The accumulation of black carbon and heavy metals furthermore demonstrates, that open soil surfaces can fulfill important sink functions in urban areas.

Contents

List of Figures

List of Tables

Part I

Introduction

This study investigates the properties of highly artificial soils, the partially sealed soils in urban areas. It deals with soil material which developed between single pavestones called seam material, evaluates the effect of the pavestones on water movement - do they induce preferential flow - and answers the question, if traffic derived heavy metals are risky for the groundwater.

Partially sealed soils are highly anthropogenic. The original construction materials are technogenic and their spatial distribution and horizontal build up is completely artificial. Partially sealed soils, or in other words pavement systems, are designed to conveniently support all kinds of traffic as a stable, dry, and even ground. All other functions, which they fulfill too, are sideeffects which were not originally intended. Although it is convenient for the city's population, soil sealing is one of the most frequent and drastic soil alterations in urban areas, leading to a number of ecological, healthy and finally economical problems for city dwellers.

Compared to natural environments, the surface runoff increases and infiltration decreases (Figure 1). The consequences are fast and pronounced responses in the discharge of receiving watercourses, which can be flood relevant. Furthermore, it can cause overrunning of combined sewage systems, which induces pollution of urban rivers with untreated wastewater. This, for instance, is the most severe negative impact on water quality of the river Spree in the urban area of Berlin (Heinzmann, 1998). The result of the decreased infiltration is a smaller amount of available soil water for the evapotranspiration. The city becomes dryer. This leads to higher sensible heat and smaller latent heat: the city becomes hotter (Wessolek, 2001). The most driving factor however for the heating of urban areas is the increased absorbed netradiation at the vertical surfaces of buildings (Kuttler, 1998). Compared to surrounding not sealed and green areas, the mean annual temperature increases by 0.5 to 1 K with absolute maximum differences of up to 10 K - the effect known as "urban heat island" (Kuttler, 1998). This hotter urban climate leads to human health problems and to increased macroeconomic costs in these areas (Tol, 2002a,b; Townsend et al., 2003). The urban heat island effect cannot be avoided by de-sealing measures, but its impact on the people can be decreased. Therefore, increasing rainwater infiltration is a main goal of ecological urban planning. Pervious sealing (e.g. cobblestones, concrete slabs with open seams) can help to reach this goal.

Huge paved areas already exist. But although it surrounds thousands of people every day, comparable little is known about the paved soils. So the study not only deals with future aspects but investigates the recent status. Cities preserve and use pavements as architectural design features, which contribute to unmistakable urbanistic identity. Compared to impervious soil

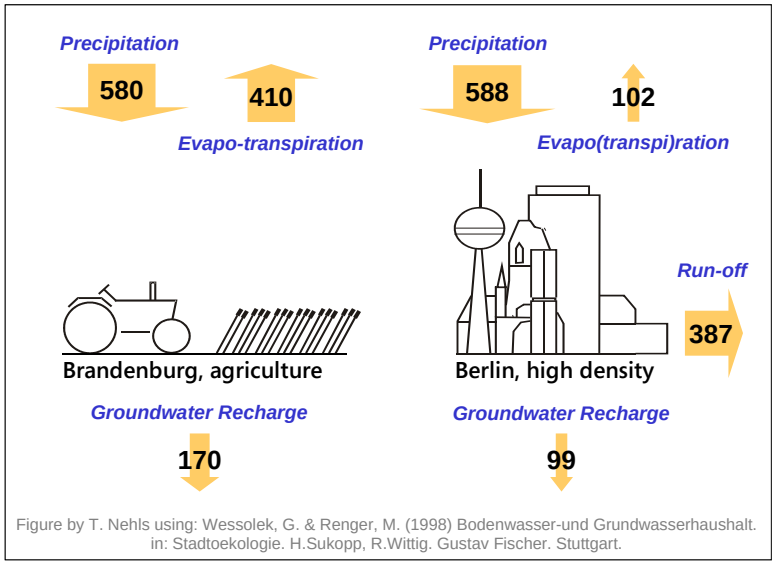

Figure 1: Illustration of long term water balances for a) an agricultural site outside Berlin and b) a site with 85 to 100 % surface sealing inside the city. The water balance components are given in mm a^{-1}.

sealing, e.g. concrete or tar surfaces, semi-perviously constructed pavements allow at least some exchange between the sealed soil and the environment. This happens via the gaps and the seam material between the pavers, which can be natural stones, concrete paving slabs or even rubber elements. Water can infiltrate through the seams or pervious pavers itself, the gas exchange is not completely restricted, evaporation is still possible (Wessolek, 2001).

De-sealing is a measure to increase infiltration. Thereby, not only the quantity but also the quality of the infiltrating water and the groundwater can be influenced. Urban areas are sites of different point and non-point emissions and immissions, depending on the circumstances like industry, traffic and so on (Harrison and Johnston, 1985; Gromaire-Mertz et al., 1999; Viidanoja et al., 2002; Dannecker et al., 1990). In Berlin, at least the traffic is a source of contaminations, e.g. heavy metals and organic contaminants like PAHs. Although pesticides were developed for agricultural use, they are used in cities too in terms of sidewalk maintenance (Spanoghe et al., 2005). Therefore, pavements allow infiltration of pollutants like heavy metals or pesticides, which are released from traffic (Hewitt and Rashed, 1991; Dierkes and Geiger, 1999; Legret and Pagotto, 1999) or actively applied (Strange-Hansen et al., 2004).

Semi-pervious pavement systems are constructed to be highly conductive by using retention-weak materials to drain water fastly in order to avoid

damages, e.g. by frost. Quantitative studies of the infiltration on different paved surfaces revealed infiltration rates, i of 7.2 to 168 $\mathrm{cm\,d^{-1}}$ (Schramm and Münchow, 1996). They are governed by the seam percentage of the pavements, but also by the age of the seam material. With increasing age, the original seam filling (usually coarse sand) becomes less conductive (Dannecker et al., 1990; Borgwardt, 1993) due to accumulations of urban dirt, which clogs the pores of the upper seam filling layer.

The term urban dirt in that context summarizes mainly urban dust, but also foliage, hairs, cigarette stumps, glass, food residues, dog feces - in short: any litter produced by urban life small enough to fit the seams. If these accumulations can fulfill filter functions has not been studied yet. However, because of these accumulations, the first layer of the seam filling gets dark. This must be due to depositions of organic carbon (C_{org}), as it works for natural soils. Consequently, Dannecker et al. (1990) demonstrated that the 0 to 2 cm upper layer had a higher clay and C_{org} amount than the layer below. Wenikajtys and Burghardt (2002) described the same phenomenon and characterized the depositions by carbon to nitrogen ratios (C/N). It could be shown, that depending on the site, the depositions consisted of natural material, e.g. deposited soil material, showing a narrow C/N or were mainly man-made, showing a wide C/N. Here, this study broadens the knowledge base about this anthropogenic carbon form and investigates the role of the so called "Black Carbon" for the build up of seam material's organic matter.

By the accumulation of organic matter the physical and chemical characteristics of the seam filling material must change. A new soil horizon is derived, which is called seam material. **The term "seam material" describes the soil material in between single pavestones of pavements, which developed from technogenic sand by deposition of all forms of organic residues in urban areas.** In the seam material, plants and animals are frequently found. The paved soil takes part in exchange processes, is a living habitat (Staikos, 2005) and therefore, it is a soil. It has been already given a name: "Dialeimmasol" (Wenikajtys and Burghardt, 2002), which considers the regularity of the soil in between the pavers.

The seam material can potentially act as a filter for contaminations. Simultaneously, these deposits are contaminants themselves. It is known for instance, that during combustion, heavy metals and organic particles are bound together (Krauss and Wilcke, 2002; Lau and Stenstrom, 2005). Which of the functions, source of contamination, or sink for contaminations, is more important for the heavy metal displacement through the pavement system?

On a bigger scale, not only the seam material influences solute transport, but also the non-pervious pavers. It is hypothesized that through the seams, the gaps between the pavestones, water is canalised into a certain flow

pattern given by the pavement geometry. Flow patterns in soils can be investigated by dye tracer experiments, especially the light colored construction sand promises good visability. In the last decade, dye tracer experiments substantially contributed to our current knowledge of flow patterns and flow mechanisms in the vadose zone. Flury et al. (1994) for instance found preferential flow to be the most common case in soils, except in sandy soils. In their well recognised study the authors show, that only in the sandy soils a uniform infiltration, can be found. However, I expected to find pavement related infiltration patterns in semi-perviously sealed soils caused by an introduced fingering through the seams.

It is the final aim of this study to assess the combined impact of preferential flow and the physical and chemical characteristics of the seam material and construction sand on the purity of infiltrating water. Heavy metals have been chosen to be the exemplary contamination. Computer simulations are good measures to study the influence of chemical and hydraulical parameters on the water and solute transport. Here, a numerical simulation offered the chance to integrate all the newly achieved information and to answer the question whether there is a risk of groundwater pollution by heavy metal displacement from paved urban soils. The programme package HYDRUS 1D/2D was used.

This dissertation is structured in three parts. After this introduction the part II follows, which consists of four chapters: on basic properties of the unknown soil substrate, the role of black carbon as a seam material constituent, the pore system properties and the chemical filter properties. Part III consists of two chapters. First, the dye tracer experiments are explained and then a new method, developed for heterogeneously colored soils is introduced. In the second chapter, the results of the dye tracer experiments are presented. In the part IV the heavy metal displacement simulation is presented. The importance of flow patterns and seam material for the retardation capacity of the whole system is assessed.

Part II

Characterisation of the Seam Material

Chapter 1

Basic Properties of the Seam Material

1.1 Introduction

"There is life in the gap!" was the head line of a news paper article about this study (Schubert, 2003), in which it was reported that the microbial activity in the seam material can be even higher than in natural soils.

Although the biological features of that soil material are not in the focus of this work, I did some investigations about the biological activity in the seam material. Reports about a very high microbial activity could be proven (Wessolek, 2001; Staikos, 2005). This is astonishing, because the seam material represents a habitat with some extreme conditions. An infrared photograph of a pavement, taken in summer 2003, shows temperatures of up to 70 °C in the seam material, while the mosaic pavement stones were colder (Figure 1.1). This phenomenon can be explained by the darker color of the seam material compared to the pavers. A lack of water in the seam material avoided a cooling of the seam material by evaporation like it is described by Wessolek and Facklam (1997). On the other hand, the seam material is subject to freezing in the winter, salt application and regular water saturation and complete drying, which leads to a regular change in redox conditions.

In this part of the study, the general properties of the seam material are studied and the seam material itself is introduced.

Concerning soil color it was observed that the seam material is always darker than the original seam filling, which should be due to inputs of organic matter (OM). Furthermore, it is expected, that this OM is different from OM of "natural" soils, because of the predominance of anthropogenic sources of carbon.

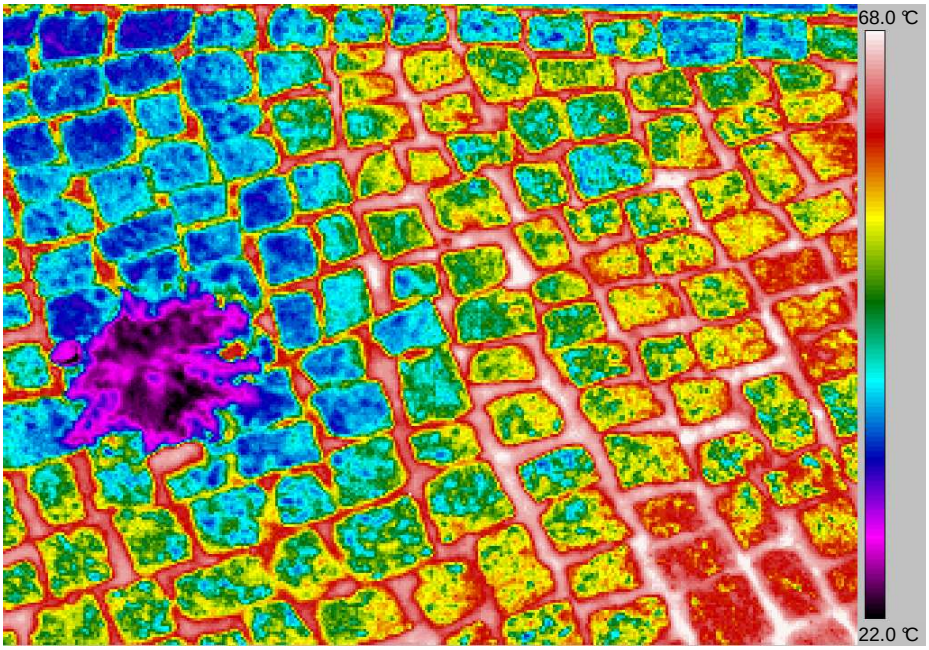

Figure 1.1: Infrared image of a mosaic pavement at the site Grosser Stern. Notice the plant causing the cooler areas at the left side. IR photo taken at the 11.08.2003, 3:13 pm, at ambient temperature of 28 °C, AGEMA infrared systems.

A parameter for the quality of the OM is the ratio C/N, which is expected to be high in case of anthropogenic sources and low for inputs of natural litter, although there are examples for high C/N in the natural environments too, e.g. coniferous foliage. One result of incorporation of OM should be an increased cation exchange capacity (CEC), which is dependent on organic substances, at least in "natural", non-urban soils (Renger, 1965).

All the samples were taken adjacent to roads in order to test for the relevance of traffic as input source. Some of the samples were taken in winter 2003. Therefore, the electric conductivity (EC) is a good parameter to describe the input of traffic due to spray and deicing salts. So, comparable high salt contents indicated by high EC are expected, which also should lead to comparable high pH. Furthermore, due to deposited abrasions from pavers, buildings and streets, the pH in general was expected to be in the neutral range.

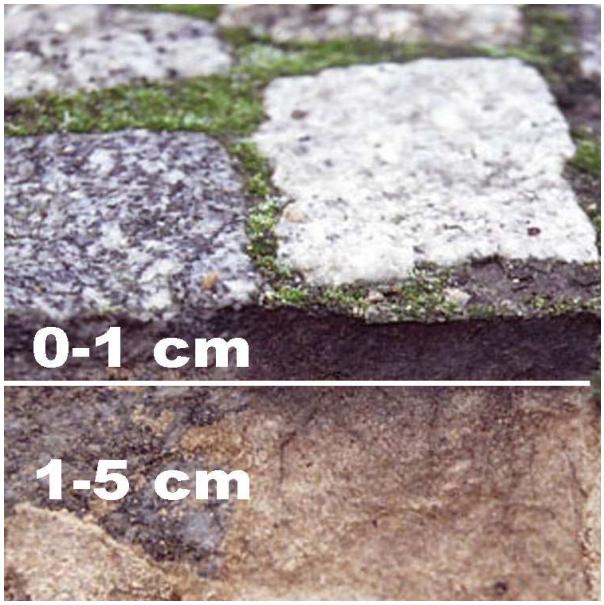

Figure 1.2: Dark seam material (0 to 1 cm) compared to the lighter original sandy seam filling at Weidendamm, Berlin.

1.2 Materials and Methods

1.2.1 Sites and Sampling

Berlin and Warsaw, two cities with similar geographic conditions (climate, soils, elevation etc.) but different environmental conditions (industry, traffic, environmental policy) were chosen to be the sampling sites. The samples consisted of the material that fills spaces between single stones of pavements, which were located adjacent to or directly on roads. The dark layer at 0 to 1 cm depth was always distinguishable from a much brighter 1 to 5 cm layer (Figure 1.2).

Obviously, the upper layer consists of material, influenced by external factors and deposits, while the deeper one represents the material, which is not visibly altered substantially by deposits. In Berlin (samples indicated by B), the 0 to 1 cm layer and 1 to 5 cm layer were sampled, whereas only the 0 to 1 cm layer was sampled in Warsaw (W - samples). Samples were taken in the following streets: B1, B1a Monbijouplatz, B2, B2a Weidendamm, B3, B3a Schnellerstraße, B4 - B8, B4a from different places at the Großer Stern, W1 Emilii Plater, W2 Jerozolimskie, W3 Pulawska, W4 Rzymowskiego, W5 Stanow Zjednoczonych, W6 Modlinska, W7 Slowackiego, W8 Wilanowska and W9 Rowecki Bridge. Sampling sites were located on sidewalks within two meters from roads with different traffic intensity, while the samples B9

and B10 Pfluegerstrasse were sampled directly on the road. Here, B9 was sampled in the middle of the street, whereas B10 was taken from the edge of the street. Samples B1a - B4a come from the same points as B1 - B4, but consist of material from the 1 to 5 cm layer. It was nice experiencing the great interest of pedestrians and policemen in this work and explaining them why I was scraping up the "dirt" from the sidewalks.

1.2.2 Analyses

The pH was determined in 0.01 M $CaCl_2$ with a combined glass/calomel electrode in a 2/1 (solution/soil) suspension. The EC was determined in a 2:1 (solution/soil) suspension with deionized water using a conductivity meter (WTW, Weilheim, Germany).

The potential CEC was determined at pH 8.2 using a batch method with cation exchange by ammoniumacetate and re-exchange by bariumchloride (Mehlich, 1984). This rather work-intensive method was used because of expected high salt and carbonate contents in the samples. Barium was analyzed using the atom absorption spectrometry (Perkin Elmer, B1000).

The N_{tot}, C_{tot} and C_{org} (after HCl-treatment to remove carbonates) were determined conductometricaly after combustion using a C/N analyzer (Carlo Erba Instruments, Milano, Italy). The soil material was ground and homogenised.

1.3 Results and Discussion

The pH of the seam material varies from 6.5 to 7.5. The inorganic carbon (mainly carbonate) as the difference of C_{tot} and C_{org} varies from 1 to 8 g kg^{-1}. The slightly higher pH of the Warsaw samples may be due to salinity effects, indicated by significantly higher EC in Warsaw compared to Berlin (Table 1.1). These ECs indicate a higher influence of deicing salts on the Warsaw seam materials compared to Berlin seam materials. The reason might be a more frequent use of deicing salts in Warsaw. More important, the Warsaw samples were taken in the winter. Although, sampling took place in a non frosty period with some rain, there might have been residues of de-icing salt in the seam material. In Berlin, these residues might have been leached already.

As observed, the seam material is always much darker than the underlying material. In Table 1.1 the objective Munsell colors are presented, which prove the statement. Like in "natural" soils this coloration can be explained by depositions of OM (for further discussions see chapter 2).

Table 1.1: General characteristics of seam materials and original seam fillings from Berlin and Warsaw.

Site	Munsell Color	pH ($CaCl_2$)	EC $10^{-6}\,S\,cm^{-1}$	C/N	CEC_{pot} $cmol(+)\,kg^{-1}$	C_{tot}	C_{org} $g\,kg^{-1}$	C_{inorg}
			Berlin, 0 to 1 cm					
B1	2.5Y3/2 (very dark grayish brown)	6.84	107	17.5	1.78	19.20	14.33	4.87
B2	2.5Y3/2 (very dark grayish brown)	7.07	93	18.7	1.65	18.70	16.23	2.47
B3	2.5Y2.5/1 (black)	7.11	-	22.5	1.96	33.37	27.60	7.36
B4	2.5Y3/1 (very dark gray)	7.22	143	25.3	1.98	25.49	23.16	2.33
B5	2.5Y3/1 (very dark gray)	7.28	161	27.5	1.86	23.01	21.80	1.21
B6	2.5Y3/1 (very dark gray)	6.80	76	29.7	1.23	17.55	12.01	5.54
B7	2.5Y3/1 (very dark gray)	7.21	87	28.1	1.21	21.00	18.60	2.40
B8	2.5Y3/1 (very dark gray)	7.08	101	29.4	1.29	15.81	13.06	2.75
B9	10YR2/1 (black)	7.05	79	18.3	1.82	22.92	18.40	4.52
B10	10YR2/1 (black)	6.58	114	17.2	4.78	52.69	48.20	4.49
			Berlin, 1 to 5 cm					
B1a	10YR4/6 (dark yellowish brown)	7.12	48	16.1	0.76	5.11	3.80	1.31
B2a	10YR5/6 (yellowish brown)	7.03	21	19.8	0.18	1.78	1.67	0.11
B3a	2.5Y4/3 (olive brown)	7.05	-	24.9	-	4.42	3.08	1.35
B4a	2.5Y5/3 (light olive brown)	7.13	28	-	0.43	2.24	1.69	0.55
			Warsaw, 0 to 1 cm					
W1	2.5Y2.5/1 (black)	-	306	34.2	2.14	29.47	22.84	6.63
W2	2.5Y2.5/1 (black)	6.91	402	26.5	1.89	43.40	35.37	8.03
W3	2.5Y2.5/1 (black)	7.35	328	25.0	3.36	32.30	27.90	4.40
W4	2.5Y3/1 (very dark gray)	7.41	409	45.4	1.69	26.86	20.80	6.06
W5	10YR2/1 (black)	7.29	426	37.6	2.06	35.58	27.93	7.65
W6	2.5Y3/1 (very dark gray)	7.34	440	39.7	1.50	32.32	25.70	6.62
W8	2.5Y3/1 (very dark gray)	7.23	2040	39.2	0.70	18.74	12.40	6.35
W9	2.5Y3/2 (very dark grayish brown)	7.36	1927	36.5	1.20	21.80	15.56	6.24

Figure 1.3: Litter milled by pedestrians to fine pieces fitting the seams of pavements.

The C_{org} contents varied from 12 to 48 g kg^{-1} in the 0 to 1 cm layer and were much lower in the 1 to 5 cm layer (less than 3 g kg^{-1}). The C_{tot} contents varied from 16 to 52 g kg^{-1} and from 0.2 to 3 g kg^{-1}, respectively (Table 1.1). The ten times higher C_{org} contents in the 0 to 1 cm layer compared to the 1 to 5 cm layer can be explained by OM, which is deposited from above and trapped in the upper layer, due to pores clogged by deposited particles. Thereby immobilized and immobilizing particles can be identically. Measurements of particle size distributions delivered an argument for this statement (Chapter 3.3.1). A transport, however, of OM into the 1 to 5 cm layer cannot be excluded, but the low C_{org} contents show the clearly lower impact of depositions on this material, which is assumed to be original and no altered. Besides that, it cannot be excluded, that the construction sand already contained different amounts and forms of OM. Sites were sampled, where the traffic density was known, because it was hypothesized, that C_{org} contents can be explained by traffic density. However, no clear correlation can be found, indicating the higher importance of other sources for the soil organic matter (SOM) formation, e.g. age, situation in the city, trees.

The CEC of the 0 to 1 cm layer in Berlin is not significantly different from CEC in Warsaw. With 0.5 cmol(+) kg^{-1}soil, the CEC of the 1 to 5 cm layer is significantly smaller than in the first layer. Compared to the original seam filling represented by the 1 to 5 cm layer, the depositions of urban dirt lead to an approximately four times higher CEC in the 0 to 1 cm layer. Compared to "natural" soils the CEC of seam materials is rather low, as this will be

discussed more detailed in Chapter 4.3.1 at page 63.

The C/N ratio indicates the character of depositions. The C/N ratios of the material vary from 17 to 45 with an average of 29 in the 0 to 1 cm layer and from 16 to 25 with an average of 20 in the 1 to 5 cm layer. The sites B1 and B9 (B10) for instance are streets with big old Linden trees (*Tilia spec.*) and show the narrowest C/N ratios. The input of foliage into the small seams of pavements is possible because pedestrians play the role of (possibly) absent natural litter decomposers like isopoda and collembola and mill the foliage into small pieces just by walking over it (Figure 1.3).

The Warsaw sites show significantly higher C/N ratios than the Berlin sites, indicating substantial different composition of Warsaw and Berlin urban dust, which might be due to the more industrial character of Warsaw. A second reason could be the choice of sampling sites in Warsaw. There, mainly arterial roads were sampled, because only here traffic data were available. These streets do not have trees along them but were planed as broad open streets in the typical socialistic magistrale-style, where the traffic influence is more pronounced than in residential areas of Berlin. Only one Warsaw site, the Emilii Plater street, has street trees but shows a comparable high C/N of 34. May be, here street cleaning service is working more frequent than in Berlin, thus leaving less leaf litter at the sidewalks.

Chapter 2

Combustion Residues as Seam Material Constituents

2.1 Introduction

If one pokes around in the spaces between single pavestones of old cobblestone pavements, the distinct color difference between the first and the second layer is immediately recognised. The first layer, mostly only one cm thick, is much darker than the layer below. At the site Weidendamm (samples B2 and B2a) a change from yellowish brown to very dark greyish brown was observed during only one year (see Table 1.1). It is hypothesized, that the deposition and incorporation of dark urban dust particles cause these color alterations. Similar is known for natural soils, as the dark color of chernozems is caused by charred residues of natural prairee gras fires (Schmidt et al., 1999). These substances are called "black carbon" (BC). In the following, formation and recent sources of BC are introduced.

The term "black carbon", was defined as "combustion-produced black particulate carbon, having a graphitic microstructure" by Novakov (1984). It summarizes pyrogenic carbon, which is formed as a byproduct of incomplete combustion of biomass or fossil fuels (Goldberg, 1985). Therefore, it includes elemental carbon, char and charcoal but also condensates like soot. Chemical features and analysis of BC have been discussed by Schmidt and Noack (2000). There is a great variety of methods used for investigations of BC, depending on the environmental compartment studied ranging from comparable easy methods involving hydrogenperoxide oxidation of other SOM components to highly sophisticated methods using gaschromatography. Because of the complex structure of BC, a direct analysis is not possible. The discussion of different methods, their advantages and disadvantages is not

content of this study, details on different methodologies can be found in Brodowski (2005).

The annual worldwide formation of BC was estimated to range from 50 to 200×10^{12} g (Kuhlbusch, 1998). Released in such amounts and highly susceptible for wind transport, it is ubiquitous in atmosphere, hydrosphere, and pedosphere (Goldberg, 1985; Kuhlbusch, 1998). In soils, BC represents a stock of stable OM (Skjemstad et al., 1996; Schmidt et al., 1999). Because of its hydrophobic character and the lack of N it is hardly decomposable (González-Pérez et al., 2004). Furthermore, strong adsorption of BC to other soil OM or minerals have been reported to hinder transport and decomposition (Brodowski, 2005). In an other publication, the same author found a accelerated co-metabolic decomposition of BC in a laboratory experiment: the decomposition was supported by the formation of BC-SOM complexes (Hamer et al., 2004). Probably, the decomposition question cannot be solely answered at the molecular scale but only under consideration of other soil properties like the redox regime, the availability of labile forms of OM, and the abundance of surface active substances, which increase microbial availabilty of BC. Furthermore, the soil moisture governs the hydrophobicity of BC enveloping soil components (Taeumer et al., 2005). It is possible, that the amount and distribution of BC might evoke its decomposing specialists. Several findings of charcoal at archaelogical sites and huge amounts of BC substances in soils however support the hypothesis, that BC is hardly decomposable. It is at least much more stable than other forms of SOM. It is still unknown, how much BC is stored in soils at the global scale. However, some impressive examples for high amounts have been reported.

In natural soils have mostly contents of 1 to 6 % (González-Pérez et al., 2004) BC of the total C_{org}. Higher contents are reported from anthropogenic influenced soils. Glaser et al. (1998) reports of amounts of BC in C_{org} of up to 35 % in man made Amazonian Terra Preta soils in Brazil (Glaser et al., 2001). Black carbon makes up to 80 % of C_{org} in brown coal dust contaminated soils near the city Halle/Saale, Germany (Schmidt et al., 1996). Glaser (2005) found up to 7.4 % of the C_{org} to be BC in soils near a federal highway in Bavaria, Germany.

However, BC has never been investigated in partially sealed or urban soils, although high amounts can be expected. However, urban air has already been investigated for BC. Because of the abundance of fossil fuel combustion processes in cities, urban dust contains BC (Köhler et al., 2001; Viidanoja et al., 2002; Zhu et al., 2002). Viidanoja et al. (2002) found 7 % of the PM 10 fraction to be BC in Helsinki, Finland.

A study focussing the input rates of BC into urban soils is still missing. For the Berlin Gründerzeit quarter, in which the site B10 is situated, a

deposition rate of dust of $82\,g\,m^{-2}\,a^{-1}$ was measured in 1991 (Senstadt-Berlin, 2001). Hoeke (2003) found higher dust deposition rates in the Ruhr area of up to $146\,g\,m^{-2}\,a^{-1}$.

Urban areas act as important sources of BC. Distinct industrial point sources are discussed separately from diffuse emissions from traffic or domestic heating based on coal or oil on the regional scale (Miguel et al., 1998; Fernandes et al., 2003; Schmidt et al., 1999). The traffic related BC emissions were quantified to range from $99 \pm 34\,mg\,vehicle^{-1}\,km^{-1}$ ($0.8 \pm 0.3\,mg\,kg^{-1}$ fuel) in 1996 near San Francisco (Miguel et al., 1998) to $1440 \pm 160\,mg\,kg^{-1}$ fuel in Vienna in 2004 (Laschober et al., 2004) or to be $3.7 \times 10^3\,kg\,day^{-1}$ (Dreher and Harley, 1998) in the San Francisco Bay area, USA. The global annual BC emission caused by fossil fuel burning was estimated to be 7 to 24×10^{12} g. At the global scale, traffic was not separated from other fossil fuel consumpting processes (Kuhlbusch, 1998).

Besides the lack of information about BC quantities in urban soils, nothing is known about the functions of BC in partially sealed urban soils. Therefore, the role of BC for artificial OM build up in seam materials and its impact on contaminant retention cannot be assessed. It is known, that BC can act as a sorbent not only for organic but also for inorganic contaminants like heavy metals (Hiller and Bruemmer, 1997). Lehmann et al. (2005) for the first time showed the hypothesized oxidated functional groups at the edges of BC particles, which cause their cation exchange capacity. However, the circumstances and the time-frame of that oxidation in soils remain unclear.

It is the goal of this chapter to quantify the BC content in partially selaed urban soils of Berlin, Paris and Warsaw. It is expected, that the content of BC is higher in seam material than in "natural" soils.

The BC stocks in urban soils should be approximated in order to assess the significance of these soils as sinks.

Traffic is hypothesized to be a major source of BC in partially sealed soils near streets.

It is expected, that BC influences the functionality of seam material, especially towards pore properties (Chapter 3) and heavy metal adsorption (Chapter 4).

2.2 Materials and Methods

2.2.1 Sites and Traffic Data

It was hypothesized, that the BC contents in the seam materials are dependent on the traffic density of adjacent streets. Therefore, places with

different traffic densities have been chosen for sampling. Only some of the samples, introduced in subsection 1.2.1 were analysed for their BC content. The choice was necessary because of limited analysing capacity. Additionally, three samples of a transect of seam materials from the Place Charles de Gaulle (Arc de Triomphe) in Paris were included. This site is one of the most trafficked places in Europe (Table 2.1).

The used traffic density information, comes from automatic measurements and was delivered by the municipalities of Berlin, Warsaw and Paris. Unfortunately, data from different years originating from different counting methods were delivered.

Light duty (LDV) and heavy duty vehicles (HDV) were seperated whenever it was possible, because of different BC formation rates of the two fuel types gasoline and diesel (Miguel et al., 1998). It is assumed, that HDVs use predominantly diesel engines. There was no data available about the portion of diesel engine powered LDVs. So they were negelcted.

In Berlin, the separation criterion for LDV and HDV data of the year 2001 was a tonnage of 7.5 tons ($\times 10^6$ g) (Senstadt-Berlin, 2001). In Warsaw, the traffic density was measured in 2003 and the HDV density was estimated because of a length criterion. Cars longer than 6.5 m were counted as HDV. In Berlin and Warsaw, busses were count as HDV. In Paris, LDV and HDV were not differentiated. Therefore, the average percentage of diesel consumpting vehicle of Berlin and Warsaw, 12 % was assumed for Paris. All traffic data therefore comes with a great portion of uncertainty. The analysis of original data of one day at the site B4 for example revealed a variation coefficient(CV), for the HDV fraction of 50 %. However, the standard error (SE) is only 2.7 %.

As the site B2 is situated near the river Spree, information about the shipping traffic at the river Spree was also needed. The data for the year 2003 were surveyed by the Wasser-und Schiffahrtsamt Berlin and was taken from countings of passing ships at the Berlin sluices. The data contain an uncertainty as some of the tourist boats for instance never pass sluices, but cross from one sluice to the next and return several times per day in the high season.

2.2.2 Chemical Analyses

Black Carbon was analysed according to Glaser et al. (1998) and Brodowski (2005) using benzenepolycarboxylic acids (BPCA) as markers, which are build by oxidation of BC. Aliquots of 0.1 to 0.5 g of the samples, according to their C_{org}, were used. For the removal of polyvalent metal cations, the samples were hydrolysed with 0.01 l of 4 N trifluoroacetic acid (TFA) for

240 min at 378 K. After rinsing with deionised water and drying for 120 min at 313 K the sample material was quantitatively transferred into digestion tubes. Oxidation was achieved with 0.002 l of 65 % nitric acid for 320 min at 443 K under pressure. In this step the complex structure of BC is destroyed, and BPCAs with different substitution levels are the reaction products. After filtering, the fluid phases were filled up to 0.01 l with deionised water. Before purification 0.002 l aliquots were diluted with 0.004 l deionised water and mixed with the internal standard citric acid (1×10^{-4} g). For purification prior to derivatisation, cation exchange resin filled columns were used (Dowex 50 W X 8, 200-400 mesh, Fluka, Steinheim, Germany), which were successively conditioned with 2 N NaOH and 2 N HCl and rinsed with deionised water until the eluate was neutral. The BPCAs were applied to the columns and eluated five times with 0.01 l deionised water into conical flasks. After freeze drying and transferring the samples into reactivials with methanol, 1×10^{-4} g of 2,2'-dicarboxylic acid were added as a second internal standard. After drying in air stream BPCA - trimethylsilyl derivates were produced by derivatisation with 1.25×10^{-7} l of dry pyridine and 1.25×10^{-7} l of N,O -bis(trimethylsilyl)-trifluoroacetamide for 120 min at 353 K. Before measurement, the samples were stored for at least one day in order to ensure complete derivatisation. For measurements the differently susbtituted BPCAs, trimellitic acid, trimesic acid, pyromellitic acid, B5CA and mellitic acid were used as external standards. The BPCAs were quantified using a Hewlett Packard 6890 gas chromatograph (Hewlett Packard GmbH, Waldbronn, Germany) with a HP-5 capillary column ($30\,\mathrm{m}\times 3.2\times 10^{-4}$ m i.d., 2.5×10^{-7} m film). For detection a flame ionisation detector (FID) was used. The temparature programm consisted of the following steps: 373 K for 2 min, rising to 513 K at 20 K min^{-1}, keeping 513 K for 7 min, rising to 573 K at 30 K min^{-1}, keeping 573 K for 10 min. Injection and detection temperature were both 573 K, the split ratio was 50:1 and the carrier gas flux was 7.93×10^{-2} l min^{-1}. The injected sample volume was 2×10^{-6} l.

For the calculation of BPCA-contents, the retention factors were estimated using external standard calibration data. For the calculation of BC contens from BPCA contents a conversion factor must be applied which represents the formation rate of BPCAs from BC parent material. This is the very weak point of this analysis method, because this conversion factor cannot be determined but only be estimated. However, the widely accepted conversion factor of 2.71 was applied (Brodowski, 2005).

2.3 Results and Discussion

2.3.1 BC in the Seam Material

The BC contents in the seam material show an average of $3.4\,\mathrm{g\,kg^{-1}}$ (SE= $0.3\,\mathrm{g\,kg^{-1}}$) (Table 2.1). The BC contents from the three cities are not significantly different ($p<0.05$, N=16). Black Carbon makes 17 % (SE=4 %) of the C_{org} in seam materials. The ratios are not significantly different for the three cities, which is an effect of the great variety of values, especially a great heterogeneity among the cities. The ratios are a bit different for the site B2 and B2a. The deposits from ship traffic lead to a higher ratio.

In the construction material (1 to 5 cm), the average BC content is rapidly and significantly dropping to $0.5\,\mathrm{g\,kg^{-1}}$ (SE=$0.1\,\mathrm{g\,kg^{-1}}$; $p<0.05$, N=8). The ratio BC/C_{org} is 0.15 in the construction material (SE=0.02) and is not significantly different from the seam material. The BC amounts decrease with increasing depth, but the amounts of BC of C_{org} are not different for both depths. This shows, that BC has been incorporated from above after construction of the pavements. Assuming, that the original construction sand did not contain BC, the result shows also, that conventional C_{org} is transported and displaced together with BC. An accumulation or depletion of BC cannot be detected by comparing the two investigated layers. However, the data base is not broad enough to verify these statements, so they remain at the status of an educated hypothesis.

Compared to available data on BC contents in arable land, the seam material shows higher contents of BC. Brodowski (2005) reports BC contents of 0.7 to $2.9\,\mathrm{g\,kg^{-1}}$ for the upper 10 cm layer of agricultural sites in Halle/Saale, Bad Lauchstätt and Rotthalmünster, Germany. There, BC makes 2.6 to 13 % of C_{org}. Thereby, the most anthropogenic influenced site Halle/Saale shows the highest BC content, while Rotthalmünster, situated in the Alps, far away from industrial sites, federal highways, and railways shows the lowest absolute BC content, and with only 2.6 % also the smallest contribution of BC to C_{org}. With 17 % the BC of seam material also contributes substantially to the C_{org} stock in the first layer of partially sealed urban soils. Brodowski (2005) found railway traffic and browncoal industries beeing responsible for the found BC contents in Halle/Saale. The sources of BC in seam materials are discussed in the following subsection.

2.3.2 Traffic as a Source of BC in Paved Urban Soils

It was hypothesized, that traffic is the predominantly source for BC of seam material. However, there is no correlation of the seam material´s BC concen-

Table 2.1: Location of sampling sites, sampling depths, traffic densities for all vehicles, light duty vehicles (LDV), heavy duty vehicles (HDV) and total, organic and black carbon contents from samples of seam material of paved urban soils in Berlin, Warsaw and Paris. BC contents labeled with the same letter are not significantly different ($p<0.05$).

Sample	Location, Depth	Traffic	LDV d^{-1}	HDV	C_{tot}	C_{org} $g\,kg^{-1}$	BC	BC/C_{org} %
			Berlin, 0 to 1 cm					
B1	Monbijouplatz	9983	9562	421	19.2	14.3	1.2 a	8
B2	Weidendamm		shiptraffic		18.7	16.2	4.5 a	28
B3	Schnellerstrasse	35030	33019	2011	33.4	27.6	2.4 a	9
B4	Grosser Stern	79806	59471	20335	25.5	23.2	2.5 a	11
B9	Pflügerstrasse, street	648	519	117	22.9	18.4	2.3 a	12
B10	Pflügerstrasse, edge	648	519	117	52.7	48.2	3.7 a	8
			Berlin, 1 to 5 cm					
B1a	Monbijouplatz	9983	9562	421	5.1	3.8	0.6 b	7
B2a	Weidendamm		shiptraffic		1.8	1.7	0.3 b	20
B3a	Schnellerstrasse	35030	33019	2011	4.4	3.1	0.4 b	12
B4a	Grosser Stern	79806	59471	20335	2.2	1.7	0.6 b	9
			Warsaw, 0 to 1 cm					
W1	Emilii Plater	30148	25324	5427	29.5	22.8	3.5 a	15
W2	Jerozolimskie	69011	57969	11042	43.4	35.4	4.4 a	12
W3	Pulawska	68068	59900	8168	32.3	27.9	3.9 a	14
W4	Rzymowskiego	54754	51140	3614	26.9	20.9	4.2 a	20
W5	Stanow Zjednoczonych	133073	117237	15836	35.6	27.9	5.1 a	18
W6	Modlinska	33435	29423	4012	32.3	35.7	4.5 a	17
W8	Wilanomska	33928	31553	2375	18.7	12.4	2.3 a	19
W9	Grota Roweckiego	145965	90498	55466	21.8	15.6	2.0 a	13
			Paris, 0 to 1 cm					
P1	Arc de Triomphe, 0 m[(a)]	216734	189766	26968[(b)]	99.3	72.5	5.8 a	8
P2	Arc de Triomphe, 2 m	216734	189766	26968	64.4	26.6	2.3 a	9
P3	Arc de Triomphe, 4 m	216734	189766	26968	48.0	19.8	1.6 a	8

[(a)] distance from traffic lane

[(b)] calculated from average HDV portion in Berlin and Warsaw

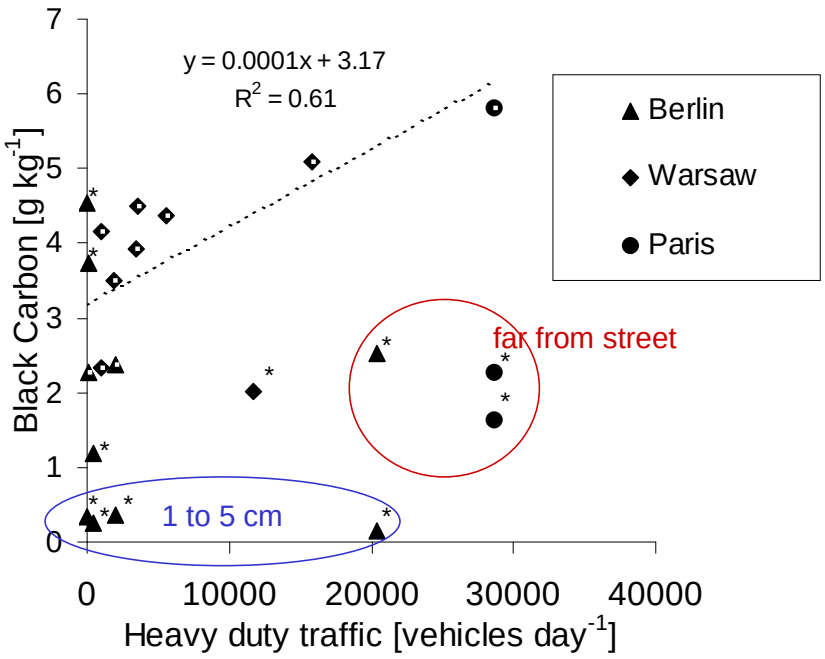

Figure 2.1: Relation between BC content in seam materials of partially paved urban soils and traffic densities at different sites in Berlin, Paris and Warsaw. Sites marked by an asterisk were excluded from the regression.

trations with the total traffic density, including all kinds of cars. If only the heavy duty vehicles, like trucks, small lorries, busses, and vans are counted, a weak relationship between traffic and BC contents occurs (R^2=0.6, N=10, Figure 2.1). This can be explained by the predominantly use of diesel engines and the corresponding diesel dust emissions. However, the outliers B2, B4, W9 had to be excluded from the dataset.

The site B2 was not considered, because this small street is almost not used by lorries. Nevertheless, the site shows a comparative high amount of BC. The site is situated at the bank of the river Spree in the historical centre of Berlin and is strongly influenced by around 15700 diesel powered sightseeing tour boats and barges per year. Using the regression between BC and traffic from figure 2.1, keeping in mind all the uncertainties, this equals the emissions of around 13000 HDV per day. From this point of view, it´s time to revise the emission guidelines for diesel powered ships at least in urban areas.

At site B4 the sampled area may not have been influenced by spray from the driving lane, like at all other sites. For the three samples from the site in Paris, a distinct decrease of BC with increasing distance from the

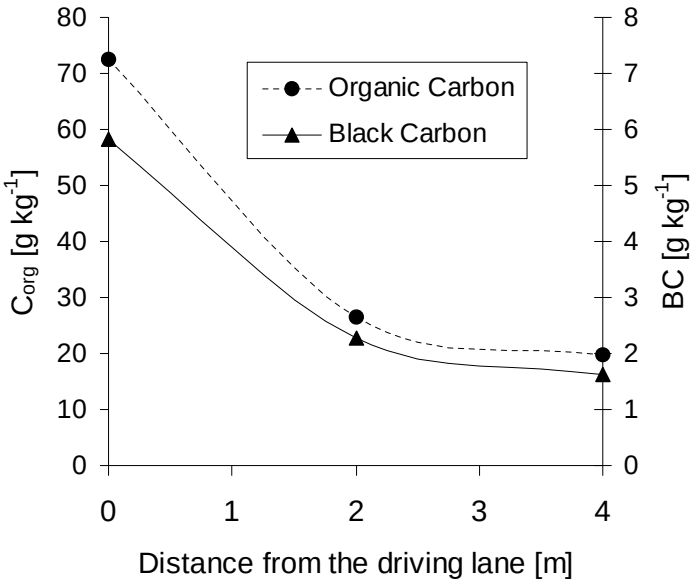

Figure 2.2: BC and C_{org} amounts on a transect at a sidewalk at the site Place Charles de Gaulle in Paris (Arc de Triomphe), France.

driving lane could be found (Figure 2.2). As it can be seen directly from the figure, the ratios of BC and C_{org} are very similar. The BC contents decrease rapidly with increasing distance from the driving lane. Glaser (2005) found the same dependency for BC and other traffic derived contaminants near a federal highway in Bavarian arable soils. Because of that findings, only the sample nearest to the driving lane was considered, if more than one sample was taken at a certain site.

The site W9 was not considered for the regression between traffic density and BC, because samples were taken at a crossing of two mayor highways under a bridge. Afterwards, it must be stated that the site was not very well chosen. The micrometeorologic conditions under a bridge are completely different to those at an open street. BC and other depositions may be dispersed by the traffic again and again. Furthermore, the pavers were partially fixed by concrete. So the incorporation of dust into sandy material like observed at all other sites is not possible.

The weak corellation of BC and traffic data can be explained by (i) stochastic effects, (ii) systematic uncertainty and (iii) lack of causal relations. The systematic uncertainties account for the majority of uncertainty. In the three cities, three different traffic counting systems are applied. The seperation of HDV and LDV is made by different criterions. For example in figure 2.1 the Warsaw samples are situated in the left part of the scatterplot.

As the HDVs are detected by their length, diesel powered, but small cars are not counted. This may underestimate the HDV fraction in Warsaw.

Another example: the sites W4 and W6 are situated near traffic lights. Incomplete combustion while acceleration is more pronounced than for uniform driving. Furthermore, also breaking for red light emits BC because of tire abrasions. Although only about 3500 to 4000 lorries per day pass the sites, very high BC contents are found. This shows, that the relation between traffic density and BC formation may not constant.

The next uncertainty is connected to the deposition of BC and the incorporation into the seam material. While the traffic data gives an educated overview for one year, the BC content is an integrating parameter for a certain timespan. This timespan varies from site to site. So the BC content represents not only the BC formation and deposition at a certain site but also the deposition history including every cigarette stump but also every construction activity, cleaning or erosion event.

Furthermore, there are other sources of BC too in urban areas. One source is at least traffic related. The tire abrasions also contribute to BC contents. Tires contain the so called "Carbon Black". This is soot, which is industrial produced in different quality for different tires and parts of tires. Of course not only HDV contribute to tire abrasions.

The site B10 shows comparable high BC contents. Here, I sampled directly in the street near the sidewalk, where rainwater runoff accumulates. This may lead to higher concentrations compared to samples coming from sidewalks. The site shows only a low traffic density, but is situated inside an old, densely populated housing area. Until modernisation in the 1970ies and 1980ies, individual heating based on coal was predominant and can still be found. This might have contributed to BC contents because of burning residues in the dust outfall. Additionally, there were accumulations of unburned coal dust from the coal delivery. The coal was put at the streets and sidewalks from where it was carried to basements or flats. All forms of coal contain BC (Schmidt et al., 1996).

Considering these uncertainties, the found correlation between the BC contents and the current HDV traffic density is quite good. However, the hypothesis, that traffic is the major source of BC in paved urban soils could not be verified. It is at least one important source of BC. In consideration of the problems described above I want to discuss two reasons for the quite good correlation: (i) The storing capacity for BC in the seam material is limited. It can only be stored in correspondingly sized pores of the original sandy seam filling material. From own observations (Chapter 3 at page 45) it is known, that this cumulative storage volume, expressed by the maximum travelling depth of particulate depositions is, depending on the grain size and

compaction of the construction material, limited to only some 1 to 2 cm. A further input might be impeded by already clogged pores. So an equilibrium between erosion of seam sealing material, caused by wind, surface runoff, traffic, and pedestrians, and the accumulation of deposits including BC is reached. The BC concentrations thereby are governed by the amount of BC in the deposited material and therefore, by the traffic density. (ii) Although the current traffic intensity data is not the same as in past years, the relation of traffic densities from one street to another stays constant for different streets. No matter what the source is, it was shown, that the seam material stores a great amount of BC. How great this amount is, is approximated in the following.

2.3.3 Approximation of BC Stocks in Partially Sealed Urban Soils

The role of urban soils as sinks for BC has not been evaluated or discussed so far, although the found BC contents in seam materials are comparable high, which could have been expected before. This leads to the question of the significance of urban areas for the global carbon sequestration.

Only a very small number of samples has been analysed, however, the goal of this subsection is to roughly approximate, how much BC is stored in roadside partially sealed urban soils worldwide. Thereby, the order of magnitude is more interesting than a accurat estimation. First, an approximation is made for Berlin soils. Then, the results of the study are extrapolated to the global scale.

In Berlin

Stored BC in Berlin is approximated based on the above introduced concentrations for the 0 to 1 cm and 1 to 5 cm layers of seam fillings (Table 2.1), and some educated assumptions about the partially sealed soils in Berlin. Three general approximations and two case studies have been calculated (Table 2.2).

The cumulative length of all streets in Berlin is 4.69×10^6 m $\approx$ 5000 km (Senstadt-Berlin, 2001). It is not known, how great the portion of partially sealed streets is. Therefore, these streets are not considered in the general approximations but in the case study for the site B10. The average width of the sidewalks is assumed to be 3 m. Of course there are some streets having broader or smaller sidewalks. It is assumed, that the majority of streets has two sidewalks. Together with the assumed sidewalk width, this is a clear

defined model. Right now, there is no information about the cumulative sidewalk length or width available for Berlin.

There are different pavement geometries with seam portions varying from 10 % (artificial stone piles) to 47 % ≈ 50 % (Bernburg Mosaic). Both seam portions as much as an average value have been employed for the approximations. Together with the seam material depth of 5 cm, a well defined soil volume was considered. The soil under the pavers and in greater soil depths was disregarded.

The mass of BC stored in seam material, m_{BC} $[g]$ was calculated using the following equations:

$$m_{BC} \;=\; l_{street}\, w_{sidewalk}\, p_{seam}\, z\, \rho_B\, c_{BC}, \tag{2.1}$$

where l_{street} $[m]$ is the cumulative length of all streets (approximations in table 2.2) respectively a chosen section of a street (case studies in table 2.2), $w_{sidewalk}$ $[m]$ is the width of the sidewalk, p_{seam} is the seam portion, z $[m]$ is the layer depth, ρ_B $[kg\,m^3]$ is the bulk density and c_{BC} $[g\,kg]$ is the BC content. The storage capacity, t_S $[a]$ can be calculated from the stored mass of BC, m_{BC}, the car specific formation rate of BC, r_{BC} $[g\,km^{-1}\,car^{-1}]$ and the amount of driven kilometers by cars per day l_d $[km\,car\,d^{-1}]$ like follows:

$$t_S = \frac{m_{BC}}{r_{BC} l_d} \tag{2.2}$$

The approximation shows the importance of roadside soils as sinks for traffic derived particulate carbon. At the site B10, the stored BC equals the emissions from cars for around 40 years!

However, the storage capacity of seam materials, is limited. Another approximation represents the function of seam material as a sink: The deposition of dust is made responsible for the formation of the seam material. Because of its ability to withstand decomposition, BC can be used as a marker for the dust accumulation history in seam materials. In 1991, the measured dust outfall (Bergerhoff technique) in the Nansenstrasse near the Site B10 was 25 g m^2 a^{-1} (Senstadt-Berlin, 2001). In the timespan 1935-1945, the dust outfall (no information about technique) has been 139 g m^2 a^{-1} (Hoeke, 2003). It is assumed, that direct World War II activity was not considered. In the last 60 years, the air pollution in Berlin drastically decreased as the overall industrial activity collapsed after 1945. It is assumed, that the dust deposition rate after 1945 was nearly the same as measured in 1991. If the dust, which has fallen only directly on the seams (seam portion 33 %) would have accumulated for 60 years and would have been compacted to a bulk density of 1.16 g cm^{-3}, this would have led only to a layer of 3.5×10^{-4}m in the pavement seams. In 60 years a BC amount of around 100 g m^{-2} would have been

Table 2.2: Approximation of BC stored in Berlin seam materials. Own measured data is compared to formation rates of BC by traffic.

Depth	street length[(a)]	sidewalk width	seam ratio	ρ_B	BC	deposited BC	emitted BC[(b)]	total driven way[(c)]	storage capacity
cm	km	m	%	$kg\,m^3$	$g\,kg^{-1}$	g	$g\,car^{-1}\,km^{-1}$	$car\,km\,d^{-1}$	a
average approximation: average seam percentage,average BC content									
0-1	5000	3	0.3	1490	2.7	3.7×10^8			
1-5	5000	3	0.3	1610	0.3	1.6×10^8			
					sum	$\mathbf{5.2\times 10^8}$	0.028	2.9×10^7	**1.8**
minimum approximation: minimum seam percentage, minimum BC content									
0-1	5000	3	0.1	1490	1.2	5.3×10^7			
1-5	5000	3	0.1	1610	0.3	5.8×10^7			
					sum	$\mathbf{1.1\times 10^8}$	0.028	2.9×10^7	**0.4**
maximum approximation: maximum seam percentage, maximum BC content									
0-1	5000	3	0.5	1490	4.5	1.0×10^9			
1-5	5000	3	0.5	1610	0.6	5.8×10^8			
					sum	$\mathbf{1.6\times 10^9}$	0.028	2.9×10^7	**5.4**
case site B10: cobble stone paved street with sidewalk									
0-1	1	6	0.3	1490	3.7	1.0×10^5			
1-5	1	6	0.3	1610	0.4	4.6×10^4			
0-1	1	5	0.4	1490	2.3	7.2×10^4			
1-5	1	5	0.4	1610	0.4	5.4×10^4			
					sum	$\mathbf{2.7\times 10^5}$	0.028	648	**41.2**
case site B3, tar paved street with sidewalk									
0-1	1	6	0.4	1490	2.4	9.0×10^4			
1-5	1	6	0.4	1610	0.4	6.5×10^4			
					sum	$\mathbf{1.6\times 10^5}$	0.028	35030	**0.4**

[(a)] Statistisches Landesamt Berlin
[(b)] Laschober et al. (2004)
[(c)] Senstadt-Berlin (2001)

accumulated assuming a BC content of 7 %, in the dust (Viidanoja et al., 2002). This would have resulted in a BC content of around $9\,\mathrm{g\,kg^{-1}}$ in the first cm of the seam material. Compared to the measured BC amount of $3.7\,\mathrm{g\,kg^{-1}}$ at B10 this value seems reasonable. It shows also, that the pavement seams can not store all dust deriving from the whole pavement. In this case a BC content of $29\,\mathrm{g\,kg^{-1}}$ would have been expected.

Together with clogging of pores and a hindered transport of BC due to binding to other SOM and minerals (Brodowski, 2005), the small amount of dust accumulated in the seams can explain, that the characteristic dark color of seam materials is limited to the first centimeter. Furthermore, the particles are physically hindered from transport. If a certain amount of particles is stored, a further incorporation is prohibited by clogged pores 3.

However, it is more likely that great portions of the accumulated dust are washed away from the pavements by surface runoff. That means, the storage capacity of urban soils can only be increased by opening of soils, if possible near roads. Together with overgrown open soils, where particles can be immobilised, particulate emissions, refered to as fine dust, PM 10, or PM 2.5 in several discussions could be sustainably decreased. For the reduction of the fine dust load it is important to immobilise particles which already had deposited. The redispersal of fine dust, especially near streets by traffic-induced turbulences seriously contributes to the high dust concentration in urban air. Precipations can wash out the particles from the air. If rainwater runoff, which contains several dust amounts, eventually collected from great sealed surfaces, can finally infiltrate, particles can be incorporated into soils and immobilised. This, apart from groundwater recharge arguments is an positive effect of reopening sealed soils in urban areas and should be regarded in the discussion about de-selaing. The relevance of paved soils for carbon sequestration on a global scale is assessed in the following.

Worldwide

The BC pool stored in partially sealed soils of urban areas on the global scale is approximated by using BC data from all the investigated sites in Berlin, Paris and Warsaw. The calculation contains two combined minimum-maximum approximations. Like for Berlin, the minimum and maximum seam portions are considered and the minimum and maximum BC contents were used for the first two layers down to 5 cm. The cumulative amounts of BC stored in raodside soils were calculated to area-based values ranging from $7.4\times 10^{6}\mathrm{g\,km^{-2}}$ to $1.0\times 10^{8}\mathrm{g\,km^{-2}}$ using the following equation:

$$BC_{global} = A_{global}\, ap_{traffic}\, p_{seam}\, z\, \rho_B\, c_{BC} \tag{2.3}$$

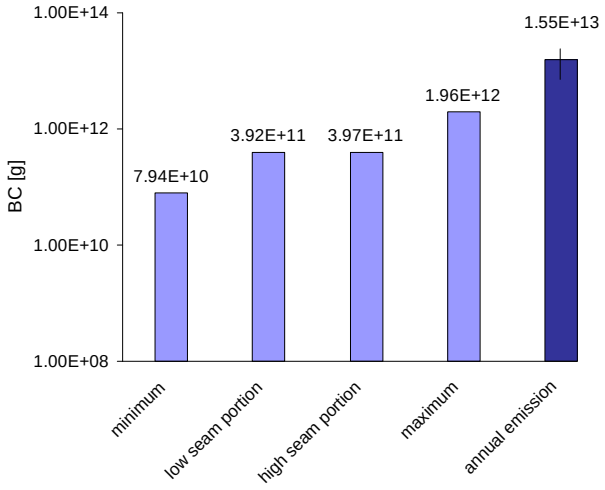

Figure 2.3: Approximation of Black Carbon (BC) stored in the first 5 cm of partially sealed urban soils worldwide. The minimum approximation combined minimum seam percentage and BC contents, the maximum approximation combined maximum seam percentage and maximum BC contents. The two intermediate approximations show the impact of both seam percentage and BC content on the result of the approximation. The most right column shows the annual global BC emission due to fossil fuel burning (Kuhlbusch, 1998).

The cumulative global urban area, A_{global} $[km^2]$ was achieved from the international "Global Land Cover 2000 Project" (ECJRC, 2003). The cartographical projection of the provided global landcover map has been transformed to the area-accurate Behrmann projection. The global urban area has been quantified to 280412 km^2 using a geo information system. Like derived from information about Berlin, Köln, Hamburg and Frankfurt, p_{seam}=16 % (Senstadt-Berlin, 2001) of this area is used for traffic purposes: 44866 km^2. This area is assumed to be similar to the areas, where the Berlin, Warsaw and Paris samples derived from. Therefore, the global urban traffic purpose area was multiplied by the area based BC storages to get the approximation for the global urban BC pool. A minimum of 8×10^{10} g up to a maximum of 2×10^{12} g BC are stored in the first 5 cm of traffic purpose urban areas worldwide (Figure 2.3).

Of course such an approximation contains large uncertainties. The data base would not have been good even for Berlin or Europe, but was used for the whole world. It can be improved by investigating soil samples from the most important urban agglomerations worldwide.

All the assumptions about traffic areas, seam portions etc. are full of uncertainties. The Global Land Cover 2000 database for instance has a

spatial resolution of 1 km^2. Therefore, smaller urban areas are not considered. This is rather an advantage than a disadvantage in this case. Smaller cities are not considered.

Obviously, the circumstances are different in Berlin, Los Angelos, Delhi, Hong Kong or Lima. The portion of urban area used for traffic is higher in the New World of northern America than in old Europe. Urban sprawl is a much more serious problem in the USA than in Hongkong. Different traffic densities, different amounts of areas used for traffic, different portions of partially sealed soils and different amounts of open soil surfaces have not been considered.

The storage capacity can be much higher if it is considered, that several cities have soils of up to some meters depth, containing layers rich in BC. In Berlin for instance, such layers can be found, where bombs caused fires in the World War II. However, no park, no housing area, no garden, no urban forest has been investigated. Only partially sealed urban soils have been focussed in this study. It is clear however, that soils of all the other compartments of a city contain BC in different amounts too. So there is a uncertainty concerning the soil layer depth and the horizontal dimension of the approximated soil area.

However, a better approximation does not exist and has not been the primary goal of this study. Keeping all these difficulties in mind, it is clear, that this approximation is only a guess. It is rather the starting point for a more detailed study, a question, than an result. From the numbers shown in Figure 2.3 one can learn however, that the BC storage capacity of partially sealed urban soils´ first 5 cm is up to 10 % of the global annual emission caused by fossil fuel burning. This number in turn has it´s own uncertainty. At least, the stored amount in only 5 cm is high enough to show the relevance of urban soils as sinks in global carbon sequestration models.

2.4 Conclusions

The BC contents of different partially sealed urban sites in three European cities have been investigated. Values of up to 5.8 $g\,kg^{-1}$ have been found resulting in BC percentages of up to 20 % of the C_{org}. Therefore, the values are higher compared to "natural" soils, which can be explained by the vicinity of sources like traffic. Partially sealed urban soils can contribute to the immobilisation of BC.

The amount of BC stored in urban soils worldwide can be expected to be up to 10 % of the annual formation rate caused by fossil fuel burning. Therefore, the ignoration of urban soils in global carbon circles and in the

international carbon sequestration discussion is not acceptable.

From a more practice oriented point of view, the importance of open spaces, possibly overgrown, for the immobilisation of dust have been shown. This argument should be considered when discussing de-sealing measures in urban areas.

The annual BC input rate at the site B10 has been approximated to be $0.15\,\mathrm{g\,kg^{-1}\,a^{-1}}$. However, an experimental verification is needed. Given the shown relevance of BC as an seam material constituent, it is interesting to study the adsorption characteristics of seam material which are influenced by BC. This is done in chapter 4.

Chapter 3

The Pore-System of the Seam Material

3.1 Introduction

The seam material as the first layer of the seam filling, may influence all exchange processes including the water behavior in the pavement system. Although some physical characteristics and infiltration capacities of different pavements have already been investigated (Wessolek and Facklam, 1997), characteristics of the pore system of seam materials have not been studied yet. Thus, a lack of material properties hinders the simulation of water fluxes in the pavement system. These parameters can not be derived from known soils because of the different genesis and unknown soil constituents, as Wenikajtys and Burghardt (2002) showed.

The objective of this part of the study is to investigate the pore system of the seam materials and to obtain data that is needed for the simulation of water flow in partially sealed soils. Therefore, some general characteristics including particle size distribution, water retention function and saturated hydraulic conductivity were studied. Furthermore the pore system is described in terms of total porosities, average pore sizes, pore-size distribution functions (PSD) and fractal dimensions. With these measurements, it is possible to describe the impact of the various accumulations on ecological functions of the seam material. It is also possible to describe the accumulations itself e.g. in terms of its grain-size distribution.

3.2 Material and Methods

3.2.1 Porosity Measurements

The grain size distribution was determined according to DIN-ISO 11277 (Deutsches Institut für Normung, 2002). It is difficult to characterise the PSD over a wide range of pore sizes with a single method. The interesting range for exchange processes spans from 10^{-9} to 10^{-3}m. Therefore, a combination of different methods is appropriate and was employed (Roquerol et al., 1994). Water vapor desorption, mercury intrusion porosimetry (MIP) and soil water retention functions were combined. The pore size ranges measured by these techniques overlap. However, the nomenclature of pores in this study is linked to the individual method.

Water-vapor desorption isotherms were used to study pores ranging from about 10^{-9} to 10^{-7} m, which are named micro pores in the following. Water-vapor sorption is the most appropriate method to simulate natural conditions. In contrast to N_2 adsorbate (Brunauer et al., 1938), the dipole character of H_2O allows to address the hydrophilic and hydrophobic character of the seam material. The samples were placed as 2×10^{-3} m thick layers in weighing vessels and closed in vacuum chambers at the temperature T = 294±0.1 K, where the relative water-vapor pressure (p/p_0) was controlled by sulfuric acid solutions of stepwise increasing concentrations. The amount of adsorbed water, (a), at given p/p_0 was measured after 48 h of equilibration by weighing the samples three times. The dry masses of the samples (dried 24 h at 378 K) were determined after completing the isotherm measurements. Results of triple weightings always had a coefficient of variation (CV) of less than 2 %.

Mercury intrusion porosimetry measurements were used to study pores ranging from about 10^{-7} to 10^{-5} m (named meso pores) using a porosimeter (Model "2000", Carlo Erba Instruments, Milano, Italy). Prior to the measurements, the samples were dried overnight at 378 K and degassed in vacuum at lab temperature. The volume of mercury intruded in the sample vs. the intrusion pressure, was registered. Triple measurements had a $CV < 4$ %.

Water-retention functions were used to characterize pores with diameters from 10^{-6} to 3×10^{-3} m (named macro pores). Small 3.3 cm^3 metal cylinders were filled with homogenized seam material in the laboratory. The material then was wetted and dried eight times in order to stabilize the structure. For measurements at high matric potentials the suction plate method was applied. Water contents at low matric potentials were measured using the pressure-chamber method (Kutilek and Nielsen, 1994). The matric potential is expressed by the pF value, the decadic logarithm of the pressure head.

Figure 3.1: Undisturbed sampling of seam material. Small 3.3 cm^3 cylinders taken from the intersection of cobble stone pavement seams at the site Pflügerstrasse, Berlin.

The dependencies were expressed on the dry mass basis. The dry masses of the samples (24 h, 378 K) were determined after completing the experiment. The water-retention measurements were conducted in four replicates ($CV < 10\,\%$). The measurements required a good contact between the ceramic plates and the samples. However, while de-watering, some samples showed a pronounced shrinking and the contact was lost. Thus, a measurement was not possible. Additionally, 18 (0 to 1 cm) respectively 10 (1 to 5 cm) different samples of site B10 (named B10* respectively B10*a) were measured. The samples were taken from positions evenly distributed across the street and taken undisturbed at intersections of pavement seams, where the small $3.3{\times}10^{-2}\,m^3$ cylinders fitted (Figure 3.1).

The samples were measured in order to estimate the spatial variance of the water retention characteristics and to compare undisturbed versus disturbed sampling. Average values and standard errors of the measurements are presented in table 3.1.

The Mualem - van Genuchten model:

$$S_e = (1 + \alpha\,|\Psi|^n)^m \tag{3.1}$$

with

$$S_e = \frac{\Theta - \Theta_r}{\Theta_s - \Theta_r} \tag{3.2}$$

has been fitted to the experimental data. Mualem-van Genuchten parameters n ($m = 1 - \frac{1}{n}$), Θ_r, Θ_s and α were gained using the software RETC 6.0 (U.S. Salinity Laboratory USDA-ARS, 1991, Riverside, CA, USA; see also: vanGenuchten et al. (1991)).

Particle density (ρ_P) was estimated using helium pycnometry. Dry bulk density (ρ_B) was measured by weighing the mass of the given volume of the homogenized sample after water retention function measurements.

Table 3.1: Measured water retention functions of seam materials of paved urban sites of Berlin and Warsaw and fitted Mualem-van Genuchten parameters ($m = 1 - 1/n$); values for B10* (B10*a) are arithmetic means. Values in brackets are standard errors N=18(10), awc = available water capacity ($\Theta_{pF1.8}$ - $\Theta_{pF4.2}$).

	measured parameters								fitted parameters				
Site	$\Theta_{pF=0}$	$\Theta_{pF=1.5}$	$\Theta_{pF=1.8}$	$\Theta_{pF=2}$	$\Theta_{pF=2.5}$	$\Theta_{pF=3}$	$\Theta_{pF=4.2}$	awc	Θ_r	Θ_s	α	n	R^2
	$m^3\,m^{-3}$								$m^3\,m^{-3}$		cm^{-1}		
Berlin, 0 to 1 cm													
B2	0.41	0.39	0.33	0.30	0.17	0.09	0.07	0.26	0.058	0.413	0.013	1.857	0.998
B4	0.40	0.39	0.36	0.33	0.13	0.09	0.06	0.30	0.069	0.396	0.008	2.729	0.998
B5	0.43	0.41	0.34	0.33	0.12	0.08	0.07	0.26	0.069	0.418	0.009	2.562	0.987
B6	0.40	0.37	0.23	0.20	0.08	0.05	0.04	0.19	0.040	0.404	0.020	2.169	0.988
B7	0.37	0.36	0.32	0.28	0.15	0.08	0.06	0.26	0.053	0.366	0.009	2.037	0.999
B8	0.39	0.37	0.32	0.30	0.11	0.08	0.07	0.25	0.069	0.375	0.009	2.660	0.992
B10	0.54	0.42	0.30	0.23	0.19	0.12	0.09	0.21	0.092	0.547	0.039	1.744	0.989
B10*	0.52	0.44	0.37	0.31	0.24	0.20	0.13	0.24	0.117	0.527	0.034	1.514	0.995
	(0.03)	(0.02)	(0.01)	(0.01)	(0.01)	(0.01)	(0.01)	(0.01)					
Berlin, 1 to 5 cm													
B2a	0.37	0.27	0.20	0.13	0.05	0.04	0.02	0.18	0.022	0.373	0.285	2.009	0.996
B4a	0.41	0.27	0.21	0.11	0.04	0.03	0.02	0.19	0.016	0.404	0.033	2.028	0.989
B10a*	0.42	0.33	0.26	0.22	0.17	0.14	0.07	0.19	0.058	0.424	0.058	1.408	0.992
	(0.02)	(0.02)	(0.02)	(0.02)	(0.01)	(0.01)	(0.01)	(0.01)					
Warsaw, 0 to 1 cm													
W1	0.42	0.38	0.36	0.33	0.31	0.20	0.17	0.19	0.129	0.410	0.016	1.367	0.964
W2	0.44	0.39	0.38	0.34	0.25	0.16	0.10	0.28	0.078	0.430	0.011	1.576	0.994
W6	0.40	0.39	0.38	0.36	0.26	0.13	0.11	0.27	0.103	0.390	0.004	2.575	0.995
W9	0.36	0.35	0.30	0.26	0.16	0.15	0.13	0.17	0.134	0.363	0.013	2.449	0.998

3.2.2 Calculation of Pore Parameters

Micro pore radius (r_{mic}) was related to p/p_0 during desorption process by the Kelvin equation (Hillel, 1998):

$$r_{mic} = \frac{2M\sigma cos\gamma}{\rho_L RTln(p_0/p)} \quad , \tag{3.3}$$

where M is the molecular mass of water, σ is the liquid surface tension, γ is the liquid-solid contact angle (assumed to be zero), ρ_L is the density of the liquid adsorbate, R is the universal gas constant and T is the temperature. The meso pore radius (r_{mes}) is related to the mercury intrusion pressure (p), by the Washburn equation (Washburn, 1921):

$$r_{mes} = -2\sigma cos\gamma p \quad , \tag{3.4}$$

where the mercury - solid contact angle γ was taken as 141.3° for all samples.

Macro pore radius (r_{mac}) was related to water-pressure head (h) by the equation (Kutilek and Nielsen, 1994):

$$r_{mac} = \frac{2\sigma cos\gamma}{gh(\rho_L - \rho_A)} \quad , \tag{3.5}$$

where g is the acceleration due to gravity, ρ_L is the density of the liquid (water) and ρ_A is the density of the air.

In all studied pore ranges, the volume of liquids filling the samples at the given pressures was taken as the cumulative volume $V_{mic,mes,mac}$ of pores associated with a given (pressure-related) radius: $r_{mic,mes,mac}$. The amount of (adsorbed) water was estimated in desorption experiments (V_{mic}), amount of intruded mercury in MIP experiments (V_{mes}) and the amount of retained water at a given pF step (V_{mac}).

After estimation the pore volume V vs. radius r dependence in the above described way, fractions of pores in the given range of radii $f(r_{ave,i})$, were calculated as:

$$f(r_{ave,i}) = \frac{V(r_{i+1}) - V(r_i)}{V_t} \quad , \tag{3.6}$$

where $r_{ave,i}$ is the arithmetic average of two subsequent, pressure-related (experimentally adjusted) radii r_i and r_{i+1} and V_t is the total pore volume e.g. maximum amount of the liquid present in the sample in a given measurement ($V_t = V_{mac}$ or $V_t = V_{mes}$ or $V_t = V_{mic}$, depending on the pore size range).

The average pore radius (r_{ave}) of the individual pore size range was obtained from:

$$r_{ave} = \frac{1}{2}\sum_{i=1}^{n} f(r_{ave,i})(r_i + r_{i+1}). \tag{3.7}$$

For the micro pore calculations it was assumed that the liquid condensation in micro pores occurs above $p/p_0 = 0.35$ (below this value, surface adsorption processes dominate). Thus, the total micro pore volume (V_{mic}) was taken as the volume of the adsorbate at the maximum p/p_0 value minus the volume of the adsorbate at $p/p_0 = 0.35$.

The average radius of meso pores was calculated for $r_{mes} < 6{\times}10^{-6}$ m because for these pores, the replicates of MIP curves showed the smallest variations. The micro pore fractal dimensions (D_{mic}) were calculated from the slopes of the linear parts of the double logarithmic plots of a vs. adsorption potential (A) using the following equation (Pfeifer and Obert, 1989; Jaroniec and Kruk, 1997):

$$ln(a) = constant + (D_{mic} - 3)ln(A) \quad , \tag{3.8}$$

where

$$A = RTln(p_o/p). \tag{3.9}$$

This equation is derived for a multi-layer adsorption region e.g. for the values of $ln(A) < 0$ (Sokolowska et al., 1999). The fractal dimension of meso pore surface (D_{mes}), was calculated from the linear parts of double logarithmic plots of the first derivate of $V = f(r)$ vs. r using the following dependence (Pachepsky et al., 1995):

$$D_{mes} = 2 - dlog\frac{\frac{dV(r)}{dr}}{dlogr} \ . \tag{3.10}$$

3.3 Results and Discussion

3.3.1 Experimental Porosity Data

Measured and calculated pore parameters of this study, which will be referred in the further discussion are included in tables 3.1 and 3.3 and figure 3.2. Sand of varying grain size was the main component of the seam material. The seam material is mainly composed of $6.3{\times}10^{-6}$ to $6.3{\times}10^{-4}$ m particles; coarser material was used for pavement construction in Berlin compared to Warsaw (Table 3.2).

A correlation between C_{org} and clay indicates, that OM is of small particle size (Clay = 2.4 C_{org} + 8.6; R^2=0.8, N=12). Therefore, the statements about pore clogging, made in chapter 1.3 could be proven.

The experimental desorption isotherms for the seam material (Figure 3.2(a)) are interpreted as the dependencies of micro pore volume vs. relative water vapor pressure, which is related to the micro pore radius according to equation 3.3.

Compared to the original sandy seam filling (1 to 5 cm), the altered seam material (0 to 1 cm) shows an increased water storage capacity (Table 3.1).

Compared to sandy forest Ah-horizons, the seam material adsorbs less than one tenth of water, at similar C_{org} contents (Hajnos et al., 2003). This difference is a hint to the specific character of the seam material's OM, e.g. its low wetability and low swelling ability. The amount of meso pores is higher in the Warsaw than in the Berlin samples due to the smaller average size of sand grains in Warsaw (Figure 3.2(b), Table 3.3). The meso porosity in the studied seam materials is much lower than in sandy forest Ah-horizons (Hajnos et al., 2003).

The water retention functions can be interpreted in terms of soil macro porosity (Figure 3.2(c)), although they include some meso pores (pores with diameters of 1×10^{-6} <r<3×10^{-3} m).

Both Berlin and Warsaw seam materials exhibit similar macro porosity. Contrary to the micro pores and meso pores, the amount of macro pores in seam material is similar to sandy forest Ah-horizons (Hajnos et al., 2003). Here, the sand fraction, which is similar in both soils, determines the water retention. The water content at saturation (Θ_s) for instance, is not significantly different in 0 to 1 cm and 1 to 5 cm layers, which, even with deposits in the upper layer, show both sandy character.

Sample B10 shows a higher porosity than the other samples. A measurement of undisturbed field samples B10* (N=18) confirms this result. This is due to the highest C_{org} and highest clay fraction among the samples, which caused the lowest dry bulk density. Contrary to other sites, at B10 Pflügerstrasse, there are trees which deliver foliage. Tree foliage contributes to high C_{org} contents, but it also contributes to humus and therefore to a good quality organic matter which might not be case in that amount at other sites.

The calculated Mualem-van Genuchten parameters n fit to the sandy character of the samples (Table 3.1). It ranges from 1.3 to 2.7. According to Rawls et al. (1982), only W1 lies between sandy loam and loamy sand.

Table 3.2: Particle size distribution and soil density data of seam materials from Berlin and Warsaw.

	Clay		Silt[%]			Sand[%]		ρ_B	ρ_P
Site		fine	medium	coarse	fine	medium	coarse	$10^3\,\mathrm{kg\,m^{-3}}$	
Berlin									
B1	1.8	0.9	1.4	5.2	35.1	43.3	12.3		2.58
B2	2.9	1.5	2.9	9.3	38.2	40.5	4.7	1.52	2.59
B3									2.54
B4								1.54	2.59
B5								1.47	2.59
B6								1.57	2.60
B7	2.3	1.6	3.0	9.3	42.5	35.7	5.5	1.64	2.60
B8								1.59	2.60
B9	2.1	0.7	1.7	7.0	45.9	38.2	4.4	1.21	2.60
B10	3.7	1.5	2.8	8.3	35.9	40.2	7.6	1.15	2.51
B1a	1.0	0.4	0.9	2.1	25.7	53.8	16.1		2.63
B2a	0.4	0.1	0.6	2.9	33.3	57.1	5.6	1.65	2.64
B3a									2.67
B4a	1.6	0.0	0.3	2.7	42.6	48.4	4.8	1.57	2.64
Warsaw									
W1								1.50	2.65
W2								1.42	2.51
W3									2.52
W4									2.59
W5	3.1	0.4	3.9	10.4	22.7	49.3	10.2		2.56
W6	3.6	0.0	4.0	13.5	36.0	39.8	4.1	1.56	2.59
W7									2.58
W8	2.5	0.7	3.2	6.8	22.6	58.3	5.9		2.60
W9	1.7	0.5	3.7	3.2	19.6	55.9	15.4	1.67	2.59

ρ_B - dry bulk density, ρ_P - particle density

Table 3.3: Pore-size distribution data of seam materials from Berlin and Warsaw.

Site	V_{mic}	V_{mes}	V_{mac}	r_{mic}	r_{mes}	r_{mac}	D_{mic}	D_{mes}
	$10^{-6}\,m^3\,kg^{-1}$			$10^{-8}\,m$	$10^{-6}\,m$	$10^{-4}\,m$		
Berlin								
B1	9.1	31.6		1.95	0.90		2.58	2.60
B2	5.7	52.8	271	1.91	2.36	1.24	2.61	2.49
B3	9.2	60.4		2.06	2.41		2.60	2.65
B4	6.3	43.6	260	1.90	1.91	0.74	2.58	2.46
B5	8.0	42.8	290	1.94	1.92	0.91	2.57	2.35
B6	4.6	33.7	253	1.91	1.30	1.65	2.60	2.82
B7	6.9	46.7	223	1.88	1.99	0.70	2.58	2.49
B8	5.7	43.9	242	1.85	1.63	1.24	2.59	2.51
B9	6.2	24.3		1.65	0.85		2.61	2.94
B10	15.7	43.7	472	2.08	1.86	4.44	2.59	2.90
B1a	3.9	13.3		1.90	0.38		2.62	2.86
B2a	1.7	2.9	227	1.71	0.13	4.66	2.48	2.89
B3a	2.5	15.9		1.94	0.68		2.67	2.65
B4a	1.1	4.4	260	2.02	0.06	5.65	2.79	3.00
W1	9.7	58.9	278	2.15	2.49	2.56	2.59	2.67
W2	12.1	72.4	309	2.21	3.16	2.21	2.61	2.43
W3	16.4	91.4		1.87	4.21		2.58	2.62
W4	9.5	51.0		2.17	2.30		2.55	2.60
W5	12.6	69.2		2.13	2.80		2.58	2.54
W6	9.7	52.1	258	2.11	2.22	0.65	2.59	2.55
W7	15.6	96.9		2.53	4.18		2.53	2.43
W8	(39.7)*	48.2		2.31	1.81		2.36	2.94
W9	(34.8)*	58.0	216	2.46	1.49	0.80	2.37	2.94

*measurements impricise due to high salinity

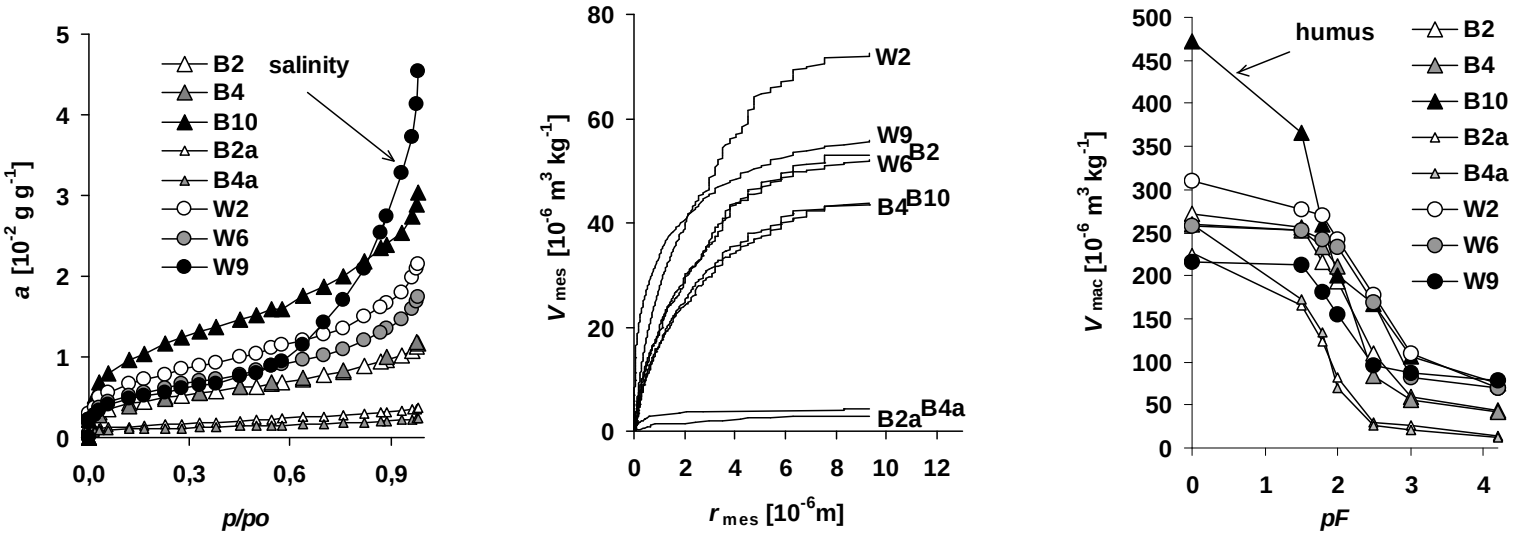

(a) (b) (c)

Figure 3.2: Porosity measurements for different pore size ranges in pavement seam materials of Berlin (B) and Warsaw (W), (a) measured water-vapor desorption isotherms as used for calculations of pore volumes in the nanometer range; (a = amount of adsorbed water; p/p_0 = relative water vapor pressure), (b) cumulative meso pore volume V_{mes} in relation to pore radius r_{mes} as calculated from mercury-intrusion porosimetry, (c) Water retention functions as used for calculation of pore volume V_{mac} in the millimeter range.

3.3.2 Calculated Pore Parameters

Micro pore size distribution functions, as calculated from desorption isotherms (equation 3.3), have similar shape for all samples except W8 and W9 (Figure 3.2(a), only W9 is shown as representative). The latter seam materials exhibit much higher water sorption at high water vapor pressure than the other seam materials. These samples are highly saline, as indicated by high EC (Table 1.1), which causes its hydrophilic property. Water contents at high relative water vapor pressures are not caused predominantly by capillary condensation. Therefore, the pore parameters cannot be evaluated for W8 and W9.

The micro pore size distribution functions are similar for all studied seam materials and exhibit broad peaks in 5×10^{-9} to 3×10^{-8} m pore radii range, while the frequencies of smaller and larger pores are low. As a consequence, r_{mic} around 2×10^{-8} m is similar for all samples and no significant differences between Warsaw and Berlin or 0 to 1 cm and 1 to 5 cm layer samples are noted (Table 1.1). As long as the amount of minerals in the clay fraction is small, mainly OM forms the micro pore system in the studied seam materials. This is probably similar for all seam materials and is a typic property of this substrate. The average micro pore radius of the sandy forest Ah-horizon, which obviously contain different OM, is about half of that of the seam material (Hajnos et al., 2003).

The volume of the micro pores exhibits fractal behavior for all samples as proven by the linearity of double logarithmic plots of adsorption vs. adsorption potential (not shown). The range of fractal scaling of the studied materials extends below the traditional multi-layer regime and covers the pore radii down to about 1×10^{-9} m. Such small pores can be referred to as surface roughness, that means structures which can be described as curved planes. The ranges of the fractal scaling (linearity intervals) are similar for all materials. A fractal dimension value, higher than 2.5 for the majority of the samples, indicates a high surface roughness and complex micro pore structure. The fractal dimensions of micro pores of seam material are in general similar to those of forest Ah-horizons. This is because of the presence of small organic particles (Hajnos et al., 2003).

Meso pore size distribution functions for the studied materials show a single peak with the maximum located at various positions depending on the sample (Figure 3.2(b)). As calculated from the PSD functions r_{mes} differs from 6×10^{-5} to 4.2 $\times10^{-3}$ m, showing smaller values for the original filling than for the altered seam material. Small amounts of meso pores together with small meso pore radii indicate that the seam materials show only a poor meso porous structure. A higher meso pore volume is caused by a larger meso

pore radius. Therefore, it seems that the dimension of pores plays a more important role for the formation of meso porosity than the number of pores. The seam material has similar meso pore radii like the forest Ah-horizon.

Meso pores of the studied materials exhibit fractal character, which is seen from the linearity of double logarithmic dV/dr vs. r (not shown). The calculated fractal dimensions vary from 2.3 to 3.0 and are larger than 2.5 for more than 70 % of the samples. This indicates a complex meso pore system. No significant differences occur between 0 to 1 cm and 1 to 5 cm layers of the seam material and between the sandy forest Ah-horizons and the seam material as well.

Macro pore size distribution functions of the studied materials show a one-peak character with the maximum located at around 2×10^{-5} m. However, high fractions of very large pores (from 1×10^{-4} to 3×10^{-3} m) cause the calculated r_{mac} to be large with 6×10^{-5} to 5.5×10^{-4} m ($r_{mac} = r_{ave}$ in equation 3.7). Variations in r_{mac} among the seam material samples are high and no differences between Warsaw and Berlin or within the layers are detectable. Concerning the macro pore volumes, the seam materials are not significantly different from forest Ah-horizons, but show a much higher variation, due to different site characteristics e.g. age or traffic density.

3.3.3 General Dependencies

Soil organic matter decreases the bulk density of natural soils, increases soil permeability and aeration (Zhang and Hartge, 1992). In the studied materials, similar phenomena occurred.

This can be seen from the decrease in ρ_P (Figure 3.3(a)) and ρ_B and the increase of micro pore and meso pore volumes with increasing C_{tot}.

Therefore, ρ_B is higher in 1 to 5 cm layers than in the C_{tot} enriched 0 to 1 cm layers (Table 1.1). However, the correlation between the particle density and C_{org} is not very strong (r^2=0.68, see figure 3.3(a)). This can be explained by light forms (humus) and heavy forms (diesel soot) of C_{org}.

Therefore, pore volumes and dry bulk densities were stronger correlated to C_{tot}, including typical urban, airborne carbonate particles (abrasions from buildings), than to C_{org}. This indicates the importance of the particulate carbonate deposits for the properties of seam material, which are connected to small pores and small particles. Therefore, the dependence of ρ_B calculated from MIP, which excludes macro pores on C_{tot} is stronger (R^2=0.73; Figure 3.3(b)) than that of dry bulk density calculated from volume and mass of soil, which includes macro pores (R^2=0.61; not shown). Here, the impact of coarser particles is stronger.

Thus, especially the micro pore volume of the studied materials is well

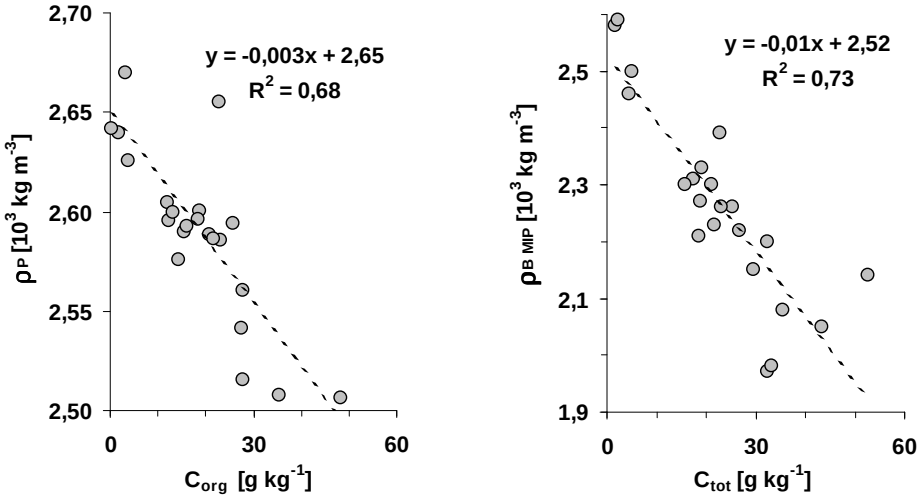

(a) (b)

Figure 3.3: Dependence of dry bulk density ρ_B on C_{tot} in pavement seam materials of Berlin and Warsaw.

correlated with the amount of C_{tot} (Figure 3.4(a)). The regression line intersects close to origin, which indicates a small input of non-carbon components to micro porosity.

Compared to micro porosity, the contribution of non-carbon components to meso porosity is larger. This leads to a weaker correlation and a higher intersection point (Figure 3.4(b)).

Consequently, the macro pore volume shows the weakest correlation with C_{tot} and the highest intersection point of the regression line (Figure 3.4(c)), because macro porosity is mainly affected by the sand fraction particles. Furthermore, the correlation disappears, if the sample B10 is excluded (then: R^2=0.31, intersection = $229\times10^3\,m^3\,kg^{-1}$).

The statements mentioned above can be quantified as following: The intersection points of the regression lines at $V_0 = f(C_{tot} = 0)$ mark the contribution of non-carbon components to the individual pore volumes. Given by the regression, higher pore volumes, e.g. V_{ave}, are connected to higher C_{tot} contents. Therefore, the ratio $(V_{ave} - V_0)/V_{ave}$ in a given pore range is an estimate for the contribution of carbonaceous components to V_{ave}. One obtains: 85 % for micro pores, 70 % for meso pores and 29 % (including B10) for macro pores. Thus, carbonaceous material contributes more to microporosity than to mesoporosity and least to macroporosity of seam material. The average pore radii and fractal dimensions do neither correlate with C_{tot} nor with C_{org} but seem to rather depend on quality than on quantity of C.

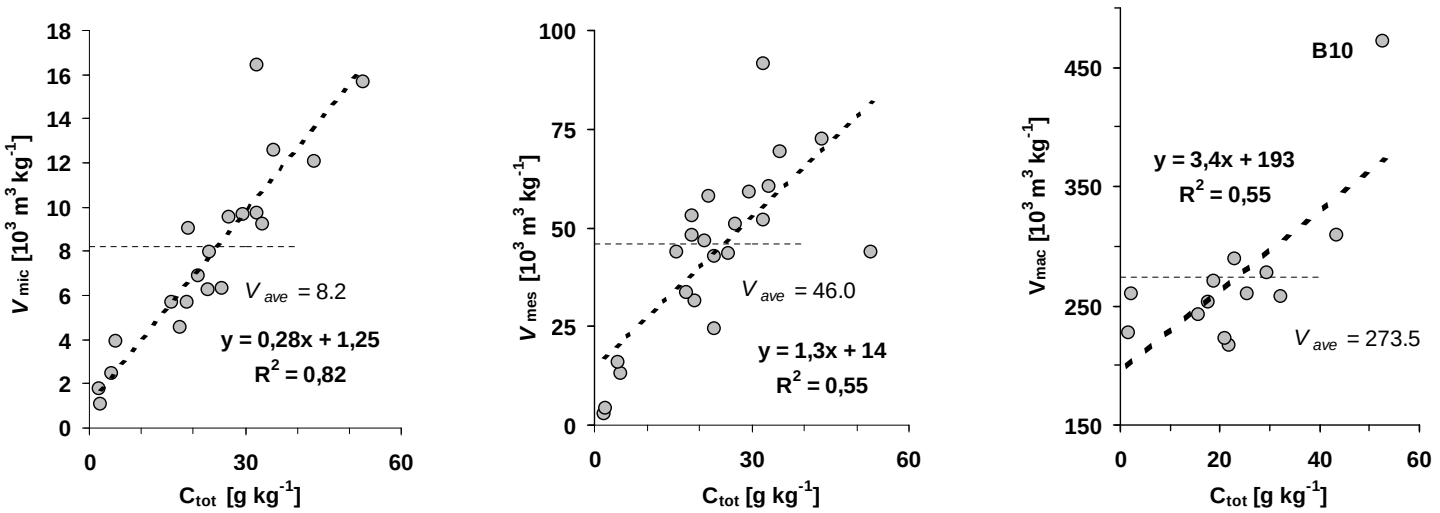

(a) (b) (c)

Figure 3.4: Dependence of pore volumes V_{mic}, V_{mes}, and V_{mac} on C_{tot} for pavement seam materials of Berlin and Warsaw. Two saline seam materials W8, W9 are not included in the figure. V_{ave} indicates the average pore volume of the corresponding pore size range.

3.4 Conclusions

This study shows that carbonaceous deposits govern the formation of the pore system of the investigated seam materials. The volume of the nanometer-size pores depends almost solely on the amount of deposited carbon, while the millimeter-size pores are mainly influenced by the grain sizes of the sand fraction. The volumes of the micrometer-size pores seem to be related to both above-mentioned factors. Therefore, the seam materials have different physical properties and ecological functions, e.g. an improved water storage capacity compared to the original sandy seam filling. The organic deposits in the seam materials seem to have a rather particulate character. Thus, they differ from natural soil organic matter (SOM). Therefore, varying pore properties were found in the seam material compared to sandy forest Ah-horizons with similar C_{org} contents. Although various sites in two different cities have been sampled, the seam materials exhibit similar pore properties in a wide range of pore sizes.

Chapter 4

Surface Properties of the Seam Material

4.1 Introduction

Because of the negative ecological effects of decreased water infiltration due to soil sealing, increasing rainwater infiltration is among the main ideas of recent ecological urban planning.

As rainwater runoff in urban areas is often contaminated (Harrison and Johnston, 1985; Gromaire-Mertz et al., 1999; Viidanoja et al., 2002), increasing infiltration implies the risk of a groundwater contamination (Dannecker et al., 1990).

Like in arable or natural soils, the fate of pollutants in the pavement system is governed by their interaction with the soil, e.g. decay, adsorption. Pavements are constructed from conductive and retention–weak materials, mainly sand, which is low in adsorption capacity. Neither the role of the seam material as a pollutant's transport pathway, possible heavy metal filter and/or waste accumulation medium nor the pollution risks are completely assessed because the chemical properties of seam materials are largely unknown. It is hypothesized, however, that because of its increased C_{org} contents, the seam material acts as a filter for heavy metals. To what extent is not clear and cannot be predicted from knowledge about conventional soils, because the seam material's OM is different from conventional SOM.

In this part of the study, the surface properties of the seam material are investigated based on ion exchange and water vapor adsorption measurements. Exchange capacities, surface areas, surface charge densities, and adsorption energies were studied in relation to basic chemical parameters (carbon and clay content) and compared to natural soil´s parameters. The adsorption

behaviour of Pb and Cd, two toxic heavy metals of different mobility, were studied. Freundlich's adsorption model was parameterised with the measured isotherms in order to get input data for modelling heavy metal solute transport through the pavement.

4.2 Materials and Methods

4.2.1 Surface Property Measurements

The surface area was calculated from water vapor adsorption isotherms, which were measured in triplicate using the vacuum chamber method at the temperature $T = 294 \pm 0.1\,K$ (see subsection 3.2.1 for further details). Here, p/p_0 was controlled by sulfuric acid solutions of stepwise decreasing concentrations. Results of triple weightings had a coefficient of variation c_v, of 3.7 %. The higher the relative pressure, the longer the time for equilibration gets, at the highest p/p_0 more then one week is necessary. The simple the measurement is, the more complex gets the calculation of surface area and adsorption energy, which is explained in detail in Hajnos et al. (2003). These measurements were conducted in the "Institue of Agrophysics" of the Polish Academy of Sciences in Lublin by Prof. M. Hajnos and his colleagues.

4.2.2 Adsorption Isothermes for Cd and Pb

Heavy metal adsorption isotherms were obtained for the two most relevant, toxic traffic related heavy metals (HM) with different mobility: C_{org} affected, immobile Pb and mobile Cd. The OECD guideline N°106 (OECD, 2000) was followed. One gram of soil has first been equilibrated with 45 ml 0.01 M $CaCl_2$ overnight. Then, heavy metals were added as a typical cocktail (Pb, Cd, Ni, Cu, Zn) in 5 ml 0.01 M $CaCl_2$ solution. Thus, the resulting isotherms include realistic adsorption concurrence. For all samples five stepwise rising solute concentrations including destilled water were added. Therefore, the resulting adsorption isothermes include one desorption step and span over a wide range of concentrations (liquid concentrations range from 0.05 to $10\,mg\,L^{-1}$ for Pb and from 0.001 to $5\,mg\,L^{-1}$ for Cd). After two hours of shaking, the original pH of the samples were re-adjusted with KOH. Liquid phase HM concentrations were measured in the supernatant after 20 min of centrifugation at $1000 \times g$.

Because of a great inhomogeneity even in the three replicates, it was not possible to calculate the adsorbed quantities from the differences of the liquid phase concentrations before and after adsorption. Instead, the solid phase

was analysed additionaly.

Urban soils in general are heterogenously. From preliminary tests it was known, that the solid phase contents of three aliquots of one sample varied with CVs of up to 35 % for Pb and up to 20 % for Cd. These variances can be caused e.g. by pieces of blast furnace slag, regularly found in the seam material. The material was extracted with concentrated nitric acid (soil/acid ratio = 1/20) for 360 min at 453 K under pressure. The concentrations of Pb and Cd were measured with a maximum CV of 2 % respectively 5 %. In order to consider only the HM fraction which is involved in adsorption processes, the 0.025 M $(NH_4)_2$EDTA (pH 4.6) extractable portion has been determined for the original soil samples (Welp and Brummer, 1999). The according residual contents have been excluded from the adsorption isotherm.

After the analyses, isotherm data was checked for inconsistencies and outliers. Isotherm data for solid (C_s) or liquid phase (C_l), smaller than the limit of quantification were set to 0.001 mg l^{-1} or mg kg^{-1}, because $\log 0$ is not defined. Outliers were checked for differing pH compared to the original pH and if the difference was more than 1 unit, eliminated. The solid phase concentrations (C_s) then were plotted against the liquid phase concentrations (C_l), showing non-linearity. In $\log C_s$ vs. $\log C_l$ plots, data behaved linear. A Freundlich conformity test was applied. Thereby, isotherm points were eliminated, which were dramatically lying outside the isotherms. These outliers could be explained by great variances in the solid phase, in most of the cases.

After the analyses, isotherm data was checked for inconsistencies and outliers. In $\log C_s$ vs. $\log C_l$ plots, data behaved linear. Thus, adsorption processes dominated the partition, other processes like precipitation can be neglected. Data sets were not considered, which were dramatically lying outside linear isotherms.

For the fitting of an adsorption isotherm to the experimental data with complex solid phases like soils, the use of the Freundlich model is widely recommended (Stumm and Morgan, 1996) before Langmuir, because it does not expect similar energy sites but can be seen as a sum function Langmuir isotherms for the individual energy sites (Sposito, 1980). So it is adequate to describe the seam material which is a mixture of sorbents with varying surface characteristics:

$$C_s = K_f {C_l}^m \quad , \tag{4.1}$$

where C_s is the concentration in the solid phase, C_l is the concentration in the liquid phase, K_f is the Freundlich coefficient, describing the soil material's affinity to the solute. m is a exponent and a measure for linearity.

The adsorption characteristics are studied to describe the mobility of the heavy metals. A good method to compare different adsorption characteristics with different degrees of linearity is to calculate the retardation factor R, which derives from the convection–dispersion equation and describes the resulting mobility of substances in a solid-liquid system (Equation 7.2):

$$R = 1 + \frac{\rho_B}{\Theta} \frac{\partial C_s}{\partial C_l} \quad , \tag{4.2}$$

where ρ_B [kg L^{-1}] is the dry buld density and Θ [m^3 m^{-3}] is the water content of the soil. For non–linear adsorption of solutes R becomes:

$$R = 1 + \frac{\rho_B}{\Theta} m K_f C_l^{m-1} \quad . \tag{4.3}$$

4.3 Results and Discussion

4.3.1 Surface Properties and Cation Exchange

The higher CEC of seam materials compared to the original seam filling can be explained by greater surface areas. The SSA correlates to higher C_{org} amounts in the seam material compared to the 1 to 5 cm layer (Table 1.1 at page 25 and table 4.1 at page 65). With 1.2 to 4.8 cmol(+) kg^{-1} the CEC of the seam material is low compared to values of 12 to 20 cmol(+) kg^{-1} for non-urban German sandy soils (Renger, 1965) or compared to values of 8 to 36 cmol(+) kg^{-1} for Berlin sandy forest soils with similar C_{org} contents (Wilczynski et al., 1993). Like for other sandy soils (Renger, 1965) the CEC of the seam material depends mainly on OM.

The CEC of the seam material‘s OM is low. It is only 74 cmol(+) kg^{-1}C, as the slope of the CEC vs. C_{org} trend line of the studied seam materials (Figure 4.1) indicates. Slightly worse correlation is obtained for CEC and C_{tot} (CEC=0.68C_{tot} + 0.77; r^2=0.70). The CEC of common, more natural SOM has been estimated to be around 300 cmol(+) kg^{-1} C by Parfitt et al. (1995) for New Zealand soils and by Krogh et al. (2000) for Danish soils. Higher values of up to 680 cmol(+) kg^{-1} C were observed in acidic sandy forest soils (Wilczynski et al., 1993).

The comparable low CEC of the seam material´s OM can be explained by its quality. As mentioned above the OM consists of different constituents, not everything can be referred to as humus. The combustion residues for instance have been quantified in chapter 2. Although BC contributs to the CEC of soils its contribution is lower than that of humus (Tryon, 1948). Consequently, the CEC of the OM rises, if not C_{org} but (C_{org} - BC) is applied

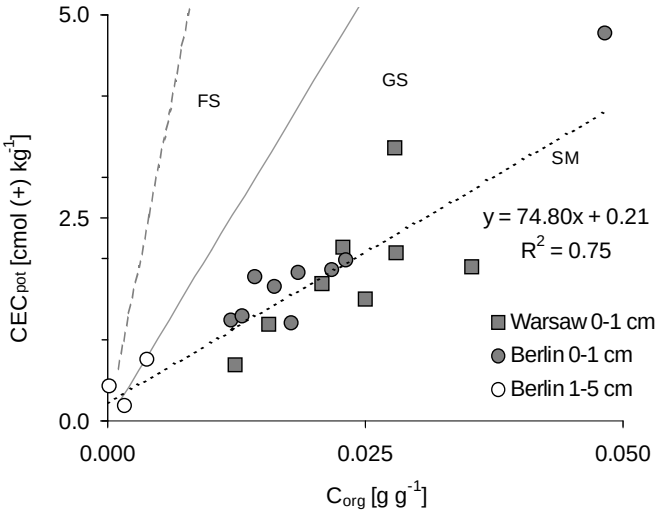

Figure 4.1: CEC depending on C_{org} in seam materials (SM, doted), sandy German soils (GS, solid) (Renger, 1965) and sandy forest soils (FS, dashed) (Wilczynski et al., 1993).

for the correlation. If the OM is held solely responsible for the CEC of the samples, one gets a contribution of 83 cmol(+) kg^{-1}C (r^2=0.74) for C_{org} wheras the contribution rises to 93 cmol(+) kg^{-1}C (r^2=0.74) if C=C_{org}-BC is apllied. However, OM seems to be solely responsible for the cation exchange process in the seam materials, as their CEC is directly proportional to C_{org}. The regression lines of the above dependencies intersect the y-axis close to (0;0), which indicates that only C_{org} compounds contribute substantially to CEC.

The specific surface area (SSA) is higher in the 0 to 1 cm layers than in 1 to 5 cm layers which can also be explained by C_{org} (Table 4.1). The surface areas of conventional SOM can be much higher than that of the seam material (Figure 4.2). This is a hint to the specific character of the seam materials OM. The samples from Berlin and Warsaw show a very similar behavior resulting in a quite good correlation between C_{org} and specific surface area (r^2 = 0.8). As it can be seen from the slope of the linear regression line, the specific surface area of the seam material's OM is about 516 m^2g^{-1}. Wilczynski et al. (1993) investigated a Berlin forest soil using the same methodology for measuring specific surface areas. They found the contribution of OM to SSA to be 501 or 1062 m^2g^{-1} depending on situation of the sampling site in the forest micro relief having ridges and furrows. However, compared to the seam material, these samples show higher CEC. This can be explained by the higher surface charge density (SCD) of the forest soils.

Table 4.1: Surface characteristics and heavy metal adsorption parameters of seam material from Berlin and Warsaw.

	Surface parameters			Freundlich adsorption parameters									
Site	$A_s(H_2O)$ $m^2\,g^{-1}$	SCD $\mu mol(c)\,m^{-2}$	E_a	k_{Pb} $mg^{1-m}\,L^m\,kg^{-1}$	m_{Pb}	r^2	C_{Pb} $mg\,kg^{-1}$	$R_{Pb}^{(a)}$	k_{Cd} $mg^{1-m}\,L^m\,kg^{-1}$	m_{Cd}	r^2	C_{Cd} $mg\,kg^{-1}$	$R_{Cd}^{(a)}$
Berlin, 0 to 1 cm													
B1	14.81	1.20	3.08	2638[(b)]	1.00	0.87	68.5	19919	20.4	0.70	0.98	2.0	147
B2	12.44	1.32	3.22	2133[(b)]	1.00	0.71	91.0	15916	17.0	0.38	0.99	9.5	155
B3	17.00	1.15	2.82					n.a.					
B4	12.17	1.62	3.30	1321	0.45	0.93	309.5	8685	19.4	0.62	0.99	n.d.	162
B5	13.56	1.37	3.06	977	0.44	0.96	290.2	6398	12.2	0.54	0.94	2.0	108
B6	8.87	1.39	3.41	1111	0.54	0.84	190.1	7901	12.2	0.21	0.93	6.1	82
B7	12.69	0.95	3.06	1376	0.93	0.96	222.0	10518	13.0	0.25	0.96	8.4	100
B8	11.03	1.17	3.22	1056	0.58	0.91	163.4	7653	16.5	0.29	0.98	6.9	121
B9	14.03	1.30	3.04	1416	0.62	0.86	203.5	10476	14.2	0.48	0.94	2.0	119
B10	29.25	1.64	2.82	2483	0.57	0.95	480.0	17914	15.2	0.28	0.98	6.1	110
Berlin, 1 to 5 cm													
B1a	7.46	1.02	3.41	499	0.92	0.96	38.3	3817	6.9	0.63	0.81	2.1	62
B2a	5.30	0.34	3.86	272[(b)]	1.00	0.99	49.6	2056	5.4	0.41	0.99	5.2	53
B3a	5.20	n.d.	3.88					n.a.					
B4a	3.00	1.44	4.32	833	0.55	0.95	72.6	5961	5.7	0.40	0.69	4.0	43
B9a		n.a.		738	0.62	0.93	135.6	5449	8.6	0.34	0.99	13.0	82
Warsaw, 0 to 1 cm													
W1	13.82	1.55		12558[(b)]	1.00	0.97	148.1	94817	20.3	0.30	0.98	2.9	145
W2	20.41	0.93	3.10	8052	0.89	0.97	180.9	61784	11.9	0.18	0.85	5.1	87
W3	27.76	1.21	2.91	4699	0.76	0.95	159.3	35982	12.1	0.15	0.76	5.5	77
W4	12.80	1.32	2.79					n.a.					
W5	17.76	1.16	2.71	2738	0.91	0.87	99.7	20965	33.6	0.28	0.90	8.5	280
W6	15.85	0.94	2.90					n.a.					
W7	17.21	n.a.	2.81					n.a.					
W8	11.32	0.61	2.64	2234	0.75	0.98	98.5	17088	8.4	0.10	0.89	5.2	42
W9	14.85	0.80	1.27	3078	0.88	0.89	270.7	23627	79.2	0.55	0.99	5.0	485

[(a)] ρ_B=1.5 g cm^{-3}, C_l=0.1 mg L^{-1}, Θ=0.3 m^3 m^{-3}

[(b)] isotherms were fitted with 0≤m≤1

n.d. not detectable; n.a. not analysed

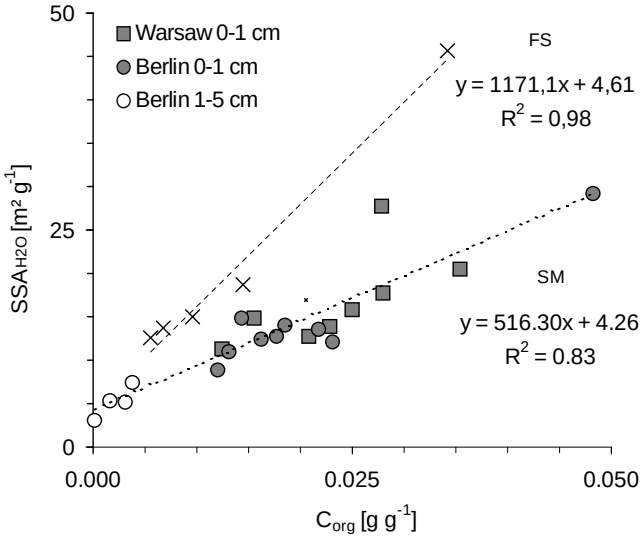

Figure 4.2: Contribution of seam material's C_{org} to specific surface area measured by water vapour desorption isothermes SSA_{H_2O} compared to forest soil's C_{org}.

4.3.2 Surface Charge Density and Adsorption Energies

The surface charge density (SCD)

$$SCD = \frac{CEC}{SSA} \tag{4.4}$$

is characteristic for the OM and is a measure for the quantity of polar functional groups. The SCD of the seam material is seven times lower than that of sandy forest soils (Wilczynski et al., 1993; Hajnos et al., 2003), that, which causes the comparable low CEC at similar C_{org} levels (Figure 4.1. Hajnos et al. (2003) report on SCD of 2.9 to 10.6×10^{-6} mol(+) m^{-2} for Berlin sandy forest soils.

A low surface charge density indicates a low amount of polar functional groups. This statement is supported by the investigated adsorption energies (Figure 4.3). The water vapor sorption in the studied seam sealing materials is in general a low energy process (i.e. water binding forces are low), which is seen from the water vapor sorption energy distribution functions (not shown). Most of the materials show high fractions of low energy sites and only low fractions of higher energy sites. The low sorption energy fractions of the two most saline samples (W8 and W9) are the highest. In three of the studied materials, the 1 to 5 cm layer samples B2a, B3a and B4a, medium energy sites dominate. Thus, E_a is higher in the 1 to 5 cm layer than in the 0 to 1 cm

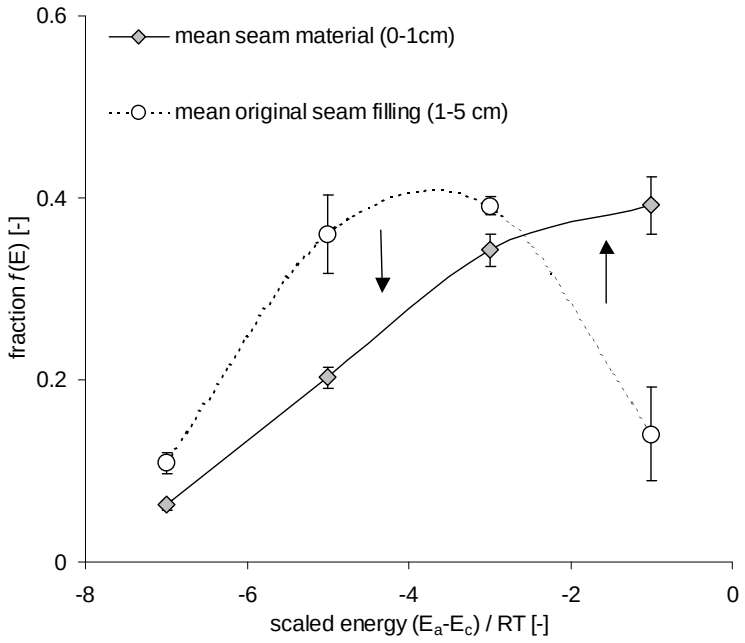

Figure 4.3: Distribution of scaled adsorption energy levels for seam materials and original seam filling (sand) from Berlin and Warsaw. The arrows indicate the shift in adsorption energy fractions due to the deposition of urban dust. Error bars show standard errors, N=19 for seam materials, N=4 for original seam filling.

layer indicating a higher polarity in the lower layer. Organic substances may have coated the polar mineral surfaces in the upper layer.

Higher polarity can result in higher SCD. However, there is no dependence between E_a and SCD. Possibly, it has been shadowed by the salt accumulation effects, because E_a was found to be related to the EC of the studied seam materials. The E_a decreases with an increase of EC which is connected logarithmicaly with low hydration energy of the salt cations (not shown). Similar relations of adsorption energy and parameters related to soil salinity are observed in natural saline environments (Toth and Jozefaciuk, 2002).

The investigation of SCD and E_a revealed characteristics of the seam materials OM, which should be validated by analysis of the quality and quantity of functional groups, e.g. using solid phase ^{13}C nuclear magnetic resonance spectroscopy (Preston, 1996; Baldock et al., 1992) or FTIR spectroscopy (Ellerbrock et al., 1999).

4.3.3 Pb and Cd Adsorption Isotherms

Beside the general parameter CEC, specific adsorption parameters are needed for assessing transport of heavy metal solutes. The results of the investigation of adsorption isotherms and its parameterisation can be found in table 4.1 and exemplarily in figure 4.4. After assuming ρ_B=1.51, Θ=0.3 and C_L=0.1 to be constant the mobility of Pb and Cd can be compared by its retardation factors, including different isotherm linearities.

Pb

In general, K_f for Pb in Warsaw is higher than in Berlin, while m implies stronger non-linearity in Berlin. In Berlin, K_f values for Pb are higher in the 0 to 1 cm layer than in the 1 to 5 cm layer indicating a higher adsorption capacity in the upper layer. The values for m are similar for both depths. However, a comparison of K_f without considering m is not meaningful. Therefore in table 4.1 the retardation factors, which consider non-linearity (equation 4.3) are presented. Obviously, seam material absorbs more Pb than the original seam filling. This corresponds to the higher C_{org} contents in the upper layer. The great relevance of OM for the adsorption of Pb in Berlin seam materials is expressed by the correlation of K_f and C_{org} (K_f = 43.6 C_{org} + 581.3; r^2 = 0.84) and can be explained by OM´s contribution to the SSA (K_f = 83.1 SSA + 273.7; r^2 = 0.81).

However, there is no correlation of C_{org} and K_f for the Warsaw samples. That may indicate, (i) different kinds of OM in Warsaw and Berlin, exhibiting different amounts of adsorption sites for Pb or (ii) it may show the greater importance of other adsorbers than the studied OM for the Warsaw samples. However, the lacking correlation could also be an effect of (iii) the small number of samples compared to the high spatial variability in urban soils.

In general, the Pb_{tot} contents correlate very well with C_{org}, indicating same sources, e.g. combustion processes or strong adsorption of Pb on OM. Due to the standardised methodology (OECD, 2000) used for determining the adsorption isotherms, initial Pb_{tot} contents influence the magnitude of K_f. This may contribute to the observed different behavior of Warsaw and Berlin samples. For a more realistic analysis, the use of a weaker extractant than nitric acid, e.g. EDTA, might be more advisable.

Furthermore, there is a correlation between K_f and BC (Figure 4.5(a)), indicating BC functioning as a heavy metal adsorber. BC is inert and therefor its contents are not reduced in time due to decomposition. One can extrapolate the retention capacity for seam materials, that contain different accumulated amounts of BC (see Figure 4.5(b)). The BC accumulation rate

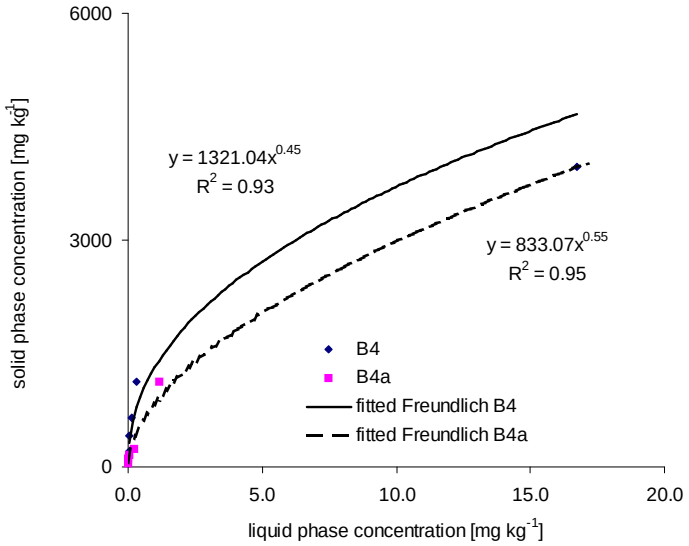

Figure 4.4: Adsorption isotherm for Pb in seam material (B4) and original seam filling (B4a) at site Grosser Stern, Berlin.

was assumed to be 0.15 and 0.5 g kg^{-1} a^{-1} as it was calculated in section 2.3.3. The effect of accumulating BC on heavy metal transport is discussed in part IV.

However, the correlation is not very strong. Therefor a laboratory experiment was conducted, in which the influence of different amounts of charcoal in sand on the Pb-adsorption was tested. Mixtures between sand and 0, 5, 10, and 100 g charcoal per kg sand were analysed for their Pb adsorption isotherms like the other soil samples. Figures 4.6(a) and 4.6(b) show the results of this experiment. It can be clearly seen, that charcoal, which stands for BC, enhances the adsorption properties of sand. However, the charcoal contains ash and water. The employed charcoal had an BC content of 80 % as measuered after 5 h of combustion at 1000 °C. The charcoal enrichment steps only influence the level of adsorption, but not the slope of the isotherms. The 0 % mixture of course behaves different. Here the adsorption isotherm of the mineral components like iron-oxides where characterised, which shows a lower slope of the adsorption isotherm than the charcoal mixtures.

Cd

As expected, the resulting retardation factors for Cd are much lower than for Pb indicating the much higher mobility. For Cd the retardation is higher

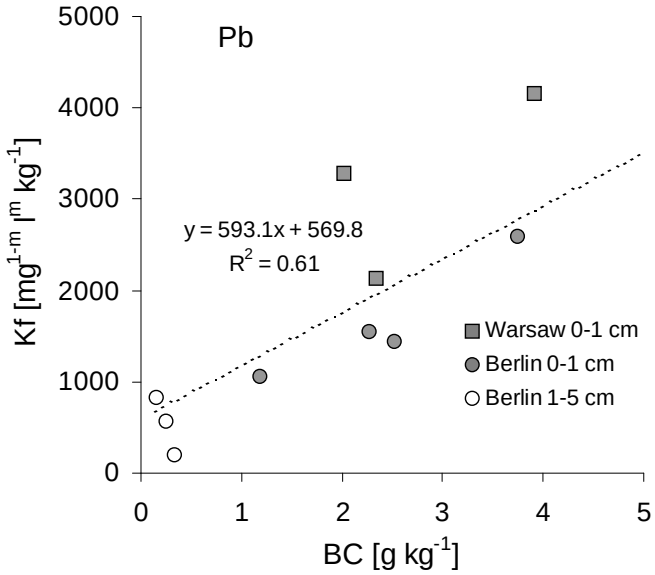

(a)

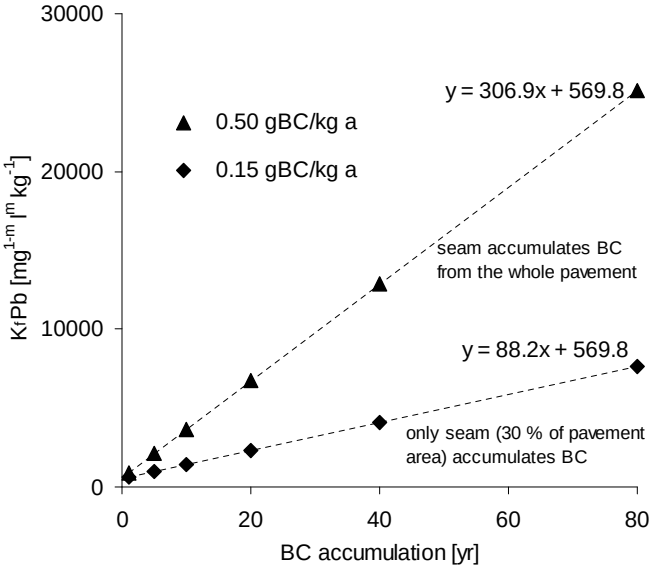

(b)

Figure 4.5: (a) Freundlich K_f for Pb adsorption depending on Black Carbon in seam materials from Berlin and Warsaw and (b) rising retention capacity as indicated by rising K_f with time due to BC accumulation at different rates depending on accumulating area.

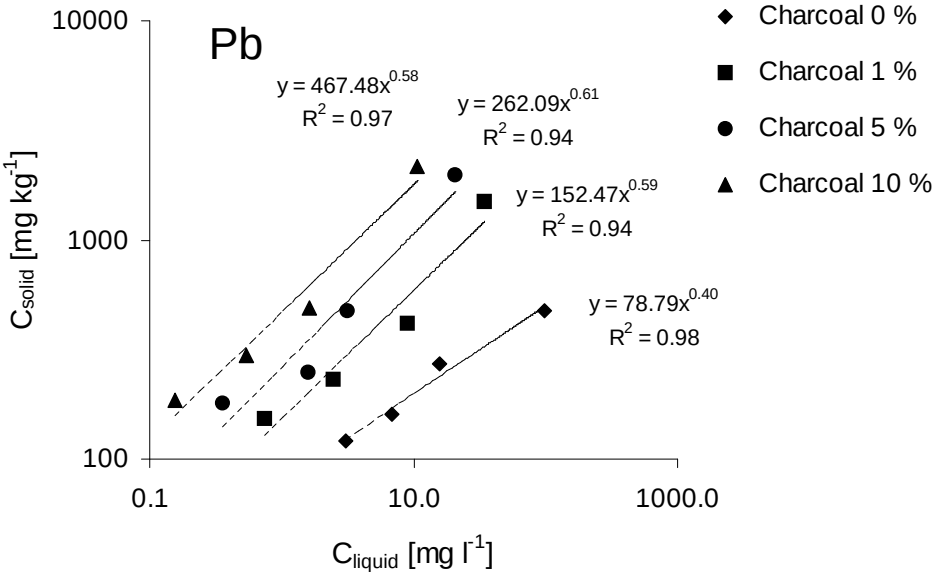

(a)

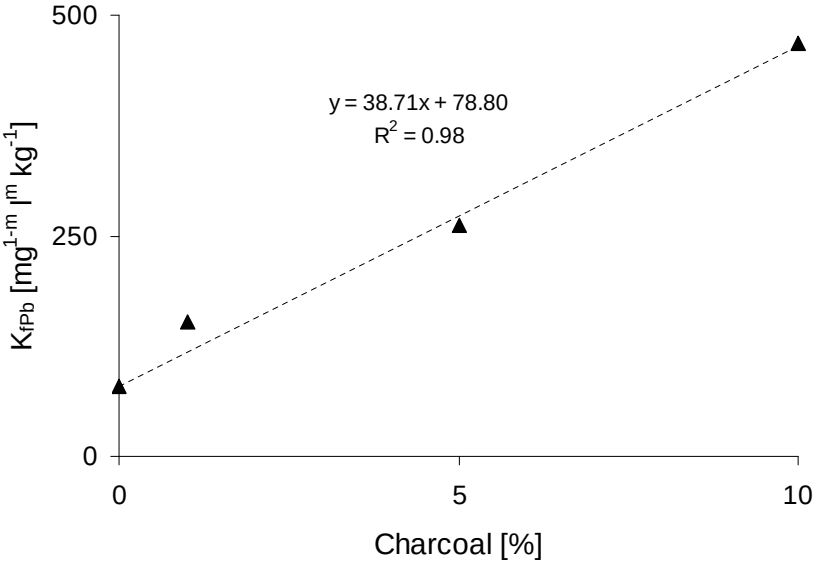

(b)

Figure 4.6: The charcoal amount of different sand/charcoal mixtures influences their Pb adsorption.(a) Pb adsorption isotherms for different mixtures of sand and charcoal.(b) Pb retention capacity as indicated by the Freundlich K_f of different sand and charcoal mixtures.

in the seam material than in the original seam filling material too. However, this can not be explained by deposited OM. Other deposited substances and particles must be more relevant, e.g. iron-oxides. From own studies (Proll, 2005), it is known, that the magnetic susceptibility, a proxy for iron oxides in urban areas (Kapicka et al., 2003), is higher in the seam material than in the sandy seam filling (Appendix). Hoeke (2003) reports the same for urban dust compared to urban soils. This proves the increased amount of Fe-oxides in the seam material, and shows its source in air borne particles. However, no correlation between magnetic susceptibility and K_f could be found neither for the Berlin nor the Warsaw samples.

4.3.4 Heavy Metal Adsorption of Seam Material Compared to Other Soils

Some published adsorption data are presented in table 4.2. The soils are compared by the retardation factors for the individual element.

Kocher (2005) investigated soils along federal highways in Germany focussing a similar scientific question like in this study. The transport of traffic derived heavy metals was investigated using Freundlich-parameters. A more general and inventory question motivated Adhikari and Singh (2003) to investigate English and Indian soils concerning the adsorption of Cd and Pb.

Compared to the Cd retardation capacity of roadside soils or the English and Indian sandy soils, the seam material is a clearly weaker filter. Concerning Pb, seam material shows comparable retardation with some samples showing better and some showing weaker adsorption capacity. Here, a clear statement concerning "the" seam material is not possible, the heterogeneity in between the seam material samples is too high.

For the transport of Pb through pavements, this leads to the expectation of travel times comparable to these known soils. In case of Cd this travel time will be much shorter, like hypothesised above and it will also be shorter than in comparable known soils. A quantitative statement can not be given here because of the special geometry of the pavement and because the influence of the only one centimeter thick seam material remains unclear. However, the Freundlich sorption parameters allow numerical simulations to predict introduced heavy metal transport under varying boundary conditions (see part IV).

Table 4.2: Adsorption data for soils with similar organic matter and clay content.

soil	Pb			Cd		
	K_f	m	$R^{(a)}$	K_f	m	$R*$
	dm^3kg^{-1}	-	-	dm^3kg^{-1}	-	-
Kocher (2005)						
jAh,0 to 10 cm,A1,1m	6849	0.24	47118	120	0.50	949
jAh,0 to 25 cm,A2,1m	8495	0.18	50017	101	0.50	800
jAh,0 to 18 cm,A3,1m	43720	0.08	143973	97	0.55	751
Adhikari and Singh (2003)						
Eng2, Norfolk	2239	0.73	15188	316	0.92	1752
Ind2, Ganges plains	102094	0.73	693895	1409	0.80	8973
Ind5, Desert sand	1135	0.42	9065	76	0.62	564

$^{(a)}$ ρ_B=1.5 g cm^{-3}, C_l=0.1 mg l^{-1}, Θ=0.3 m^3 m^{-3}

4.4 Conclusions

This part of the study showed the remarkable role of deposited urban dirt, especially of deposited OM for adsorption properties of pavement seam materials. The quantity of deposited OM governed cation exchange capacities, surface areas and heavy metal adsorption. So the C_{org} enriched pavement seam material has a much higher filter capacity compared to the original sandy seam filling. Whether this filter capacity is important for solute fluxes can not be evaluated without taking into account the layer thickness of only 1 cm and the similarly deposited contaminations itself.

Compared to natural soils, the pavement seam material can only act as a weak barrier for pollutants travelling through urban pavements toward the groundwater, but it is a hint for the role of urban soils as sinks for pollutants and different forms of C_{org}.

Part III

Flow Paths in Paved Urban Soils

Chapter 5

A New Image Analysis Tool to Distinguish Tracer Colors from Heterogeneous Soils

5.1 Introduction

Because of the strong anthropogenic impact and their dynamic genesis, urban soils are very heterogeneous. They are different from "natural" soils in many aspects. Therefore, they are good test cases for methodology validation. Sometimes these tests fail.

I wanted to use a well established method (Forrer et al., 2000), developed for arable soils, to investigate the flow paths in urban soils. Already the first experiment failed and a new image analysis method had to be developed. The special experimental setup for paved urban soils and the new digital image analysis method are introduced in this chapter.

Digital image processing has been used as a valuable tool for the analysis of dye tracer experiments in both, laboratory and field studies (Forrer et al., 1999; Kildsgaard and Engesgaard, 2002). Besides qualitative description of dye patterns, the quantification of dye concentrations and flow path cross sectional areas are main goals of tracer experiments. Therefore, these are main questions to answer by digital image processing.

The distinction of dye stained pixels from unstained, not through-flown regions by an explicit, objective and reproducible method is an important analyse step. If the contrast between the unstained soil and the dye stained soil region is high, this step might be easy. Obviously, the information content of stained regions is limited in dark soil regions, or if soil and dye tracer emit light in similar wavelengths. Consequently, the application of fluorescent

tracer techniques in soil science was forced (Stadler et al., 2000). However, special equipment is needed for such experiments. It is expensive and makes the experiment design more complex.

That's why, the use of dye tracers like the food dye Brilliant Blue (BB, CI 42090, E133) is favorable wherever possible. Brilliant blue is cheap, non-toxic, easy to handle and well described (Flury and Flühler, 1995). It is suitable for preferential flow tracing, multiple tracing approaches and was used dozens of times in different natural soils and artificial laboratory substrates.

Compared to urban soils, these soils and substrates were either homogeneously colored (Kildsgaard and Engesgaard, 2002) or the soil layering admitted a description of spatial heterogeneities as a function of the soil depth (Forrer et al., 1999). In urban soils, heterogeneity patterns are rarely to describe by such models. The chaotic mixture of light and dark colored soil regions is a characteristic of anthropogenic soils. It is a major barrier for the distinction of dye stained pixels from unstained pixels in digital image processing. A digital image processing method has been developed, which can extract dye tracer information from images of heterogeneously colored soils.

Using this method the application of cheap and harmless dye tracers can be expanded to a greater group of soils which allows systematic investigation of flow pattern types in different soils under different conditions.

5.2 Dye Tracer Experiments

The flow patterns of different urban sites in Berlin have been investigated using BB dye tracer solution (Table 6.1 at page 88). The solution was infiltrated from a pond (3-6$\times 10^{-2}$ m) using a special infiltration frame (1 m$\times$1 m). Thus, the experiment simulated infiltration from a sidewalk pond like it is frequently found in Berlin. After 24 hours, horizontal sections of the soil were excavated using tiny brick trowels and a ruler with water level. The central 0.75 m $\times$ 0.75 m area of each of the sections was photographed including a gray-scale, a color reference, and a frame for geometrical and illumination correction of the later digitized images. I used a reference line and a perpendicular to place the frame exactly in the same relative position in consecutive depths. The pictures were taken with an old fashioned photo camera with a 50 mm lens. The use of such a lens results in little geometrical distortion of the photos. Slide films have been used (Kodak Elite chrome ASA 200). The camera was mounted on a special horizontal tripod construction which allowed to adjust the distance from camera to soil section similar for all pho-

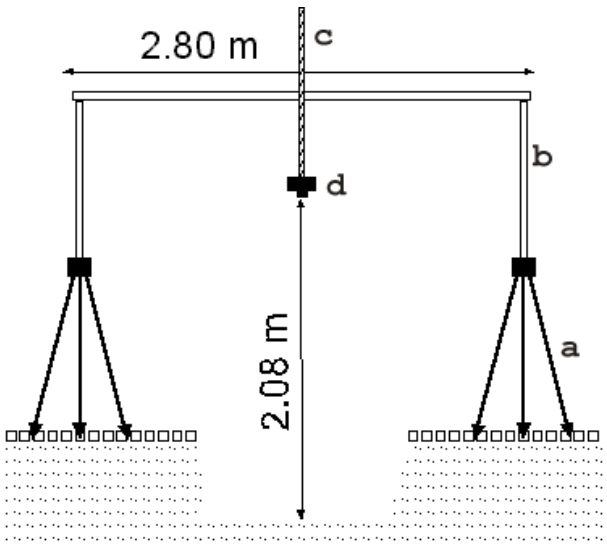

Figure 5.1: Setup for photographing horizontal soil sections after dye tracer experiments; (a) tripods, (b) framework, (c) spindle, (d) camera, (e) distance between camera and soil.

tographs (Figure 5.1). So, the spatial information is the same for pictures from different depths.

After the photo of a prepared soil depth has been taken, soil samples from variously colored soil regions have been taken. The samples were numbered and their locations were documented with a second photo.

In the lab, BB was extracted from the soil samples with a water/acetone (4/1) mixture. The mass of 0.5 g was extracted with 50 ml of the extracting solution using beakers and a vacuum system. Then, the BB contents were photometrically analysed. The calibration included concentrations from 0 to 20 $\mathrm{mg\,l^{-1}}$, the detection limit was 0.1 $\mathrm{mg\,l^{-1}}$.

5.3 Image Pre-processing

The slide films were digitised in a commercial photo laboratory, image files were delivered on a Kodak Photo CD. The images were corrected for geometrical distortion. That includes first, the spatial transformation of pixels using the tie point concept and second, the gray-level interpolation (Gonzalez and Woods, 2002). The corners of the 0.75 m $\times$ 0.75 m section of the gray frame were used as tie points. The gray frame was used for illumination correction (Forrer et al., 2000). The resulting images show the same combination of red, green and blue reflectance values (RGB) for the same color (e.g. at color reference). Prior to these corrections, the image resolution was reduced

to 400 × 400 pixels in order to reduce calculation time. So one pixel represents a quadratic soil area of 3.5 mm^2. All following image processing steps were programmed using the programming language package IDL, version 6.0 (Interactive Data Language, Research Systems, Inc., Boulder, CO, USA).

For dye tracer distribution analysis, "bluish pixels" need to be detected. This sounds trivial, but it is not, if the method should be objective and possibly automatized.

Each of the bluish pixels represents not only the tracer intensity, but also the background color of the soil. Due to mixture of soil and tracer colors not only one distinct blue color, but a wide range of different blue intensities and hues have to be detected. Detecting bluish pixels therefore requires separation of soil colors and dye tracer intensities. This is the objective of this method. When displayed in the RGB color model, the red channel shows the highest BB reflectance, while the blue channel contains almost no tracer intensities but contains the soil color information ((b) in figure 5.2). As it can be seen in this figure, the red channel is not appropriate to distinct stained pixels from unstained. Note the "clown face" in the center of the images.

This effect lead to the idea, to change the color model in order to erase or amplify color information in the different channels. It is the goal, to get an new color model: soil color-soil color-BB (S_1S_2BB) instead of RGB in which the color information caused by BB is perpendicular to the color information caused by the soil colors. The three-dimensionality of the color model implies the need to represent the heterogeneous soil color by no more than two dimensions. Then, one dimension is left for the dye tracer information, which then could be easily separated. So the main step of this image analysis tool is the reduction of the three-dimensionality of the soil colors. Therefore, the channels of the images, or in other words, the axises in the three-dimensional coordinate system must be transformed. This can be realised by an axis transformation. The transformation matrix is obtained from a principal component analysis (PCA), which was done with a set of unstained pixels (I_u). It was derived from the picture itself. The unstained parts of the image excluding bluish pixels has been used. Here, it seems the snake bites itself in the tail, the goal of the whole method seems already reached or necessary. But this first masking step can be rough. Unstained pixels can be excluded as well, as long as no stained pixel remains. It is also possible to use a training set of images of unstained soil sections. The PCA however is conducted with unstained, not bluish pixels. The result of this PCA is a new coordinate system, which reduces the variability of the soil color information to a maximum of two axes. This means, two channels are sufficient to represent the same information as in the RGB image. The

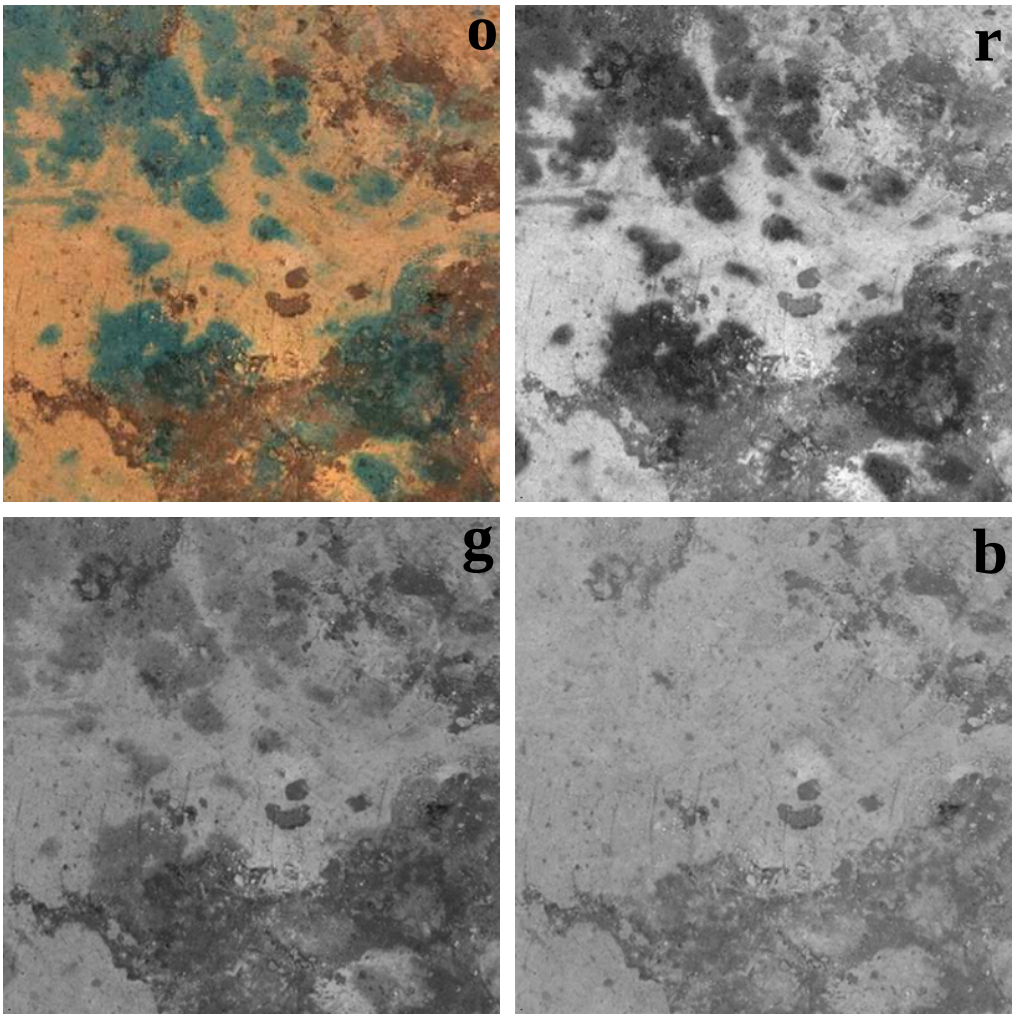

Figure 5.2: Visualization of a horizontal soil section under mosaic pavement at Monbijouplatz, Berlin, depth 11 cm; (o) original RGB image and gray-scale images of (r) the red channel, (g) the green channel and (b) the blue channel.

way, how the axes were transformed in the PCA is described by a transformation matrix. Afterward, a set of pixels including bluish pixels (I_t) is processed based on this transformation matrix. As the result, the BB channel of this S_1S_2BB color model shows only the BB information. The following requirements must be fulfilled to use this method: (i) the soil colors must be mixtures of not more then two colors, in order to be representable by two channels, (ii) the tracer dye must be different from this colors. This is true for BB compared to yellow and brown soil colors, but it might be problematic for red Rhodamin and reddish soil colors. And, (iii) the image subset I_u must represent all soil colors appearing in the image (set I_t). The necessary transformations and calculations are described in detail in the following.

The calculations are done with an RGB image ($I_{(RGB)}$), for example, the image shown in figure 5.2. Such an image has a horizontal resolution (h) and a vertical resolution (v) resulting in the number of pixels $p = v \times h$. In case of the quadratic RGB image MP-11, with a side length of 400 pixels, p is $400 \times 400 = 160.000$ pixels and n as the number of channels is three (Red + Green + Blue). Now, the image can be expressed as a 3 level matrix I [3,400,400] which means the matrix

$$\begin{array}{c} \\ 1 \\ 2 \\ \vdots \\ j = v \end{array} \begin{array}{c} \begin{array}{cccc} 1 & 2 & ... & i = h \end{array} \\ \begin{pmatrix} x_{00} & x_{10} & ... & x_{h0} \\ x_{01} & x_{11} & ... & x_{h1} \\ \vdots & \vdots & \vdots & \vdots \\ x_{0v} & x_{1v} & ... & x_{hv} \end{pmatrix} \end{array}$$

exists 3 times with x=R,G and B.

First, all bluish pixels are erased from the image to get I_u. Therefore, a rough masking is sufficient, the only quality criterion is to exclude all bluish pixels. A corresponding flow path mask (FP) is build after the image was converted into the hue-saturation-value color model (HSV) (Gonzalez and Woods, 2002) where choosing appropriate threshold values for "blue" is more intuitive than in RGB. Here "blue" is equivalent to a number in the hue channel (0 to 360) and is not a combination of red, green and blue.

$$I[(red, green, blue), h, v] \rightarrow I[[hue, saturation, value], h, v] \tag{5.1}$$

$$FP = \begin{array}{c} \\ 1 \\ 2 \\ \vdots \\ j = v \end{array} \begin{array}{c} \begin{array}{cccc} 1 & 2 & ... & i = h \end{array} \\ \begin{pmatrix} x_{00} & x_{10} & ... & x_{h0} \\ x_{01} & x_{11} & ... & x_{h1} \\ \vdots & \vdots & \vdots & \vdots \\ x_{0v} & x_{1v} & ... & x_{hv} \end{pmatrix} \end{array} \tag{5.2}$$

Because the human color perception is the only quality criterion for this step, the security margins should be large. In the 8-bit example image MP-11, pixels with a hue higher than the lower threshold (lt) of 29 and less than an upper threshold (ut) of 190 were excluded. This erased some unstained pixels too. Erasing in this context means that the pixels are set to $(0, 0, 0)$, the placeholder however remains!

$$I(hue, h, v) = \begin{array}{c} \\ 1 \\ 2 \\ \vdots \\ j = v \end{array} \begin{array}{c} \begin{array}{cccc} 1 & 2 & ... & i = h \end{array} \\ \begin{pmatrix} hue_{00} & hue_{10} & ... & hue_{h0} \\ hue_{01} & hue_{11} & ... & hue_{h1} \\ \vdots & \vdots & \vdots & \vdots \\ hue_{0v} & hue_{1v} & ... & hue_{hv} \end{pmatrix} \end{array} \tag{5.3}$$

$$x_{ij} \in FP = 1, where\ lt < hue_{ij} \in I_{hsv} > ut \tag{5.4}$$

Now, that the positions of the bluish pixels (FP), are known, we can extract the subset I_u from I. The subset I_u is transformed into the $n \times p_u$ Matrix, or pixel list, with $p_u = p - FP$

$$I_u : I[3, h, v] \rightarrow I[3, h \times v]\ where\ FP \neq 1 \rightarrow \begin{array}{c} \\ 1 \\ 2 \\ \vdots \\ p_u = \end{array} \begin{array}{c} \begin{array}{ccc} R & G & B \end{array} \\ \begin{pmatrix} R_1 & G_1 & B_1 \\ R_2 & G_2 & B_2 \\ \vdots & \vdots & \vdots \\ R_p & G_p & B_p \end{pmatrix} \end{array} \tag{5.5}$$

Because of the high number of pixels, the remaining unstained pixels should still represent the soil colors. If this requirement is doubtful, the set of unstained pixels can be enlarged by pooling the unstained pixels of different depths. One can also use an independent set of unstained pixels, coming from a second soil profile at the same site but without any tracer treatment. Increasing the color depths from 8 to 16 bit would further increase accuracy, but is increasing computation time also. However, this masking step is a rough and conservative classification, not useful for quantification of flow phenomena because lots of unstained pixels and therefore flow path cross-sectional area is excluded too.

The spatial information of the pixels is conserved by the sequence of the RGB-pairs in the lists. Later, knowing the spatial resolution, the original image can be reconstructed.

5.4 Principal Component Analysis

Now, the image can be treated as a cloud of points (x_{ij}) in the three dimensional space. First of all, it is the aim to move the origin of the coordinate system into the gravitational center of the cloud of points. Therefore, the mean of the columns is subtracted from the individual members of the columns. Thus, the sum of the whole matrix gets zero, while the new axises are still parallel to the original axises. In other words, all points have been moved by the negative of the vector of the center of the cloud.

$$\sum_{i=1}^{p}(R_i - \bar{R}) + (G_i - \bar{G}) + (B_i - \bar{B}) = 0 \tag{5.6}$$

The next step is to conduct the principal component analysis (PCA). Details about PCA can be found in Dunteman (1989). IDL delivers a preprogrammed function to determine eigenvalues and eigenvectors of the matrix. Afterwards it can be diagonalised to get the principal axis transformation. The transformation matrix T_1 is obtained, which transforms the original color model into a new one, which represents soil colors at the first and second axis. For the example MP-11, the first axis explains already about 94 % of the variance of the soil colors. Now, the same transformation matrix T_1 is used to transform the complete original image I including all dye stained pixels ($I_{(RGB)} \rightarrow I_{(XYZ)}$). After that step, the tracer is still represented by all axises. A second PCA is computed with the second and third channel of $I_{(YZ)}$ revealing the transformation matrix T_2 ($I_{(YZ)} \rightarrow I_{(S_2BB)}$). After that transformation the dye tracer information is represented in the BB channel, while the second channel S_2 contains only noise.

The channel BB can now be used for separating dye stained pixels from unstained pixels by setting only one threshold instead of two like described above. The success of this method can be seen in figure 5.3, where the histogram of the BB channel is compared to that of the red channel of the RGB image. In case a, the single threshold was set to separate regions. In the corresponding image it can be seen, that dark soil regions and stained soil regions cannot be separated. Both are included in one of the two peaks of the histogram. Here, it is difficult to find a threshold for separating bluish from unstained pixels. In case b, although the histogram of the BB channel shows three peaks, bluish pixels are separated from unstained pixels and only one threshold must be found (the two peaks represent two different intensities). In the corresponding color images it can be seen, that the separation is more accurate in case b. Note, that in this figure the threshold is still subjectively set and the resulting flow path mask is still imprecise. How the threshold can be set objectively is described in the following.

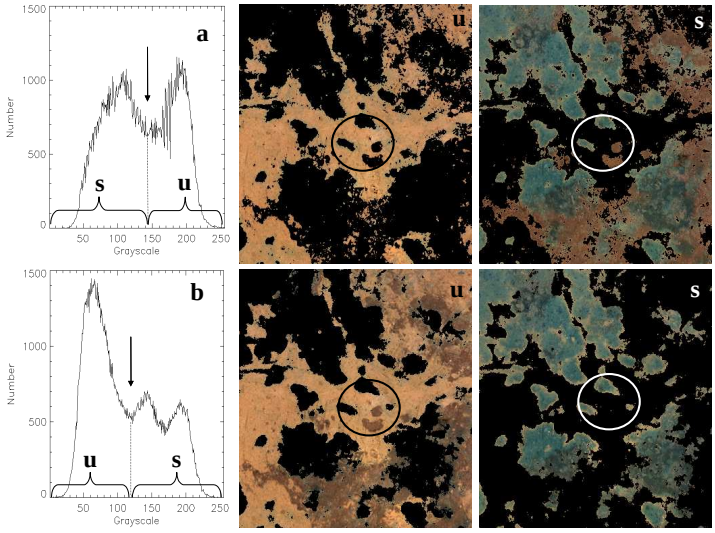

Figure 5.3: Successful colour discrimination using the new method. Comparison of histograms of a) red channel of the original image and b) BB channel of transformed image; u=unstained, s=stained.

5.5 Objective Flow Path Separation - Setting Thresholds

If the image is processed in the above described way, finding the threshold for histogram supported separation can be done objectively by employing the BB concentration data from analyzed samples. In figure 5.4 the correlation between BB concentrations of the samples and corresponding gray scales values (7×7 pixel regions arithmetic average) is shown for the example section Engeldamm in the depth of 50 cm (ED-50). The intersection of the trend line BB vs. gray-scale marks the threshold between stained and unstained pixels. Using this threshold, two masks can be build which allow to divide the original image into stained and unstained regions.

For the quantification of flow path cross sectional areas, the described histogram calculation alone is sufficient. The number of stained pixels is extracted and set in relation to the total number of pixels which results in the relative flow path cross sectional area.

5.6 Conclusion and Outlook

Because of the great heterogeneity of the colors of urban soils, already published digital image processing methods for dye tracer experiment analysis

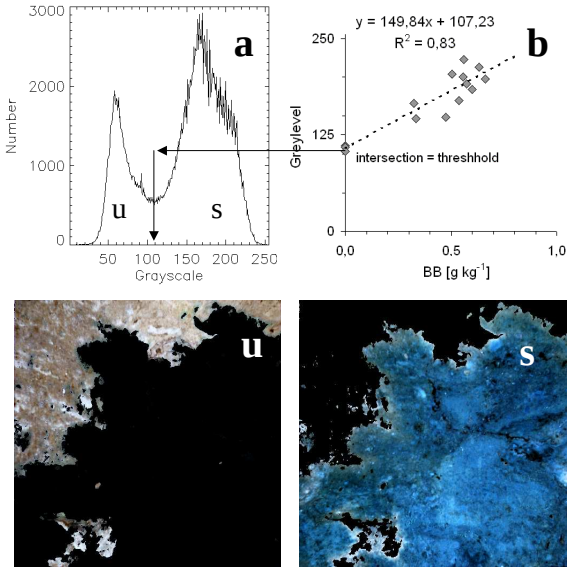

Figure 5.4: Method to objectively find thresholds to discriminate flow regions from non-flow regions using BB concentration data; figure a) shows the histogram of the BB channel of the processed image ED-50, b) shows the correlation of gray-scale values of the BB channel vs. BB concentration of the according points and the resulting threshold which divides the histogram in a) into unstained u) and stained s) parts of the original image.

were not able to seperate stained from unstained soil regions. Thus, a new method was developed, which uses the principal component analysis to transfrom the original RGB - image into a new color model, where the soil colors and the dye color are perpendicular. Thus, it allows to seperate soil colors from dye colors. By analising dark and light soil colors at the same time, the new method can be used for all soils and for horizontal as much as for vertical trenches. The method is the prerequisite to map dye tracer intensities in order to identify dye tracer concentrations from digital images. The whole dye tracer method is limited to soils, which´s colors are light enough to allow the visual detection of the dye. Paved urban soils with their great portions of technogenic sands are good observation objects.

Chapter 6

Preferential Flow in Paved Urban Soils

6.1 Introduction

Pervious pavements cover already a great portion of urban areas and are promoted as a good compromise between soil sealing and rain water infiltration (Wellner et al., 1997). The legal regulations in Germany encourage building principals and architects to use pervious sealing. Tax reductions are awarded to those, who reduce sealing by pervious sealing instead of impervious sealing (German law about Building activity, BauGB § 1, Abs.6 and the according regulations in the several counties). Yet, it is unknown how this kind of pavements qualitatively influence water movement in the soil below. Water flow simulation models like HYDRUS-2D (see 7.2.1) predict a homogeneous flow field.

Having a closer look at the pavement and the pavement system, it is obvious that due to the distribution of seams and pavers infiltrating water initially is canalized. This influence can be small in case of a mosaic pavement with a high seam percentage or may be greater in case of a cobblestone pavement, where the seam percentage is smaller. However, no experimental data are available about flow paths in pavements. It is hypothesized, that the pavements introduce heterogeneous flow path patterns, corresponding to the seam geometry, which can be still found in greater soil depths.

For a ground water pollution risk assessment, the flow characteristics in the corresponding soils must be known, because preferential flow phenomena substantially influence flow path cross sectional areas. Therefore, adsorption and breakthrough times are strongly dependent on the flow patterns.

In trend-setting and well remarked dye tracer experiments, it was shown

that preferential flow is not an exception but the rule for all soils except for sandy soils (Flury et al., 1994). In the decade afterwards, dye tracer experiments substantially contributed to our current knowledge of flow patterns and flow mechanisms in the vadose zone (Forrer et al., 1999). In subsequent studies, it was shown, that preferential flow paths can be very stable for long times (Hagedorn and Bundt, 2002).

A method to visualize flow paths in soils is to stain them by infiltration of dye tracers. Compared to conservative invisible tracers like chloride or bromide, the food dye tracer Brilliant Blue (BB) is sorbed much stronger. Therefore, it is not appropriate to predict the fastness of water movement but is an appropriate model substance for sorbing pollutants like heavy metals or pesticides (Flury and Flühler, 1994). The main advantage compared to invisible tracers is that the spatial resolution of sampling can be higher and sampling is much easier. One has just to take a picture (Flury and Flühler, 1995; Kasteel et al., 2002).

The aim of this part of the study is to give an overview about the shape of infiltration patterns in paved soils and to quantify the through flown cross section areas using the method described in chapter 5 in order to get a data base for simulating solute transport with consideration of the flow patterns. Thereby, it is hypothesized that the shape of the seams can be found in the shape of the dye patterns, which means that the pavement introduces heterogeneous flow.

6.2 Materials and Methods

The dye tracer experiments were conducted at five sites in Berlin, which are introduced in table 6.1. For further details concerning experiments see the materials and methods section in chapter 5 at page 75. The biggest experimental challenge was always to seal the infiltration frame against the pavement. Gypsum and different kinds of construction glues like silicon has been employed but a complete sealing was never reached. Due to that problem, it is not possible to calculate mass balances or to compare the experimental travel depth of the dye with the predicted travel depth in case of homogeneous infiltration. Due to the same problem, the measurement of infiltration rate was not possible. A infiltration ring has been placed on the pavement which can be seen the images. Another problem was the heat in summer of 2003 which let the time domain reflectrometry device collapse, so that there are no measurements of soil water content.

After the images were taken, digitized and processed as described above, the relative cross-sectional area was determined by automatized counting of

Table 6.1: Sites in Berlin, were dye tracer experiments were conducted.

Site	label	pavement	paver dimension
Ebelingstrasse	EB	concrete slabs	30×30×5 cm
Engeldamm	ED	cobble stones	18×10×18 cm
Grosser Stern	GS	big mosaic stones	6 to 8×6×6 cm
Monbijouplatz	MP	small mosaic stones	1 to 4×4×5 cm
Pflügerstrasse	PF	cobble stones	20×18×18 cm

the stained versus the unstained pixels. Additionally, the shapes of the flow paths have been visualized by black/white figures.

6.3 Results and Discussion

The original images are shown in figures 6.1 and 6.2. Furthermore, the results of the image processing method are demonstrated in figure 6.3 for three of the sites.

The great heterogeneity of the soil in the horizontal sections can be seen at the original images. In non of the cases the simulated water infiltration pattern could be found. In opposite there were dry regions directly below the pave stones. This effect was most pronounced at the sites Engeldamm and Pflügerstrasse. The pave stones had greater dimensions than the mosaic pavement at the sites Grosser Stern and Monbijouplatz. The effect was rarely to observe at site Engeldamm. Here, a gravel layer has been placed below the pave stones which has been especially done to guarantee the pavement stability against heavy duty vehicles. However, according to newer construction regulations this kind of construction is required for all kinds of pavements nowadays. Such a layer has only been found at Engeldamm. The other pavements were constructed with a thin sand layer above the autochthonous urban soil. In case of Ebelingstrasse this urban soil consisted mainly of loamy sand, in all other cases, sand with different amounts of OM has been found.

It has been hypothesized, to find the patterns of the seams again in the flow patterns of the dye tracer. Such patterns could be found at the site Pflügerstrasse and Ebelingstrasse. The patterns of the site Pflügerstrasse profile can be clearly explained by the seam geometry. Below 19 cm a pattern of lines and right angles can be seen, which correspond to the seams.

At the site Ebelingstrasse, a pond in the sidewalk has been searched and used for the experiment. In EB-5 and EB-11 the same behavior like for the site PF can be found. The dye tracer distribution is also clearly coupled to

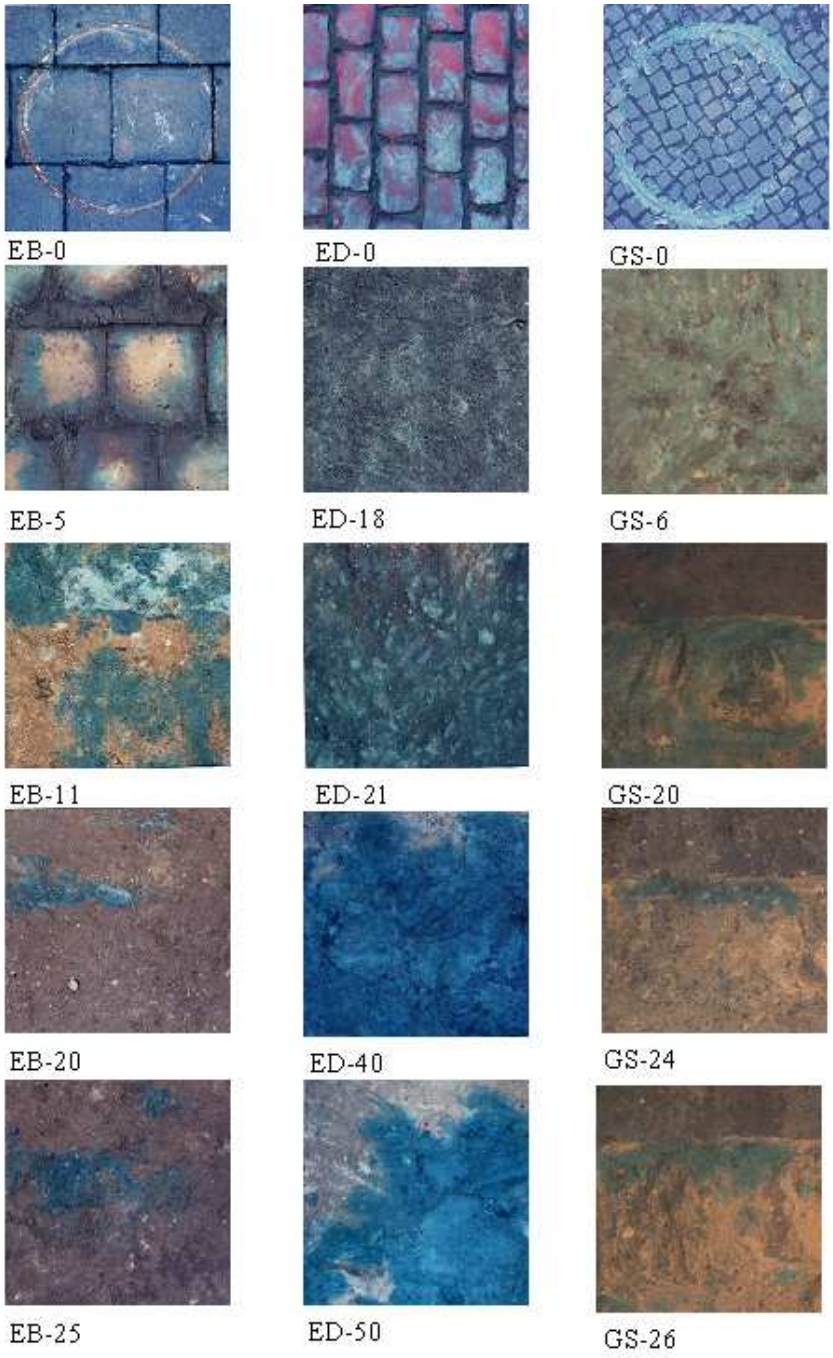

Figure 6.1: Original images of flow path patterns stained by dye tracer Brilliant Blue in urban soils under pavements at the sites Ebelingstrasse EB, Engeldamm ED, Grosser Stern GS, numbers following the site labels indicate depth in cm.

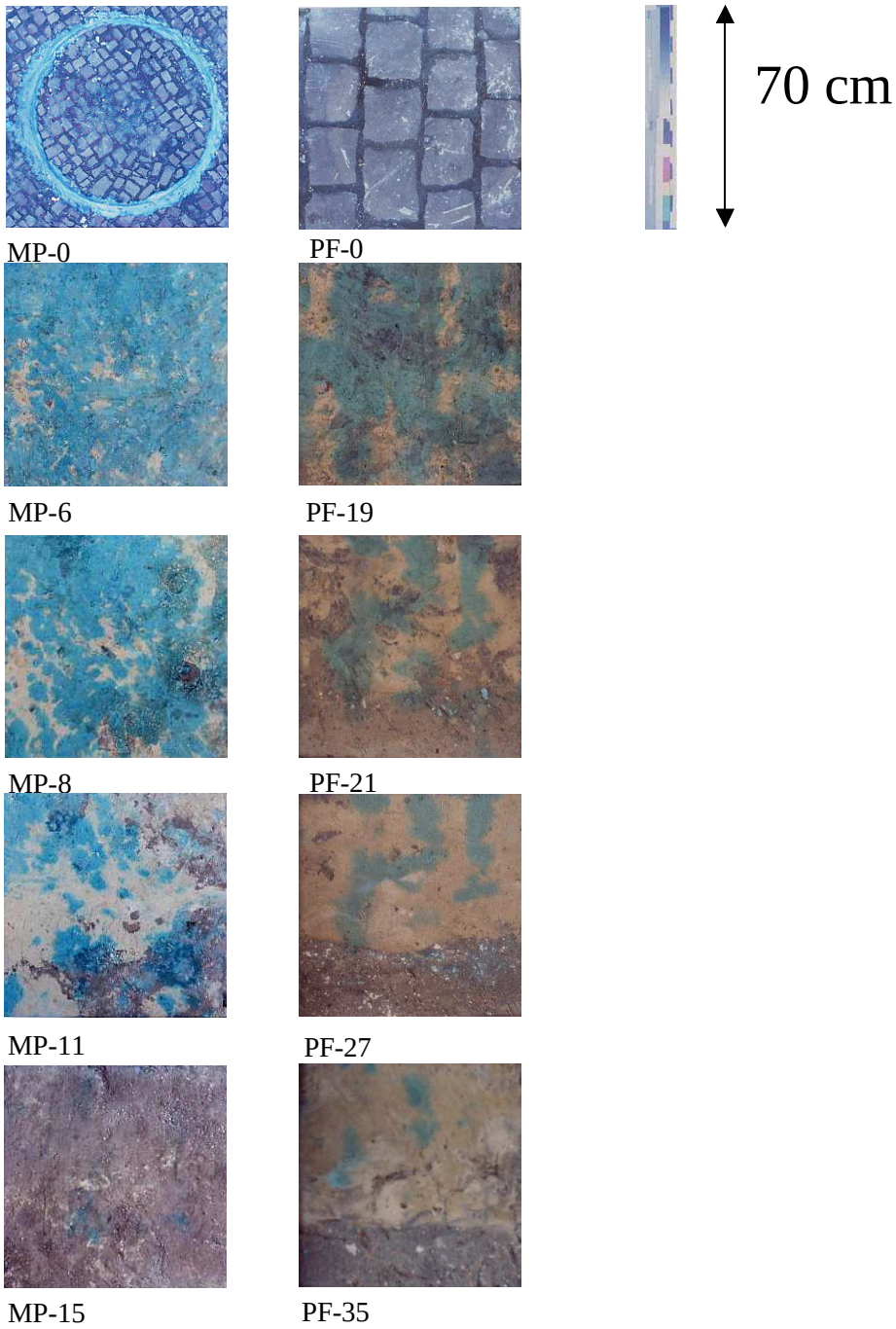

Figure 6.2: Original images of flow path patterns stained by dye tracer Brilliant Blue in urban soils under pavements at the sites Monbijouplatz MP and Pflügerstrasse PF, numbers following the site labels indicate depth in cm.

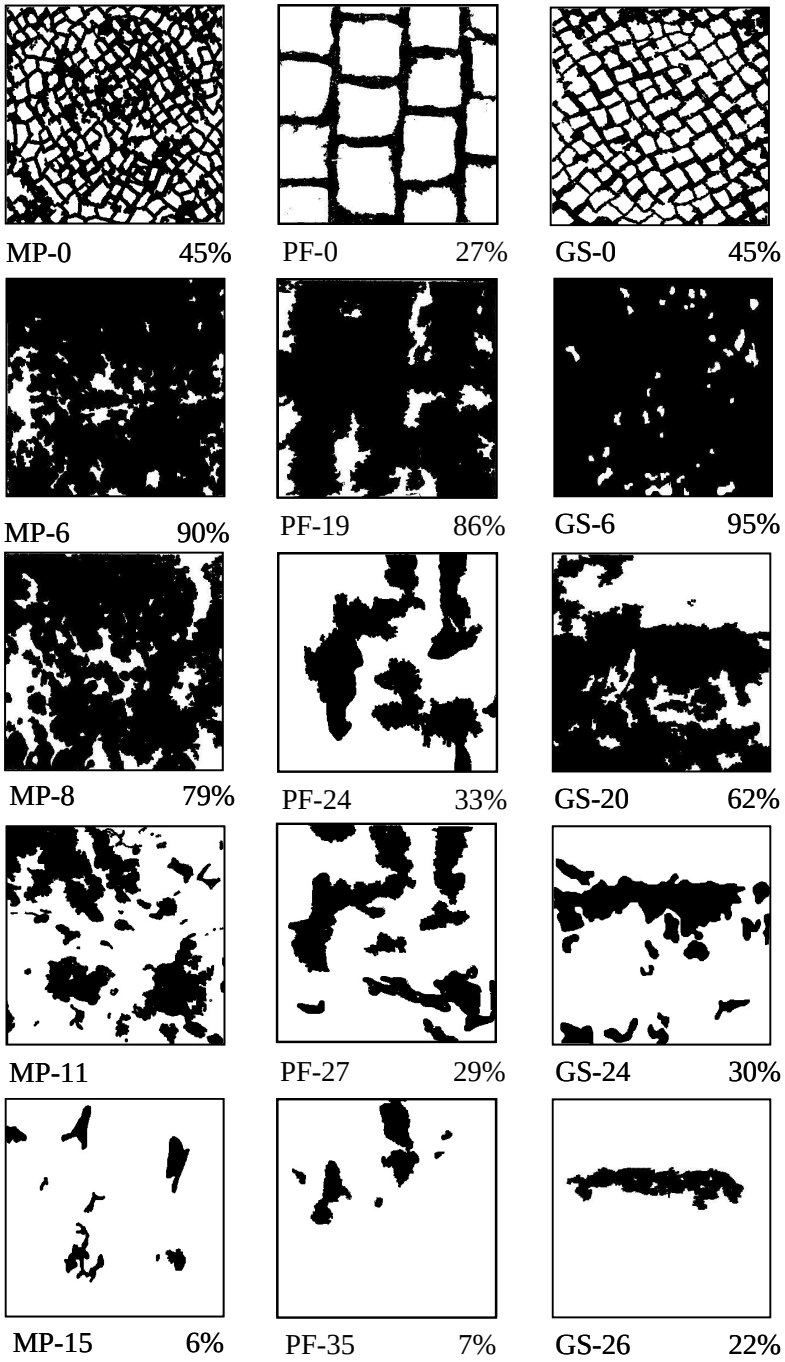

Figure 6.3: Binary images of the flow paths in paved urban soils at Monbijouplatz MP, Pfluegerstrasse PF and Grosser Stern GS, numbers following the site label indicate depth in cm, the flow path cross-sectional area is given in percent.

the pavement seams. In the greater depths, these patterns are no longer that pronounced. Now, the pond situation might be of more influence. The dye tracer can be found mainly along only one horizontal running seam and the intersection of a vertical seam with this seam (Figure 6.2).

At the site Engeldamm the soil material below the pave stones was to dark to see the tracer. However, one can distinguish differently stained patterns in the layer ED-18 which might have been caused by the seam geometry of the pavement. Below that first layer, a gravel layer followed and the patterns in the deeper layers cannot be explained by the geometry of the pavement seams. Here the gravel layer functions as a redistribution layer and allows more or less homogeneous infiltration. This is a good example for a technical measure, which inhibits preferential flow under pavements, although it has been introduced because of stability reasons.

The dye patterns in the mosaic paved profiles show a heterogeneous distribution of infiltrating water too, but here the patterns are small compared to the investigated cross section and the seam geometry is to chaotic to find a correlation between seam geometry and flow patterns. Furthermore, although heterogeneously, compared to the other sites, the infiltration at Monbijouplatz and Grosser Stern would be characterized as rather homogeneous, at least in MP-6 and GS-6. In greater depths, the patterns become more heterogeneous. The geometry of the seams is less important than other soil characteristics. At the site Grosser Stern, for instance, one can see a dark colored region in the upper part of the images. This is the autochthonous urban soil material which can be found also elsewhere, while the light sand was inserted after the installation of a electrical power supply line. The water run rather through the greater pores of the construction sand than through the OM enriched dark soil material. A depletion in the pavement situated in the center of the infiltration frame may have additionally influenced the pattern. However, in case of site Grosser Stern, after the water first infiltrated homogeneously, preferential flow patterns can be found in greater depths.

The same is true for the site Monbijouplatz, although such patterns are not that pronounced here. Until 8 cm the infiltration pattern looks rather homogeneously. Then, the water begins to prefer only a few spots for infiltration.

Besides the qualitative observation of preferential flow patterns, its quantitative measurement is important to get data for simulations. In figure 6.3 three examples for results of the image processing method, described in chapter 5 are demonstrated. If the relative cross sectional areas are plotted against the soil depth, one nearly gets the shape of a infiltration front (Figure 6.4).

In all demonstrated cases, the cross-sectional area increased after the passage of the pavement layer due to lateral dispersion. Then the cross

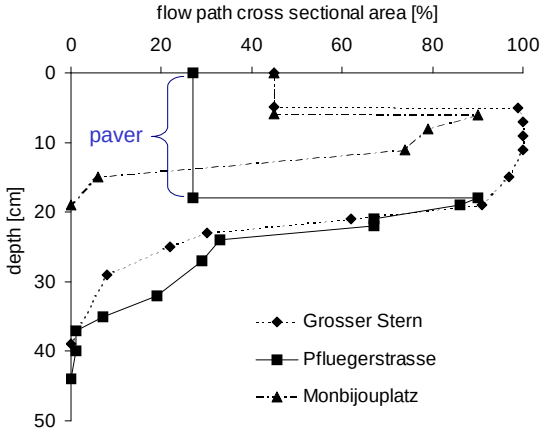

Figure 6.4: Depth profiles of the flow path cross sectional area at the sites Monbijouplatz, MP, Pflügerstrasse PF and Grosser Stern GS.

sectional areas decrease. In case of site Pflügerstrasse one can detect a part in the profile where the flow path area is not decreasing from one depth step to the next, this is between 20 and 22 cm, where the flow path area is around 66 %. Here, this might be the flow path area at steady state conditions. In the other cases, the horizontal resolution of the experiment was too small to detect such a condition in the data.

6.4 Conclusion

The results of this part of the study show the relevance of preferential flow phenomena in paved urban soils. The hypothesized preferential flow could be found at all sites. However, only under special conditions the flow patterns of the dye tracer follow the pavement seam geometry. These are great pave stones and small seam percentage. It is expected to find a certain relationship between pavestone width and seam depths, which introduces preferential flow. Due to different other conditions, preferential flow has been found regularly under pavements except for a site where a gravel layer was introduced under the pavement. Considering the high number of ponds at older pavements, one gets an idea about the importance of water accumulation processes and preferential flow for solute transport processes.

Part IV

Heavy Metal Transport in Paved Urban Soils - a Risk for the Groundwater?

Chapter 7

Prognosis of Longterm Heavy Metal Transport in the Pavement System

7.1 Introduction

Models are used to describe natural systems by reducing their complexity. This reduction is the advantage and the disadvantage of models. They will never be able to predict the whole truth but they allow at least to approximate it. Simulations are tools to ask and answer questions about models. Thereby, the advantage of a simulation is, that results of processes which take place in long timespans in nature can be predicted. Furthermore the influence of varying boundary conditions can be assessed. Therefore, simulations are often used for risk assessment.

Because of the great heterogeneity of urban soils and varying circumstances in different cities, even quarters in one city, the simulation of a contaminant breakthrough at a certain site is dependent on the individual urban soil profile with its past pollutions, the depth of the groundwater table, etc. Thus, it would be a case study with no relevance for other sites.

Instead, the heavy metal displacement was simulated only for the pavement system. It is a technical normed compartment, which can be generalised for the simulation and which can be found in similar types everywhere in Germany. It is the part which is mainly influenced by the pavestones, seam materials, and construction sand, which have been studied in this work. The results of such a simulation can be used as a input for individual investigations at different sites with their specific underlying soils. The simulations are also used to evaluate the influence of the seam material, construction

sand, infiltration rates and preferential flow patterns on the HM displacement. There is especially the question, whether seam material can substantially influence the system characteristics. Therefore, the following questions about the pavement system should be answered by appropriate simulations:

1. What is the retardation capacity of the uncontaminated construction sand and seam material (if such would exist)?

2. How would the incorporation of BC change the heavy metal retardation capacity of seam material in time?

3. What is the remaining retardation capacity of construction sand and seam material, if realistic actual heavy metal concentrations are concerned?

4. How is the retardation capacity of the whole pavement system influenced by preferential flow patterns?

5. Is there a risk regarding opening sealed soils and promoting pervious sealing for urban areas from heavy metal inputs through the pavement?

Question 1 and 2 are necessary to assess the retardation capacity of the depositions in the seam material. Thereby, it is assumed that the contaminations are not interfering the positive impacts of OM depositions. As discussed above, there seems to be an equilibrium between deposition of material in the pavement seams and its erosion due to natural impacts and street cleaning. Question 2 is intended to demonstrate the result of unhindered accumulation of dust in the pavement seams.

Question 3 assesses the remaining retardation capacity considering background contaminations. This is important to answer the question if seam material acts as a source or a sink for HMs under realistic conditions, because obviously OM is deposited together with HM contaminations.

Question 4 is asked to learn about the influence of reduced through flown cross sectional areas due to preferential flow, resulting in higher effective water flow velocity and reduced number of involved adsorption sites.

The questions have been answered by simulating different scenarios consisting of different soil profile geometries and boundary conditions. The simulations were calculated for Pb and Cd. Therefore, toxic, differently mobile heavy metals have been investigated. Because of toxicity, the results are relevant. Because of the high mobility of Cd and the low mobility of Pb, the results represent a minimum-maximum approximation, which can be transferred to other heavy metals with known mobility.

7.2 Materials and Methods

7.2.1 The Model

The linear and two dimensional HYDRUS simulation software packages were used to simulate water and heavy metal transport. The hydrological and chemical models which are used, are described in detail by Simunek et al. (1999). The important features are outlined in the following. Both programs numerically solve the Richard equation (Hillel, 1998) for saturated and unsaturated water flow:

$$\frac{\partial \Theta}{\partial t} = -\nabla \bullet [K(\Psi)\nabla\Psi] + \frac{\partial K}{\partial z}, \tag{7.1}$$

where Θ is the volumetric water content, t is time, z is the vertical coordinate (positive upward), Ψ is the matric potential, K is the hydraulic conductivity. A solution of equation 7.1 requires the knowledge of relations between Θ, Ψ and K as well as initial and boundary conditions. In the HYDRUS-1D software, the solution of the equation is forwarded to the next node in the line, in the HYDRUS-2D Software a two dimensional mesh is generated, and the solutions for the individual mesh nodes are forwarded to all neighbours.

For simulation of the solute transport, the convection-dispersion equation is solved:

$$\frac{\partial C}{\partial t} + \frac{\rho_B}{\Theta}\frac{\partial C_S}{\partial t} = \frac{\partial}{\partial z}\left[D\frac{\partial C}{\partial z}\right] - \frac{q}{\Theta}\frac{\partial c}{\partial z}, \tag{7.2}$$

where, C is the solute concentration in the liquid phase, C_S is the solute concentration in the soil phase, D is the effective dispersion coefficient and q is the specific flux rate. The transport equations also include provisions for linear and nonlinear equilibrium and non-equilibrium reactions between the solid and liquid phases. For nonlinear adsorption both Freundlich's theory as well as Langmuir's theory can be chosen to describe the data. The governing flow and transport equations are solved numerically using Galerkin-type linear finite element schemes.

The main advantage of the software package in the context of this study is the option to easily create and manipulate the two dimensional geometry of the soil region in HYDRUS-2D. So it is possible to model vertical and horizontal heterogeneous soil horizons. Therefore, this software is appropriate to model water and solute fluxes concerning the special spatial distribution of soil characteristics in a paved urban soil containing layers, pavers, stones and no-flow regions to consider preferential flow (Figure 7.1). However, movement of free water in cracks or macro pores cannot be simulated with the model.

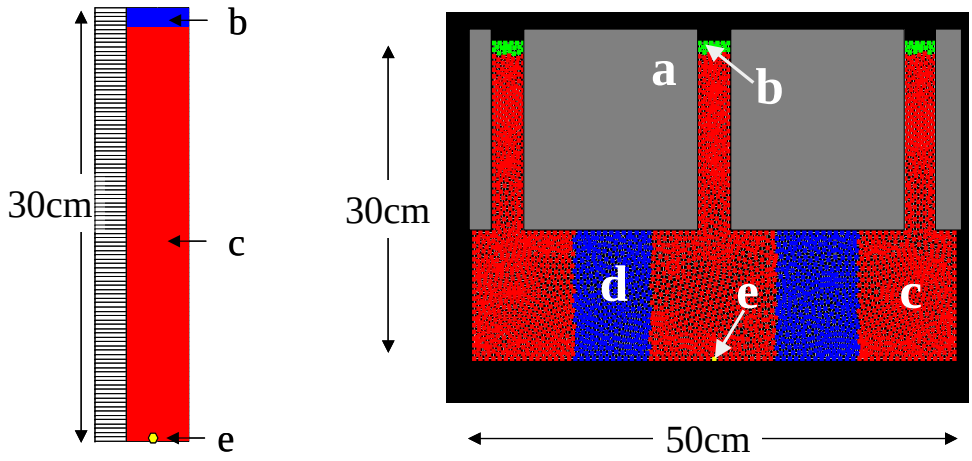

(a) HYDRUS-1D (b) HYDRUS-2D

Figure 7.1: Model geometries used for simulations of water and heavy metal fluxes in pavement urban soils. A vertical section of a cobble stone pavement was reconstructed. Thereby a) is the impervious paver, b) is the 1 cm thick seam material, c) is the construction sand, d) is the area, not through flown if preferential flow is considered, and e) marks the observation node.

7.2.2 Scenarios and Simulations

The impacts of seam material, preferential flow phenomena and source/sink function has been studied using a system of different scenarios. By comparing pairs of scenarios, the impacts of above mentioned compartments and processes are assessable. To assess e.g. the impact of the potential adsorption capacity the scenarios "potential of sand" and "potential of seam material" are compared. The scenarios are presented in table 7.1. In the following, it is explained, how these scenarios are realized in the simulations.

Use of the Software Packages

For the scenarios 1 to 4 the HYDRUS-1D package has been used, because the results of the simulations are not influenced by geometry features. The numerical solution of the non linear adsorption of heavy metals can be calculated with mass balance errors smaller than 1 % in a short computing time of less than three minutes.

Pictures of soil profiles of site B10 have been taken as example for the model geometry. The three different soil compartments can be effectively enabled and disabled by giving them different or the same soil parameters. For instance, for simulating scenario 1 "potential of sand" all three com-

Table 7.1: Scenarios and their aims for modelling heavy metal transport in the pavement system of partially sealed urban soils.

Scenario	Simulated features	Aim and applied software
1 potential of clean sand	sand, no seam material, heavy metal transport into uncontaminated sand column	assess role of construction material as filter, HYDRUS-1D
2 potential of clean seam material	uncontaminated seam material, heavy metal transport into column of seam material	assess potential of construction material as filter, HYDRUS-1D
3 realistic sand column	contaminated construction sand, heavy metal infiltration	realistic influence of sand, HYDRUS-1D
4 realistic soil column	contaminated seam material and sand, realistic solute concentration	assess role of materials as sources and sinks, HYDRUS-1D
4a realistic soil column with increased BC content	seam material after 60 years of BC accumulation	assess potential of BC as retarding agent, HYDRUS-1D
5 homogeneous flow	uncontaminated pavement system, assuming homogeneous flow	assess the impact of reduced flow cross section due to pavers, HYDRUS-2D
6 preferential flow	uncontaminated pavement system, considering preferential flow	assess the impact of preferential flow, HYDRUS-2D

partments are given the same hydraulic and reaction parameters, so there is virtually only one material involved. Thus, one model geometry could be used for all simulations and must not have been changed.

The scenarios have been compared by comparing the travel time of the solutes. Thereby, the travel time is the time necessary to detect the plume at the lower end of the soil column. The individual observation nodes are marked in figure 7.1.

Measurements of Saturated Conductivities

The saturated conductivity, K_s, can be approximated using Mualem-van Genuchten parameters which were fitted to the experimental determined water retention function. It can also be determined experimentally, which was done here. $100\,\mathrm{cm}^3$ metal cylinders have been filled with seam material according to the measured bulk densities. The construction sand has been sampled undisturbed. After saturation of the samples an overhead of water has been applied to the cylinders and the resulting water transport velocity has been measured. Solving Darcy´s law revealed K_s (Hillel, 1998). For the seam material, a K_s of $715\,\mathrm{cm\,d^{-1}}$ (SE=12 %) and for the construction sand it was $374\,\mathrm{cm\,d^{-1}}$ (SE=8 %).

Hydraulic Parameters

Water balances were not studied at the investigated sites. Therefore, the following assumptions has been used. Groundwater recharge rates of $120\,\mathrm{mm\,a^{-1}}$ (Wessolek and Renger, 1998) and of $480\,\mathrm{mm\,a^{-1}}$ (simulating infiltration from ponds) were applied. Furthermore, the open seam area of 27 %, measured at site B9, was included to get the daily groundwater recharge rates of 0.12 and $0.48\,\mathrm{cm\,d^{-1}}$ for the open seam area as the net infiltration rate at the upper boundary. Thus, evaporation was not simulated but is regarded as the groundwater recharge has been applied as an infiltration rate. The water flow was not simulated but realized by accordingly chosen boundary conditions and derived effective parameters for the site B9: K_s^* of 0.12 and $0.48\,\mathrm{cm\,d^{-1}}$, respectively and pressure heads of 0 cm for the upper and lower boundary conditions. The according artificial saturated water contents, Θ_s^* corresponded to K_s^* and was derived from $K(\Psi)$ and $\Theta(\Psi)$ functions fitted to measured porosity (Nehls et al., 2006) and K_s data (Figure 7.2, Table7.2).

Reaction Parameters

The solute concentrations of the infiltrating surface run off have been taken from Gromaire-Mertz et al. (1999) and can be found in Table 7.2. The

Table 7.2: Simulation input parameters used for the HYDRUS models according to the described scenarios.

general model parameters									
length unit: cm, time unit: day, mass unit: mg length of the column 20 cm number of nodes HYDRUS 1D:101 finite elements mesh HYDRUS-2D: 4139 nodes									
	seam material				construction sand				no-flow region
soil hydraulic parameters									
Θ_r $\left[cm^3\,cm^{-3}\right]$	0.117				0.058				0.058
Θ_s $\left[cm^3\,cm^{-3}\right]$	0.527				0.424				0.058
α $\left[cm^{-1}\right]$	0.034				0.058				0.058
n $[-]$	1.514				1.401				1.401
K_S $\left[cm\,d^{-1}\right]$	715				374				
ρ_B $\left[g\,cm^{-3}\right]$	1.16				1.51				1.51
arbitrarily adjusted water flow parameters in the model									
$\Psi_u = \Psi_l$ $[cm]$	0								
$K_S*_{1,2}$ $\left[cm\,d^{-1}\right]$	0.12, 0.48								
Θ_s* $\left[cm^3\,cm^{-3}\right]$	0.264 for K_S*_1 (0.298 for K_S*_2)				0.231 for K_S*_1(0.265 for K_S*_2)				
adsorption parameters									
	B1	B2	B4	B9	B1a	B2a	B4a	B9a	
$K_f(Pb)$ $\left[mg^{1-m}\,L^m\,kg^{-1}\right]$	2638	2133	1321	1416	499	272	833	738	1
$m(Pb)$ $[-]$	1.00	1.00	0.45	0.62	0.92	1.00	0.55	0.62	1
c_{Pb}(soil water) $\left[mg\,L^{-1}\right]$	0	0.22	0.02	0.04	0.04	0.46	0.01	0.01	0.3
c_{Pb}(rainwater) $\left[mg\,L^{-1}\right]$	0.3								
$K_f(Cd)$ $\left[mg^{1-m}\,L^m\,kg^{-1}\right]$	20.38	16.95	19.37	15.18	6.92	5.41	5.66	8.61	1
$m(Cd)$ $[-]$	0.70	0.38	0.62	0.28	0.63	0.41	0.40	0.34	1
c_{Cd}(soil water) $\left[mg\,L^{-1}\right]$	0.013	0.020	0.004	0.020	0.023	0.013	0.020	0.019	0.01
c_{Cd}(rainwater) $\left[mg\,L^{-1}\right]$	0.01								

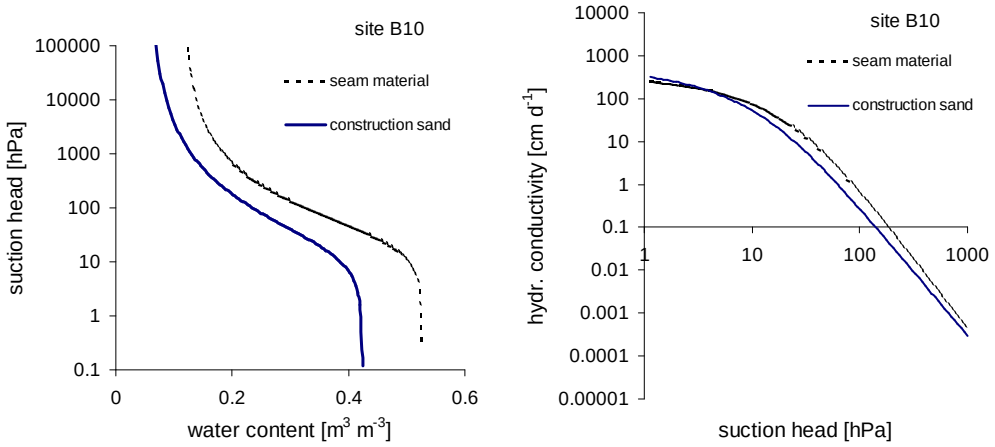

(a) (b)

Figure 7.2: Water retention function (a) and hydraulic conductivity (b) for seam material and construction sand at the site Pflügerstrasse, Berlin.

initial concentrations have been set to 0 for the clean material. For the contaminated material, liquid concentrations were applied (see Table 7.2) which have been measured as one of the steps of the adsorption isotherms. For the calculation of the solute transport itself, the investigated Freundlich parameters (same Table) have been applied.

7.3 Results and Discussion

For the groundwater recharge rate of 120 mm a^{-1}, the simulated displacement times vary from 315 to 2350 a for Pb and from 37 to 253 a for Cd (Table 7.3). At the site B2, the measured Pb concentration for the liquid phase in the soil is already higher than the chosen concentration in the rainwater runoff (which was rather too high than too low). For Cd, however all sites show higher soil water than rainwater concentrations. In these scenarios, every rainfall is a net HM displacement! Apart from these cases, the positive filter effects of urban depositions, which were already discussed by means of retardation factors, could be approved by the simulations for all cases but one. As in the simulations, apart from adsorption behaviour, also the different soil hydraulic properties and densities were considered, the effect of the smaller dry bulk sensity of the seam material can compensate the effect of stronger adsorption. The displacement of Cd at the site B4 is the one example. If the scenarios 1 and 2 for the site B4 are calculated with the

Table 7.3: Simulated heavy metal displacement through a 20 cm paved soil column at different sites in Berlin. [a] The travel times indicate the period which is needed to recover 95 % of the applied concentration at the lower boundary of the soil column.

Scenario	Pb				Cd			
	B1	B2	B4	B9	B1	B2	B4	B9
	travel time[a] [a] for 120 mm a^{-1}							
1 (potential of clean sand)	610	315	1253	1072	37	92	100.8	176
2 (potential of clean seam material)	2350	1901	1603	1578	90	185	83	253
contaminated seam material	2350	1315	1341	1392	0	0	60	0
3 (realistic sand column)	584	0	1159	1016	0	0	0	0
4 (realistic soil column)	588	0	1158	1008	0	0	0	0

original seam filling's dry bulk densities, the travel time for the seam material would be 27 a and therefore higher than that of the original seam filling. So except for the displacement of Cd at the site B4 we conclude that in general, the seam material has a positive impact on the retardation of Cd and Pb. Although the impact is detectable, it is not very high and the formation of only 1 cm thick layer of seam material leads not to substantial longer travel times. However, the potential of the urban dirt as a Pb filter is clearly to be seen if the scenarios "contaminated seam material" are compared to scenarios 1: even contaminated seam material is a much better filter than any clean construction sand can be. For Cd, the background contamination is that high, that both seam material and original construction sand act rather as a source than as a sink. For Pb however, the calculated traveltimes do not imply an acute risk of groundwater contamination.

Because of the abundance of ponds at streets and sidewalks in urban areas, we simulated the infiltration of accumulated rainwater runoff from ponds. Realizing a higher infiltration rate of 0.48 instead of 0.12 cm d^{-1} influences the soil water content and therefore the pore water velocities. However, the average ratio between the traveltimes for 120 mm a^{-1} and 480 mm a^{-1} is 1:4. This is mainly due to the fact, that the differences in the water content caused by the different water conductivities (0.12 and 0.48 cm d^{-1}) are described by the quasi-linear behaviour in the according sections of the functions $K(\Psi)$ and $\Theta(\Psi)$.

For 480 mm a^{-1}, the calculated traveltimes range from 10 to 100 a for Cd. As the pavements at the investigated sites were constructed from the early 1900s on, a substantial amount of heavy metals may already have left the

Table 7.4: Results of simulations of different scenarios for the heavy metal transport considering preferential flow at the site B9

Scenario	travel time in years	
	Pb	Cd
1 potential of clean sand	1072 (+6 %)	176(-2 %)
2 potential of clean seam material	1578 (+57 %)	253(+41 %)
3 contaminated sand column	1016 (+0.8 %)	0
4 contaminated soil column	1008 = 100 %	179*=100 %
4a potential of BC accumulation	1038 (+3 %)	-
5 homogenous flow through contaminated pavement	100 %	100 %
6 preferential flow through contaminated pavement	-3 %	-39 %

upper soil layers. The displacement risk for Pb even from ponds is rather low. However, the simulated infiltration from ponds shows the high importance of non-uniform infiltration in urban areas. It therefore underlines the need of knowledge on soil surface properties for realistic risk assessments, e.g. for more mobile substances such as glyphosate (Kempenaar et al., 2007).

The effect of the immobile soil regions due to preferential flow patterns can be seen in table 7.4. In the following, the results are discussed separately for the two heavy metals.

7.3.1 Pb Transport Considering Preferential Flow Patterns

The simulated travel time of Pb through the contaminated pavement system, containing only sand and assuming non linear adsorption is 1012 years. The infiltration through an contaminated pavement system containing additionally a realistically contaminated seam material results in an accelaration of 0.8 %. This difference is in the same order of magnitude like the mass balance error of the simulation runs. Therefore, an effect of the seam material cannot be detected, an sink or source effect is to small to be detectable. This statement is supported by scenario 4a. The seam material with the increased BC content after 60 years shows an approximately doubled K_f of 5860 $mg^{1-m}\,l^m\,kg^{-1}$. However, the travel time rises by only 3 %. This underlines the insignificance of the seam material layer for Pb retardation, which is a result of the small layer thickness.

If same column lengths are compared (comparison between scenario 1 and 2) the significance of the chemical properties can be evaluated. If the pavement would have been constructed only from uncontaminated seam material,

this would result in a 47 % slower breakthrough of Pb compared to scenario 1. Scenario 2 represents the maximum adsorption potential, all other traveltimes are smaller. The comparison of scenario 1 with scenario 3 shows the relevance of the actual contamination of the soil profile. If the sand is clean, the time the plume needs to reach the bottom is 6 % higher.

Compared to homogeneous flow, the preferential flow induced by pavers reduces the flow cross sectional area by 33 %. This results in a faster Pb transport, the traveltime is reduced by 30 a, which are 3 % less compared to homogenous flow. Compared to the impact of preferential flow on the Cd transport (see below) this is not relevant.

This result can be explained by the huge amount of free sorption sites and the strong adsorption of Pb to the soil material compared to the relative small solute concentration. Thus, the breakthrough is mainly governed by the diffusion rate. Convection is not relevant. Because the reduction of the crossectional area mainly influences convection but not diffusion, a travel time reduction due to preferential flow could not be detected for Pb. However, the resulting traveltime is 1000 years. Therefore, the infiltration of surface runoff bears not an acute but also no longterm risk of groundwater contamination at the investigated site for the tested conditions.

7.3.2 Cd Transport Considering Preferential Flow Patterns

As expected from the Freundlich parameters, Cd is relocated much faster than Pb. Because of the contamination of the soil column, there is no retardation of Cd. For the comparison, therefore the traveltime for uncontaminated soil column has been used in table **??**. Considering the seam material resulted in a 16 % faster transport compared to a sand column.

The consideration of preferential flow substantially accelerates the Cd replacement. The travel times is 39 % shorter than in the homogenous flow case and is around 109 years for the front of the contamination plume. This shows the potential of preferential flow phenomenons to increase contaminant transport. It further accelerates the actual net displacement of Cd considering the measured background concentrations.

Cd can be replaced much faster than Pb and the results indicate an acute risk for the groundwater quality. However, one needs to consider, that only the pavement system has been studied, the groundwater table is still far away. Furthermore, right now the front of the contaminant plume was detected, a considerable mass replacement has not taken place but starts after 109 years (for the uncontaminated case). However, the employed input con-

centration of 0.01 mg l^{-1} is unrealistic. Gromaire-Mertz et al. (1999) reported of concentrations of 0.6 μg l^{-1}!

Different to Pb the longterm effects of Cd transport through pavements can be relevant. In Berlin there are some older quarters were one can expect to find the first matric flow transported Cd at the bottom of pavement systems.

Now the HM transport through the pavement system is compared to an other sandy soil. Three times faster travel times have been reported by Streck (1993). This can be explained by different circumstances. Cd of concentrations of around 5 μg l^{-1} has been displaced to 60 cm in 30 years. The investigated soils showed much lower C_{org} contents, the highest of around 1 %. The pH was around 5. Thus, the resulting K_f was small (21 to 67 $\mu g^{1-m} l^m$ kg^{-1}, m=0.86). The infiltration rate was 430 mm a^{-1} resulting from wastewater application and precipitation. The predicted traveltimes could be veryfied using the HYDRUS model.

7.4 Conlusions

The study shows and quantifies the influence of the seam material and the influence of flow patterns under pavements. While the first plays no role, the latter is of importance. The results can be used for other studies too, for instance for the transport of organics such as mineral oil hydrocarbons or pesticides.

The traveltimes for Pb are high. A risk for the groundwater quality however can be stated for Cd, as the soil profiles are contaminated and the seam material further acts as a source. The risk assessment however, works with assumptions, which are worth thinking twice.

The groundwater recharge rate for densely populated housing areas of 120 mm a^{-1} was applied. In the same reference, Wessolek and Renger (1998) calculated the minimum evaporation rate in urban Berlin to 102 mm a^{-1}. If the precipitation of 588 mm a^{-1} is reduced by that evaporation, an available water amount of approximately 480 mm a^{-1} remains. If because of special conditions like ponds the water can inflitrate completely without losses due to surface runoff, the traveltimes from table 7.3 can be devided by four. If one takes a look around in the old, densely populated quarters of Berlin like at the site Pflügerstrasse, it is clear, that ponds at the sidewalk are rather the rule than the exception. Flow through macro pores or co transport by colloids has not been considered.

In reality, the contaminations in the ground, frequently found in urban soils might be more serious than heavy metals inputs from above.

However, not all risks have been investigated. Partially sealed soils show comparable high infiltration rates and a low evaporation which leads to high water flow velocities and groundwater recharge rates. Furthermore, they are sites of high input of small particles. therefore, partially sealed urban soils might be susceptible for colloid transport which would influencse the HM transport too. Flow through macropores could also not have been considered by the model, but might have an influence in reality. Here, the corresponding necessary field measurements have already began but are not part of this work.

Part V

General Conclusions and Outlook

The anthropogenically developed, urban dirt containing seam material is able to immobilise and to store deposited heavy metals - dirt cleans dirt. Thus, the seam material is a good example for artificial soils, which fulfill ecological functions generating a benefit for city dwellers - clean air and clean water. However, because of the limited layer thickness, a beneficial effect on solute heavy metal displacemant could not be observed in simulations of the actual situation. The simulations need to be verified by field monitoring. This has been prepared and is the next step in investigating the pavements.

However, if the deposition and incorporation, thus immobilisation of dust into urban soils would be improved by opening sealed soils, a positive effect would be detectable. This has been simulated too. The further incorporation of BC has a positive effect on the retardation of Pb. Increasing the layer thickness would have a much greater influence. For Cd, which is not affected by orginc matter in the same extent like Pb, the seam material is not of relevance. Here, other sorpting agents are more important, which are already part of the construction sand.

For Cd the displacement time is to a much greater extent governed by preferential flow patterns. These have been quantified by dye tracer experiments. Such experiments were done for the first time in partially sealed urban soils and showed, that the pavement geometry can substantially influence the flow patterns in the soil. This shows an option for optimizing the pavement system with the goal to prevent preferential flow. Gravel layers has been found to prevent formation of preferential flow patterns. The great heterogeneity of urban soils played an important role for the motivation to develop a new digital imgage analysing method, which can handle a great soil color heterogeneity. The method was developed for urban soils, but can now be applied to other soils too.

In the simulations, a Berlin case study was presented. Nevertheless, some properties of the seam material seem to be universal for all seam materials, at least some physical properties for Berlin and Warsaw seam materials were similar. This data and sample base could be enlarged by samples from other cities. Enlarging the sample pool and the knowledge about the sampling sites would also give the chance to determine the most important external factors for the seam material development (traffic densities, street trees etc.)

The role of partially urban soils in the carbon cycle has been investigated and a high relevance of urban soils for the global carbon cycle can be assumed because of first approximations. Only the first 5 cm of partially sealed soils, which make only 15 % of the urban area can store about half the annual anthropogen black carbon release! Here, a further research is necessary and very promising if one keeps in mind that the anthropogenic influenced layers of urban soils can reach some meters.

As other harmful substances like pesticides were not studied yet, there might be still a risk for the groundwater, coming from the pavement above. Further investigations are needed and has already been started in the second period of the graduate school.

Bibliography

Adhikari, T. and M. Singh (2003). Sorption characteristics of lead and cadmium in some soils of india. *Geoderma 114*, 81–92.

Baldock, J. A., J. M. Oades, A. G. Waters, X. Peng, A. M. Vassallo, and M. A. Wilson (1992). Aspects of the chemical-structure of soil organic materials as revealed by solid-state c-13 nmr-spectroscopy. *Biogeochemistry 16*(1), 1–42.

Borgwardt, S. (1993). Versickerung auf durchlässig befestigten Oberflächen. *Wasser und Boden 1993*(1), 38–41.

Brodowski, S. (2005). *Origin, function, and reactivity of black carbon in the arable soil environment*. Dissertation, Institut für Bodenkunde, Rheinische Friedrich-Wilhelms-Universität Bonn.

Brunauer, S., P. H. Emmett, and E. Teller (1938). Adsorption of gases in multimolecular layers. *Journal of the American Chemical Society 60*, 309–319.

Dannecker, W., M. Au, and H. Stechmann (1990). Substance load in rainwater runoff from different streets in hamburg. *The Science of the total environment 93*, 385–392.

Deutsches Institut für Normung (2002). DIN ISO 11277, Ausgabe 2002-08 (2002) Bodenbeschaffenheit- Bestimmung der Partikelgrößenverteilung in Mineralböden - Verfahren mittels Siebung und Sedimentation.

Dierkes, C. and W. F. Geiger (1999). Pollution retention capabilities of roadside soils. *Water Science and Technology 39*(2), 201–208.

Dreher, D. B. and R. A. Harley (1998). A fuel-based inventory for heavy-duty diesel truck emissions. *Journal of the Air and Waste Management Association 48*(4), 352–358.

ECJRC (2003). The global land cover map for the year 2000, the european commission joint research centre. http://www-gem.jrc.it/glc2000.

Ellerbrock, R., A. Höhn, and H. Gerke (1999). Characterization of soil organic matter from a sandy soil in relation to management practice using ft-ir. *Plant and Soil 213*, 55–61.

Fernandes, M. B., J. O. Skjemstad, B. B. Johnson, J. D. Wells, and P. Brooks (2003). Characterization of carbonaceous combustion residues. i.morphological, elemental and spectroscopic features. *Chemosphere 51*, 785–795.

Flury, M. and H. Flühler (1994). Brilliant blue fcf as a dye tracer for solute transport studies - a toxicological overview. *Journal of Environmental Quality 23*(5), 1108–1112.

Flury, M. and H. Flühler (1995). Tracer characteristics of brilliant blue fcf. *Soil Science Society of America Journal 59*(1), 22–27.

Flury, M., H. Flühler, W. A. Jury, and J. Leuenberger (1994). Susceptibility of soils to preferential flow of water - a field-study. *Water Resources Research 30*(7), 1945–1954.

Forrer, I. ., A. Papritz, R. Kasteel, and D. Luca (2000). Quantifiying dye tracers in soil profiles by image processing. *European Journal of Soil Science 51*, 313–322.

Forrer, I., R. Kasteel, M. Flury, and H. Flühler (1999). Longitudinal and lateral dispersion in an unsaturated field soil. *Water resources research 35*(10), 3049–3060.

Glaser, B. (2005). Source appointment of a highway-traffic-influenced urban areas in bayreuth (germany) using biomarker and stable carbon isotope signatures. *Environmental Science and Technology 39*, 3911–3917.

Glaser, B., L. Haumaier, G. Guggenberger, and W. Zech (1998). Black carbon in soils: the use of benzenecarboxylic acids as specific markers. *Organic Geochemistry 29*(4), 811–819.

Glaser, B., L. Haumaier, G. Guggenberger, and W. Zech (2001). The ´terra preta´ phenomenon: a model for sustainable agriculture in the humid tropics. *Naturwissenschaften 88*, 37–41.

Goldberg, E. (1985). *Black Carbon in the Environment*. New York: Wiley.

Gonzalez, R. C. and R. E. Woods (2002). *Digital image processing*. Upper Saddle River, New Yersey: Prentice Hall.

González-Pérez, J., F. González-Vila, G. Almendros, and H. Knicker (2004). The effect of fire on soil organic matter- a review. *Environmental International 30*, 855–870.

Gromaire-Mertz, M. C., S. Garnaud, A. Gonzalez, and G. Chebbo (1999). Characterisation of urban runoff pollution in paris. *Wat.Sci.Tech. 39*(2), 1–8.

Hagedorn, F. and M. Bundt (2002). The age of preferential flow paths. *Geoderma 108*, 119–132.

Hajnos, M., G. Jozefaciuk, Z. Sokolowska, A. Greiffenhagen, and G. Wessolek (2003). Water storage, surface, and structural properties of sandy forest humus horizons. *Journal of Plant Nutrition and Soil Science-Zeitschrift Fur Pflanzenernahrung Und Bodenkunde 166*(5), 625–634.

Hamer, U., B. Marschner, S. Brodowski, and W. Amelung (2004). Interactive priming of black carbon and glucose mineralisation. *Organic Geochemistry 35*(7), 823–830.

Harrison, R. M. and W. R. Johnston (1985). Deposition fluxes of lead, cadmium, copper and polynuclear aromatic hydrocarbons (pah) on the verges of a major highway. *The Science of the Total Environment 46*, 121–135.

Heinzmann, B. (1998). Improvement of the surface water quality in the berlin region. *Water Science and Technology 38*(6), 191–200.

Hewitt, N. and M. B. Rashed (1991). The deposition of selected pollutants adjacent to a major rural highway. *Atmospheric Environment 25A*(5/6), 979–983.

Hillel, D. (1998). *Environmental Soil Physics*. San Diego: Academic Press.

Hiller, D. and G. Bruemmer (1997). Mikrosondenuntersuchungen an unterschiedlich stark mit Schwermetallen belasteten Böden. 2. Gehalte an Schwermetallen und anderen Elementen in Huminstoffaggregationen, Streustoffen und Holzkohlepartikeln. *Zeitschrift für Pflanzenernährung und Bodenkunde 160*(1), 47–55.

Hoeke, S. (2003). *Identifizierung, Herkunft, Mengen und Zusammensetzung von Exstäuben in Böden und Substraten des Ruhrgebiets*, Volume 20 of *Essener Ökologische Schriften*. Essen: Westarp Wissenschaften.

Jaroniec, M. and M. Kruk (1997). Fractal analysis of composite adsorption isothermes by using density functional theory data for argon in slitlike pores. *Langmuir 13*, 1031–1035.

Kapicka, A., N. Jordanova, E. Petrovsky, and V. Podraszsky (2003). Magnetic study of weakly contaminated forest soils. *Water, Air, and Soil Pollution 148*, 31–44.

Kasteel, R., H.-J. Vogel, and K. Roth (2002). Effect of non-linear adsorption on the transport behaviour of brilliant blue in a field soil. *European Journal of Soil Science 53*, 231–240.

Kempenaar, C., L. A. P. Lotz, C. L. M. van der Horst, W. H. J. Beltman, K. J. M. Leemnans, and A. D. Bannink (2007). Trade off between costs and environmental effects of weed control on pavements. *Crop Protection 26*(3), 430–435.

Köhler, I., M. Dameris, I. Ackermann, and H. Hass (2001). Contribution of road traffic emissions to the atmospheric black carbon burden in the mid-1990s. *Journal of geophysical research 116*(No. D16), 17997 – 18014.

Kildsgaard, J. and P. Engesgaard (2002). Tracer tests and image analysis of biological clogging in a two-dimensional sandbox experiment. *Groundwater monitoring and remediation 22*(2), 60–67.

Kocher, B. (2005). *Einträge und Verlagerung strassenverkehrsbedingter Schwermetalle in Sandböden an stark befahrenen Ausserortstrassen*. Dissertation, Institut für Ökologie, Technische Universität Berlin.

Krauss, M. and W. Wilcke (2002). Sorption strength of persistent organic pollutants in particle-size fractions of urban soils. *Soil Science Society of America Journal 66*(2), 430–437.

Krogh, L., H. Breuning-Madsen, and M. H. Greve (2000). Cation-exchange capacity pedotransfer functions for danish soils. *Acta Agriculturae Scandinavica Section B-Soil and Plant Science 50*(1), 1–12.

Kuhlbusch, T. (1998). Black carbon and the carbon cycle. *Science 280*, 1903–1904.

Kutilek, M. and D. Nielsen (1994). *Soil Hydrology*. Geoecology Textbook. Cremlingen-Destedt: Catena.

Kuttler, W. (1998). Stadtklima. In H. Sukopp and R. Wittig (Eds.), *Stadtökologie*, pp. 125–167. Stuttgart: Gustav Fischer Verlag.

Laschober, C., A. Limbeck, J. Rendl, and H. Puxbaum (2004). Particulate emissions from on-road vehicles in the Kaisermühlen-Tunnel (vienna, austria). *Atmospheric Environment 38*, 2187–2195.

Lau, S. L. and M. K. Stenstrom (2005). Metals and pahs adsorbed to street particles. *Water Research 39*(17), 4083–4092.

Legret, M. and C. Pagotto (1999). Evaluation of pollutant loadings in the runoff waters from a major rural highway. *The science of the total environment 235*, 143–150.

Lehmann, J., B. Liang, D. Solomon, M. Lerotic, F. Luizão, F. Kinyangi, T. Schäfer, S. Wirick, and C. Jacobsen (2005). Near-edge x-ray absorption fine structure (nexafs) spectroscopy for mapping nano-scale distribution of organic carbon forms in soil: Application to black carbon particles. *Global Biogeochemical Cycles 19*, GB1013. DOI 10.1029/2004GB002435.

Mehlich, A. (1984). Mehlich-3 soil test extractant: a modification of mehlich-2 extractant. *Communications in soil science and plant analysis 15*, 1409–1416.

Miguel, A. H., T. W. Kirchstetter, R. A. Harley, and S. v. Hering (1998). On-road emmissions of particulate polycyclic aromatic hydrocarbons and black carbon from gasoline and diesel vehicles. *Environmental Science and Technology 32*, 450–455.

Nehls, T., G. Jozefaciuk, Z. Sokolowska, M. Hajnos, and G. Wessolek (2006). Pore-system characteristics of pavement seam materials of urban sites. *Journal of Plant Nutrition and Soil Science 169*, 16–24.

Novakov, T. (1984). The role of soot and primary oxidants in atmospheric chemistry. *The science of the total environment 36*, 1–10.

OECD (2000). Oecd guideline for the testing of chemicals no. 106 adsorption - desorption using a batch equilibrium method.

Pachepsky, Y., T. Polubesova, M. Hajnos, Z. Sokolowska, and G. Jozefaciuk (1995). Fractal parameters of pore surface areas as influenced by simulated soil degradation. *Soil Science Society of America Journal 59*, 68–75.

Parfitt, R., D. Giltrap, and J. Whitton (1995). Contribution of organic matter and clay minerals to the cation exchange capacity of soils. *Communications in soil science and plant analysis 26*(9-10), 1343–1355.

Pfeifer, P. and M. Obert (1989). *Fractals: Basic concepts and terminology.* The fractal approach to heterogenous chemistry. Cichester: Wiley.

Preston, C. M. (1996). Applications of nmr to soil organic matter analysis: History and prospects. *Soil Science 161*(3), 144–166.

Proll, K. (2005). Untersuchungen zum zeitlichen und räumlichen Verhalten von Sickerwasser unter teilversiegelten Flächen. Diplomarbeit, Institut für Ökologie, Technische Universität Berlin.

Rawls, W. J., D. L. Brakensiek, and K. E. Saxton (1982). Estimation of soil water properties. *Transactions of the ASAE 25*(5), 1316–1320,1328.

Renger, M. (1965). Berechnung der Austauschkapazität der organischen und anorganischen Anteile der Böden. *Zeitschrift für Pflanzenernährung und Bodenkunde 110*, 10–26.

Roquerol, R., D. Avnir, C. Fairbridge, D. Everett, J. Haynes, N. Pernicone, J. Ramsay, K. Sing, and K. Unger (1994). Recommendations for the characterization of porous solids. *Pure and Applied Chemistry 66*, 1739–1758.

Schmidt, M. W. I., H. Knicker, P. G. Hatcher, and I. KogelKnabner (1996). Impact of brown coal dust on the organic matter in particle-size fractions of a mollisol. *Organic Geochemistry 25*(1-2), 29–39.

Schmidt, M. W. I. and A. G. Noack (2000). Black carbon in soils and sediments: Analysis, distribution, implications, and current challenges. *Global Biogeochemical Cycles 14*(3), 777–793.

Schmidt, M. W. I., J. O. Skjemstad, E. Gehrt, and I. Kögel-Knabner (1999). Charred organic carbon in german chernozemic soils. *European Journal of Soil Science 50*, 351–365.

Schramm, M. and B. Münchow (1996). *Beregnungsversuche zur Ermittlung der Infiltrations- und Abflußcharakteristik neuer und gealterter Flächenbefestigungen.* Entsiegelung und Oberflächenversickerung mit durchlässigen Platten- und Pflasterbelägen. Troisdorf: FLL e.V.

Schubert, F. (2003). Leben in der Ritze. *Die Zeit 38*(39), 39.

Senstadt-Berlin (2001). Umweltatlas Berlin. online, Senatsverwaltung für Stadtentwicklung und Umweltschutz.

Simunek, J., M. Sejna, and M. vanGenuchten (1999). The hydrus-2d software package for simulating the two-dimensional movement of water, heat, and multiple solutes in variably-saturated media. Technical report, U.S. Salinity Labaoratory, Riverside, CA 92507.

Skjemstad, J. O., P. Clarke, J. A. Taylor, J. M. Oades, and S. G. McClure (1996). The chemistry and nature of protected carbon in soil. *Australian Journal of soil research 34*, 251–271.

Sokolowska, Z., M. Hajnos, C. Hoffmann, M. Renger, and S. Sokolowski (1999). Surface fractal dimension of thermally treated peat soils from adsorption isotherms of nitrogen. *Journal of Plant Nutrition and Soil Science 163*, 441–446.

Spanoghe, P., J. Claeys, L. Pinoy, and W. Steurbaut (2005). Rainfastness and adsorption of herbicides on hard surfaces. *Pest Management Science 61*(8), 793–798.

Sposito, G. (1980). Derivation of the freundlich equation for ion exchange reactions in soils. *Soil Science Society of America Journal 44*, 652–654.

Stadler, D., M. Staehli, P. Aeby, and H. Flühler (2000). Dye tracing and image analysis for quantifiying water infiltration into frozen soils. *Soil science society of america journal 64*, 505–516.

Staikos, N. (2005). Zur biologischen Aktivität urbaner Böden. Diplomarbeit, Institut für Ökologie, Technische Universität Berlin.

Strange-Hansen, R., P. E. Holm, O. S. Jacobsen, and C. S. Jacobsen (2004). Sorption, mineralization and mobility of n-(phosphonomethyl)glycine (glyphosate) in five different types of gravel. *Pest Management Science 60*(6), 570–578.

Streck, T. (1993). *Schwermetallverlagerung in einem Sandboden im Feldmaßstab - Messung und Modellierung*. Dissertation, Naturwissenschaftliche Fakultät der Technischen Universität Carolo-Wilhelmina zu Braunschweig.

Stumm, W. and J. Morgan (1996). *Aquatic Chemistry* (3 rd ed. ed.). New York: John Wiley and Sons, Inc.

Taeumer, K., H. Stoffregen, and G. Wessolek (2005). Determination of repellency distribution using soil organic matter and water content. *Geoderma 125*, 107–115.

Tol, R. S. J. (2002a). Estimates of the damage costs of climate change - part i. benchmark estimates. *Environmental and Resource Economics 21*, 47–73.

Tol, R. S. J. (2002b). Estimates of the damage costs of climate change - part ii. dynamic estimates. *Environmental and Resource Economics 21*(2), 135–160.

Toth, T. and G. Jozefaciuk (2002). Physicochemical properties of a solonetzic toposequence. *Geoderma 106*(1-2), 137–159.

Townsend, M., M. Mahoney, J. A. Jones, K. Ball, J. Salmon, and C. F. Finch (2003). Too hot to trot? exploring potential links between climate change, physical activity and health. *Journal of Science and Medicine in Sport 6*(3), 260–265.

Tryon, E. (1948). Effect of charcoal on certain physical, chemical and biological properties of forest soils. *Ecological Monographs 18*(1), 82–114.

vanGenuchten, M., F. Leij, and S. Yates (1991). The retc code for quantifying the hydraulic functions of unsaturated soils. Technical Report EPA Report 600/2-91/065, U.S. Salinity Laboratory USDA, ARS Riverside.

Viidanoja, J., M. Sillanpää, J. Kaakia, V.-M. Kerminen, R. Hillamo, P. Arnio, and T. Koskentalo (2002). Organic and black carbon in pm 2.5 and pm 10:1 year of data from an urban site in helsinki, finland. *Atmospheric Environment 36*, 3183–3193.

Washburn, E. (1921). A method of determining the distributionof pore sizes in a porous material. *Proceedings of the national academy of sciences USA V.7*, 115.

Wellner, F., M. Köhler, and D. Ulonska (1997). *Richtig planen und ausführen - Dauerhafte Verkehrsflächen mit Betonpflastersteinen*. Bonn: Deutsche Beton- und Fertigteilindustrie e.V.

Welp, G. and G. W. Brummer (1999). Adsorption and solubility of ten metals in soil samples of different composition. *Journal of Plant Nutrition and Soil Science-Zeitschrift Fur Pflanzenernahrung Und Bodenkunde 162*(2), 155–161.

Wenikajtys, M. and W. Burghardt (2002). Dialeimmasol - Ritzenboden von Gehwegpflastern. *Mitteilungen der Deutschen Bodenkundlichen Gesellschaft 99*, 23–24.

Wessolek, G. (2001). Bodenüberformung und -versiegelung. In H.-P. Blume, P. Felix-Henningsen, W. R. Fischer, H.-G. Frede, R. Horn, and K. Stahr (Eds.), *Handbuch der Bodenkunde*, Volume 11, pp. 29. Landsberg/Lech: ecomed.

Wessolek, G. and M. Facklam (1997). Standorteigenschaften und Wasserhaushalt von versiegelten Flächen. *Journal of Plant Nutrition and Soil Science 160*(1), 41–46.

Wessolek, G. and M. Renger (1998). Bodenwasser- und grundwasserhaushalt. In H. Sukopp and R. Wittig (Eds.), *Stadtökologie*, pp. 186–200. Stuttgart: Gustav Fischer.

Wilczynski, W., M. Renger, G. Jozefaciuk, M. Hajnos, and Z. Sokolowska (1993). Surface area and cec as related to qualitative and quantitative changes of forest soil organic matter after liming. *Zeitschrift für Pflanzenernährung und Bodenkunde 156*, 235–238.

Zhang, H. and K. Hartge (1992). Zur Auswirkung organischer Substanz verschiedener Humifizierungsgrade auf die Aggregatstabilität durch Reduzierung der Benetzbarkeit. *Journal of Plant Nutrition and Soil Science 155*, 143–149.

Zhu, Y. F., W. C. Hinds, S. Kim, S. Shen, and C. Sioutas (2002). Study of ultrafine particles near a major highway with heavy-duty diesel traffic. *Atmospheric Environment 36*(27), 4323–4335.

Appendix A

The investigated sites

Table A.1: Investigated sites in Berlin, Warsaw and Paris.

Site ID	Street	Latitude	Longitude
B1	Monbijouplatz	52°31'24.69"N	13°23'55.08"E
B2	Weidendamm	52°31'19.80"N	13°23'26.46"E
B3	Schnellerstraße	52°27'19.23"N	13°30'42.35"E
B4-B8	Grosser Stern	52°30'49.49"N	13°21'2.14"E
B9-B10	Pflügerstraße	52°29'28.25"N	13°25'25.81"E
W1	Emilii Plater	52°13'35.76"N	21°0'23.58"E
W2	Jerozolimskie	52°13'30.09"N	21°0'23.58"E
W3	Pulawska	52°8'18.36"N	21°1'5.50"E
W4	Rzymowskiego	52°10'17.47"N	21°0'20.92"E
W5	Stanow Zjednoczonych	52°13'42.54"N	21°3'46.68"E
W6	Modlinska		
W7	Slowackiego	52°16'19.89"N	20°58'11.06"E
W8	Wilanowska	52°10'42.32"N	21°1'39.52"E
W9	Grota Rowecki	52°17'26.11"N	21°0'8.88"E

Figure A.1: Site B1, Berlin, Monbijouplatz.

Figure A.2: Site B2, Berlin, Weidendamm.

Figure A.3: Site B3, Berlin, Schnellerstraße.

(a)

(b)

Figure A.4: Site B4-8 and soil profile, Berlin, Großer Stern.

Figure A.5: Site B9-10 and soil profile, Berlin, Großer Stern.

Figure A.6: Site W1, Warsaw, Emilii Plater.

Figure A.7: Site W2, Warsaw, Aleji Jerozolimskie.

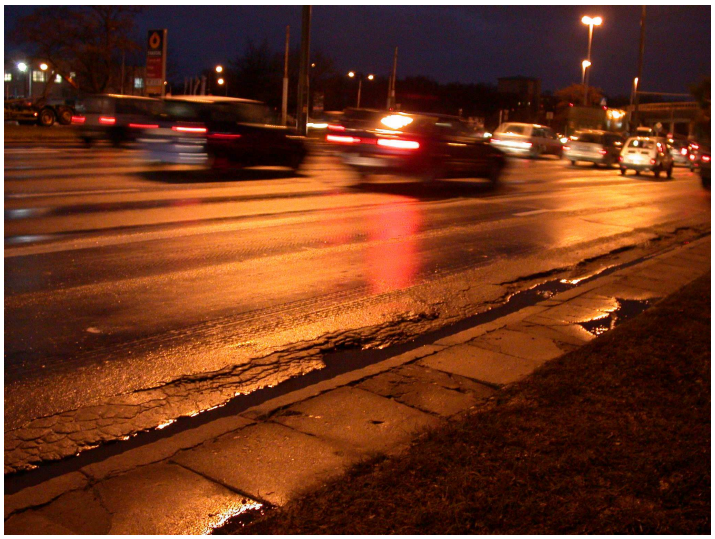

Figure A.8: Site W3, Warsaw, Pulawska.

Figure A.9: Site W4, Warsaw, Rzymowskiego.

Figure A.10: Site W5, Warsaw, Aleji Stanow Zjednoczonych / Most Lazenskiego.

Figure A.11: Site W6, Warsaw, Modlinska.

Figure A.12: Site W7, Warsaw, Slowackiego.

Figure A.13: Site W8, Warsaw, Wilanowska.

Figure A.14: Site W9, Warsaw, Grota Rowecki.